RESURGENT SODIUM CURRENT MODULATION BY AUXILIARY SUBUNITS IN DORSAL ROOT GANGLIA NEURONS AND POTENTIAL IMPLICATIONS IN PAIN PATHOLOGIES.

Cindy M. Barbosa Nuñez

Submitted to the faculty of the University Graduate School
in partial fulfillment of the requirements
for the degree
Doctor of Philosophy
in the Department of Pharmacology and Toxicology
Indiana University

June 2016

Accepted by the Graduate Faculty, Indiana University, in partial

fulfillment of the requirements for the degree of Doctor of Philosophy.

_____
Theodore R. Cummins, Ph.D., Chair

_____
Jill C. Fehrenbacher, Ph.D.

Doctoral Committee

_____
Andy Hudmon, Ph.D.

April 11, 2016

_____
Grant D. Nicol, Ph.D.

_____
Richard Day, Ph.D.

DEDICATION

This work is dedicated to my parents whose love, encouragement and support have given me the strength to follow my passion for science and helping others.

ACKNOWLEDGEMENTS

I would like to acknowledge the people and the support received which made this dissertation possible. First, I would like to thank God for your enduring love and care which has given me the strength and motivation throughout my Ph.D. studies and will continue to guide me in my future ventures.

Secondly, I would like to thank my family. Mom and Dad thank you for your prayers. Mom thanks for your care, support and daily calls to make sure I was on track and lifting my spirit when things did not work as anticipated. Dad thanks for helping me keep focus on the big picture and not to lose sight of my end goals. To my brothers, Omar and Marcos, thanks for your love and motivation.

I would also like to give special thanks to my mentor, Dr. Theodore Cummins. Thank you for giving me the space to explore new ideas and pushing me to be a better scientist. I am immensely grateful for all your support, attention and guidance that allowed me to be grow and be productive. Thanks to my past mentors, Dr. Jorge Colon and Dr. Alexander Obukhov for investing in me. Your teachings and advice, I carried with me and have helped me through this process. I would also like to acknowledge my fellow SPINES and mentors from the Marine Biology Lab Course 2013. Your friendship, mentorship and advice

helped me in more ways that I can explain. Thank you for believing in me and motivating me to go beyond my comfort zone and dare to dream.

I would like to thank my thesis committee advisors, Dr. Grant Nicol, Dr. Richard Day, Dr. Andy Hudmon and Dr. Jill Fehrenbacher. Thank you for challenging me to think about my research from different points of view. Thank you for training me in new techniques and providing advice on experimental procedures which truly helped me throughout my research. Your feedback and constructive criticism has enhanced the quality of this research.

I would also like to thank our collaborators who have been instrumental for our research. Many thanks to Dr. Michael Vasko, Dr. Ruizhong Wang, Dr. Jun-Ming Zhang, Dr. Wenrui Xie and Dr. Judith Strong. Your knowledge, training, and feedback were pivotal to overcoming key hurdles.

Special thanks to past and present members of the Cummins lab, Yucheng Xiao, Andrew Piekarz, Zhiyong Tan, Zifan Pei, Reesha Patel, James Jackson, Adrienne Jackson, Emily Mason, Claudia Pan and Andrew Johnson for all your support. It has been fun sharing science, our lives (the ups and the downs) and watching each other grow into new stages of our lives and career.

Thanks to the administrative staff from the Pharmacology and Toxicology department Joanna Plew, Lisa King, Amy Lawson, Dan Smith, Andy Boyll,

Alexandra Guzik and STARK Neuroscience Research Institute, Nastassia Belton, for your help and support. Thank you for helping me navigate the grant submission process, paperwork for my graduate studies and keeping me on track. Thanks to all the students, post-docs and faculty from the Department of Pharmacology and Toxicology for your valuable input in seminars and journal clubs.

Thanks to the IUSM Graduate Department. In particular, past and present directors Monica Henry and Tara Hobson-Prater. Thanks Monica for making the transition from Puerto Rico easier, knowing that I had someone that I could count on and had my best interest at heart made me feel confident during this process. Tara, I have no words to say how much you have helped. Thank you for always being available to help and for your support as I navigated future directions. Thanks for believing in a more inclusive and diverse student body, your help with SACNAS and for letting me be part of recruitment process. I truly enjoyed being part of the IUSM community.

Lastly, this research would have not been possible without the support of the National Institute of Medicine. In particular, thanks to the National Institute of Neurological Disorders and Stroke for funding my training through Diversity Supplement-NS053422 and Ruth L. Kirschstein National Research Service Award Individual Predoctoral Fellowship-F31NS090837.

Cindy M. Barbosa Nuñez

Resurgent sodium current modulation by auxiliary subunits in dorsal root ganglia neurons and potential implications in pain pathologies.

Increased electrical activity in peripheral sensory neurons contributes to pain. A unique type of sodium current, fast resurgent current, is proposed to increase nerve activity and has been associated with pain pathologies. While sodium channel isoform Nav1.6 has been identified as the main carrier of fast resurgent currents, our understanding of how resurgent currents are modulated in sensory neurons is fairly limited. Thus the goal of this dissertation was to identify resurgent current modulators. In particular, we focused on sodium channel beta subunits (Navβs) and fibroblast growth factor homologous factors (FHFs) in dorsal root ganglion (DRG) neurons. We hypothesized that Navβ4 and FHF2B act as positive regulators by mediating resurgent currents and modulating Nav1.6 inactivation, respectively. In contrast, we hypothesized FHF2A negatively regulates resurgent current by increasing the probability of channels in inactivated states. Thus, the aims of this dissertation were to 1) determine if Navβ4 regulates fast resurgent currents in DRG neurons, 2) examine the effects of Navβ4 knockdown on resurgent currents, firing frequency and pain associated behavior in an inflammatory pain model and 3) determine if FHF2A and FHF2B functionally regulate Nav1.6 currents, including resurgent currents in DRG neurons. To examine the aims, we used biochemical, electrophysiological and

behavioral assays. Our results suggest that Navβ4 is a positive regulator of resurgent currents: in particular, the C-terminus likely mediates these currents. Localized knockdown of Navβ4 decreased inflammation-induced enhancement of resurgent currents and neuronal excitability, and prevented the development of persistent pain associated behavior in an inflammatory pain model. FHF2B increased resurgent currents and delayed inactivation. In contrast, FHF2A limited resurgent currents; an effect that is mainly contributed by FHF2A's N-terminus activity that increased accumulation of channels in inactivated states. Interestingly, in an inflammatory pain model FHF2B was upregulated and FHFA isoforms were downregulated. Together these results suggest that FHF2A/B modulation might contribute to enhanced resurgent currents and increased neuronal excitability observed in the inflammatory pain model. Overall, our work has identified three resurgent current modulators FHF2A, FHF2B and Navβ4. Manipulation of these proteins or their activity might result in novel strategies for the study and treatment of pain.

Theodore R. Cummins, Ph.D., Chair

TABLE OF CONTENTS

LIST OF TABLES

LIST OF FIGURES

LIST OF ABBREVIATIONS

AP	Action Potential
AU	Arbitrary Units
CAM	Cell Adhesion Molecule
CNS	Central Nervous System
CTFC	Corrected Total Cell Fluorescence
DI-IV	Domains of Voltage-gated Sodium Channels
DMEM	Dulbecco' modified Eagle's Medium
DRG	Dorsal Root Ganglia
FBS	Fetal Bovine Serum
FHF	Fibroblast growth factor Homologous factors
FHFA	Fibroblast growth factor Homologous Factor Type A
FHFB	Fibroblast growth factor Homologous Factor Type B
HEK	Human Embryonic Kidney
I/V	Current-Voltage
IACUC	Institutional Animal Care and Use Committee
IRES	Internal Ribosome Entry Site
IUSM	Indiana University School of Medicine
LID	Localized Inflammation of the DRG
n.t.	non-targeting
Nav	Voltage-gated Sodium Channel isoform
Nav	Sodium channel Beta subunit
PBS	Phosphate Buffered Saline
PEPD	Paroxysmal Extreme Pain Disorder
PKC	Protein Kinase
PNS	Peripheral Nervous System
POD	Post Operative Day
S1-6	Segments within Domains of Voltage-gated Sodium Channels
SEM	Standard Error of the Mean
shRNA	small hairpin Ribonucleic Acid
siRNA	small interfering Ribonucleic Acid
TG	Trigeminal Ganglia
TTX	Tetrodotoxin
TTXR	Tetrodotoxin-Resistant
TTXS	Tetrodotoxin-Sensitive
VGSC	Voltage-gated Sodium Channel
WT	Wild-type

INTRODUCTION

Overview

Pain is one of the prevalent reasons why people in the United States seek medical care. According to the National Center for Health Statistics, around 76.2 million people experience persistent pain (1). A third of these people who experience pain find that it is so significant that it impacts their daily routine (2). One of the main problems faced in pain management, especially management of persistent pain, is that the available therapeutics either are ineffective or have unwanted side effects (1). Such a high incidence of pain and inadequate relief creates a need for the development of new therapeutics.

Peripheral sensory neurons are an important component of the neuronal network that processes pain sensations. In mammals, these neurons are pseudounipolar neurons, possessing one axon that sends branches into two areas: one to the periphery (e.g., skin, muscle, internal organs) and the other to the spinal cord & brainstem of the central nervous system (CNS). The peripheral branch can detect changes in mechanical, thermal or chemical input and relay the information through the branch that projects to the CNS. Typically, when a noxious stimulus is encountered, “pain-sensing” peripheral sensory neurons or nociceptors are activated (3). Alterations in the signaling process that relays painful stimuli to the CNS (i.e. nociception) are a common mechanism in pain

pathologies. In particular, increased firing of nociceptors in dorsal root ganglia (DRG) and trigeminal ganglia (TG) often results in increased pain (4-7).

Voltage-gated ion channels contribute to the excitability of sensory neurons. In particular, voltage-gated sodium channels (VGSCs or Nav) are classically viewed to generate the rising phase of the action potential (AP). There is strong evidence from genetic and pain model studies that support the functional relevance of VGSCs in pain sensations (8-12). For example, in humans and mice loss-of-function of the VGSC isoform, Nav1.7, is associated with congenital indifference to pain. Furthermore, alterations to the activity of other VGSC isoforms such as Nav1.3, Nav1.6, Nav1.8 and Nav1.9 have also been associated with pain pathologies (13-16). This evidence suggests that inhibition of specific VGSC isoforms or selective blockade of altered activity may provide new therapeutic strategies for pain. In particular, specific patterns or modes of sodium current activity are likely to be important in the perception of noxious stimulus (i.e., nociception) and the transmission of pain sensations. A novel target for altered activity in VGSC that has emerged is resurgent sodium current.

Resurgent currents, an atypical VGSC current, are thought to increase the firing frequency of neurons by providing a depolarizing drive at repolarizing voltages (17-19). Increased resurgent currents in sensory neurons have been implicated in paroxysmal extreme pain disorder (PEPD), sea anemone toxin

ATX-II induced pain, and oxaliplatin acute cooling-aggravated painful neuropathy (19-26). Under baseline physiological conditions, resurgent currents are observed in a subpopulation of DRG neurons where the major contributing isoform is Nav1.6 (27). Nav1.6 has been implicated in inflammatory and neuropathic pain models since knockdown of Nav1.6 blocks the development of persistent pain associated behaviors and increased activity of sensory neurons (14, 15). Together these findings suggest that targeting resurgent currents may provide novel strategies for pain therapeutics. However, our understanding of how resurgent currents are modulated in peripheral sensory neurons is limited. Thus, the main goal of this dissertation was to identify potential modulators of resurgent currents. In particular, we focused on the modulation of Nav1.6-mediated currents by auxiliary subunits such as beta subunits and fibroblast growth factor homologous factors (FHF).

Brief history of voltage-gated sodium channels

Our current knowledge of VGSC was spearheaded by the work of Hodgkin and Huxley in the 1950s (28-31). Hodgkin and Huxley conducted a series of experiments using the voltage clamp technique (32, 33), which enabled them to "clamp" the membrane of the squid giant axon at a specific voltage and examine the ionic currents that contributed to the generation of the action potential. They identified three main ionic currents: sodium, potassium and a small leak current (which included Cl^-). Upon depolarization the sodium conductance was

transiently activated, whereas, the potassium conductance slowly activated. Returning to the initial resting membrane potential terminated both sodium and potassium conductances. Based on their findings, they proposed a mathematical model in which the ionic conductance was dependent on the ion's permeability and electrochemical gradient (34). Additionally, they introduced a novel concept of regulation for the sodium and potassium conductances by charged particles that acted as gates. Movement of these gates was dependent on the membrane potential (i.e., voltage-gated) and time. Therefore, based on their model, sodium currents contributed to the rising phase of the action potential, whereas sodium current inactivation coupled with potassium current activation contributed to the downward phase of the action potential.

Years later, it was discovered that toxins derived from pufferfish and shellfish selectively inhibited sodium currents (35-39). In contrast, the quaternary ammonium cation, tetraethylammonium ion (TEA), selectively inhibited potassium currents (37, 38, 40, 41). These experiments confirmed that sodium and potassium currents were generated by specific channels or receptors which Hogdkin and Huxley eluded to as "particles occupying the membrane" (34). During the 1960-70s, several functional properties of "sodium receptors" were elucidated giving birth to new conceptual models for an ion selectivity filter, pore structure of the channel, and activation and inactivation gates (42-48). However, the actual VGSC protein was not identified until the 1980s, when the subunits of VGSC were purified from brain tissue. These studies revealed a multimeric

complex composed of large alpha (α)-subunits associated with smaller beta (β)-subunits (49-51). It was during this time that a major breakthrough was achieved, the first sodium channel α subunit was cloned (52, 53). Expression of the α subunit was sufficient to produce a functional channel. Together, cloning of VGSC subunits and the advancement of high resolution patch clamp techniques, propelled the study of VGSCs (54, 55).

Voltage-gated sodium channel

VGSCs are transmembrane proteins that selectively mediate the inward flow of sodium ions generating the rapid upstroke of the AP (56). Nine α subunit genes that encode VGSC isoforms (Nav1.1 - Nav1.9) have been identified in mammals. The overall structure of the nine α subunit isoforms is highly conserved as a single polypeptide sequence (~2,000 amino acids) organized into four homologou*s* domains (DI-DIV) each with six transmembrane segments (S1 - S6; Figure 1A). The α subunit folds into a pseudotetrameric tridimensional structure in which S5/6 segments within each domain form an aqueous pore module selectively permeable to sodium ions**.** The S1-4 segments form the voltage sensor domain arranged around the pore module. In particular, S4 within each domain contains positive residues sensitive to changes in membrane potential and movement of the voltage sensors produces conformational changes in the protein structure (53, 57, 58). In this manner, VGSCs change between conformations that either conduct sodium ions (open state) or are

nonconducting (inactive states and closed states). Classically, sodium currents are generated when the membrane is depolarized and channels become activated or open. Sodium currents are then terminated by channel inactivation (Figure 1B-C). There are different modes of inactivation and these are discussed below. The most common mode of inactivation is fast inactivation which is mediated by the cytoplasmic linker between DIII-DIV. In particular, the IFM (Isoleucine-Phenylalanine-Methionine represented as the inactivation particle in Figure 1) motif within this linker is essential (59). Movement of the inactivation particle occludes the pore as a hinged lid by interacting with a putative receptor in the VGSC structure (60). Once inactivated, VGSCs become refractory and require repolarization of the membrane to recover before they are available again (61).

Many of the α subunits have developmental and tissue specific distributions (62). For example, Nav1.4 is predominantly expressed in skeletal muscle (63). In contrast, Nav1.5 is predominantly in cardiac tissue (64). Nav1.3 is predominantly expressed immature neurons and downregulated in mature neurons (65). Nav1.7, Nav1.8 and Nav1.9 are predominantly expressed in the peripheral nervous system (PNS). In contrast, in mature CNS neurons the predominant isoforms are Nav1.1, Nav1.2 and Nav1.6, however Nav1.1 and Nav1.6 are also expressed in PNS (66, 67).

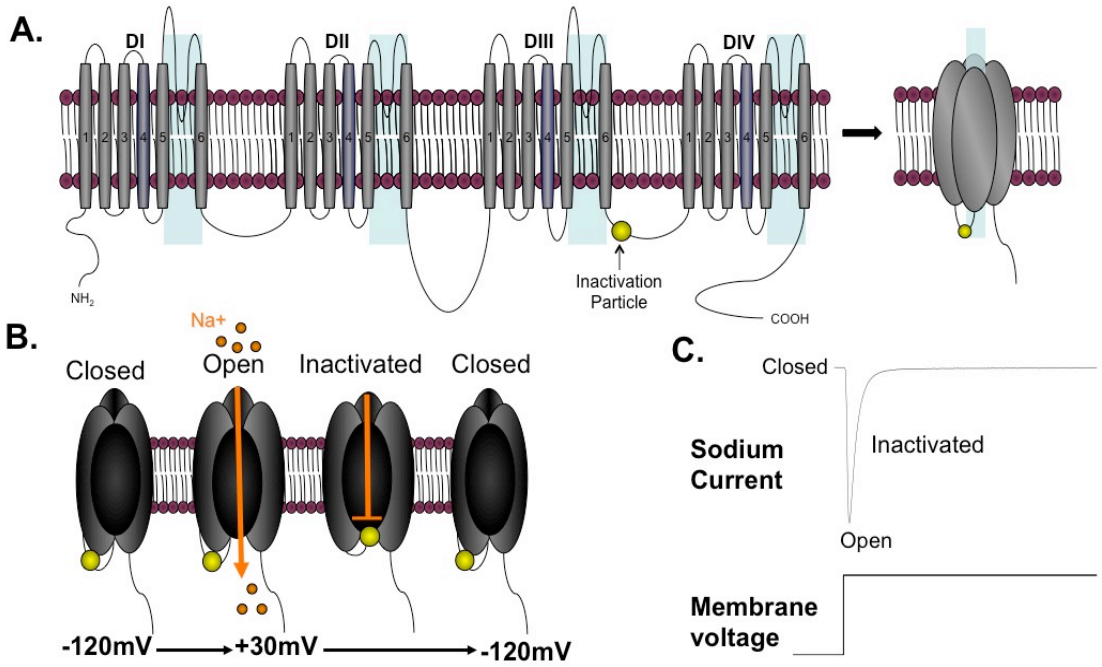

Figure 1: Structure and function of VGSC. ***A***, Linear Representation of VGSC α subunit. Regions highlighted in blue represent the regions between S5 and S6 that yield the aqueous pore module selectively permeable to sodium. ***B***, Cross-sectional representation of VGSC conformational changes in response to changes in membrane potential. ***C***, Representative trace of whole cell patch clamp recording of sodium current upon a depolarizing voltage step stimulus and corresponding state transitions from closed–open-inactive states.

Sodium channels in DRG neurons

Peripheral sensory neurons, at least in mammals, differ from neurons in the CNS neurons in a number of ways, including morphology and physiology (68). Although it has been written that with VGSCs “one is impressed more with the similarity of function than with the differences”(56) , this is clearly not the case with sodium currents in peripheral sensory neurons where sodium currents exhibit broad diversity. While sodium currents in the CNS are, for the most part, highly sensitive to pufferfish’s tetrodotoxin (TTX; IC50s near 10nM), distinct

components of the complex currents that can be elicited in peripheral DRG and TG neurons are roughly 1,000 to 50,000 fold less sensitive. As such, VGSC currents in DRG neurons can be classified as TTX-sensitive (TTXS) and TTX-resistant (TTXR).

The kinetic diversity of sodium currents in peripheral sensory neurons is also greater than that in the CNS. Peripheral neurons may express fast, slow and persistent sodium currents (see Figure 2) (69, 70). The fast gating current can be generated by multiple TTXS isoforms including Nav1.1, Nav1.3, Nav1.6 and Nav1.7. In adult DRG neurons, Nav1.3 is not expressed but expression can be triggered following nerve injury (71). The kinetics and voltage-dependence of TTXS currents contribute to the initiation of the AP. Some isoforms may also generate small persistent currents that can influence the threshold for AP generation (72, 73). In contrast, the large slowly inactivating and persistent currents observed in peripheral sensory neurons (74-76) are TTXR. In adult DRG neurons, the slow component is mainly generated by Nav1.8. This isoform exhibits a more depolarized voltage-dependence of activation and inactivation relative to TTXS channels and contributes in a major fashion to the upstroke of AP in neurons where it is expressed (77, 78). In contrast, Nav1.9 channels can activate at more hyperpolarized membrane potentials where other VGSCs are quiescent generating the large persistent component observed in DRG neurons (Figure 2D). Expression of Nav1.5, a TTXR channel, is detected in embryonic DRG neurons but is downregulated to negligible levels in adult neurons (65, 79,

80). As such, it is not considered to be a major VGSC contributor of TTXR sodium current in adult DRG neurons (13).

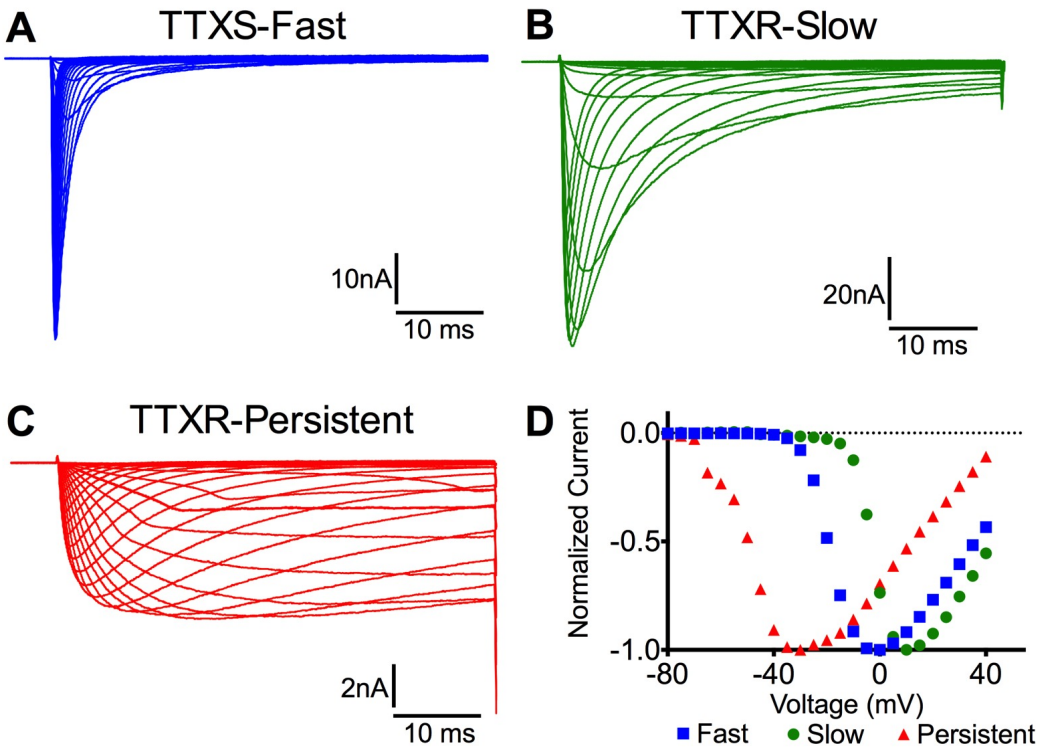

Figure 2: Examples of the sodium current diversity in DRG neurons. Endogenous sodium current recordings were obtained from dissociated DRG neurons grown in culture. A single pulse of 50ms from -80 to 40 mV was used to examine the current voltage relationship of the sodium currents.. ***A***, Representative traces of a DRG neuron with fast TTXS sodium currents. ***B***, Representative traces of a DRG neuron with TTXR-slow sodium currents. ***C***, Representative traces of a DRG neuron with TTXR-slow sodium currents. For panel B and C recordings were obtained in the presence of 500 nM TTX. Sodium currents were normalized to the peak sodium current of the DRG neurons. **D**, Normalized current as function of voltage shows that slow sodium currents (green circles) exhibit a more depolarized voltage-dependence relative to fast (blue squares) and persistent currents (red triangles). In contrast, persistent currents exhibit a more hyperpolarized voltage correlation relative to fast and slow currents.

The expression of VGSC α subunits varies between the different classes of peripheral sensory neurons. Three main classes of sensory fibers (C, Aδ and Aα/β) can be differentiated based on conduction velocity, soma diameter, and

activation threshold (Table 1). These different types of sensory fibers are activated selectively by the mode and intensity of the peripheral stimulus. Fibers, that are activated by a noxious stimulus, are termed nociceptors. Nociceptors are generally classified as high threshold neurons (81). While nociceptors are classically identified as fibers in the C-Aδ class, there is substantial evidence that supports that a subset of Aβ fibers also likely function as nociceptors (82). In C-fiber neurons, the predominant VGSCs expressed are Nav1.7, Nav1.8 and Nav1.9 (74, 75, 83, 84). In contrast, A-fiber neurons predominantly express Nav1.1, Nav1.6 and, (to a lesser extent) Nav1.7 with the exception of a discrete subpopulation that also expresses Nav1.8 at high levels (83, 85, 86).

Fiber class	***Aα/β***	***Aδ***	***C***
Soma diameter	>35um Large	25-35um Medium	<25um Small
Myelination	Thick	Thin	None
Conduction	35-75m/s	5-30m/s	0.5-2m/s
Threshold	Low - high	Low - high	Low - high
VGSC **(predominant α subunits)**	Nav1.1, Nav1.6, Nav1.7 *Unique subpopulation express Nav1.8		Nav1.7 Nav1.8 Nav1.9

Table 1. Classification of peripheral sensory neurons

The focus of this dissertation is TTXS currents, in particular Nav1.6-mediated currents. Therefore, we used the differences of VGSCs sensitivity to TTX inhibition to isolate currents from a specific isoform in transfected DRG neurons. When examining endogenous sodium currents in DRG neurons, we use

the voltage-dependence and kinetic differences between TTXS/TTXR channels to digitally subtract the TTXR component.

VGSCs and pain

Because Nav1.7, Nav1.8 and Nav1.9 are preferentially expressed in peripheral neurons and highly expressed in typical nociceptor neurons, a great deal of attention has focused on these three isoforms. Studies of pain mechanisms in animal models, transgenic mice, and mutations identified in humans have confirmed that these three isoforms play important roles in nociception. For example, multiple studies indicated that Nav1.8 currents are substantially altered in animal models of nerve injury and inflammation (13, 87-91). A number of mutations in *SCN10A* (the gene that encodes Nav1.8) have been identified in humans with painful neuropathies (92, 93).Several of these mutations have been shown to increase sensory neuron excitability when expressed in preclinical models , helping to validate the importance of Nav1.8 in pain. In contrast, mutations in *SCN11* (Nav1.9 gene) have been identified in humans with abnormal pain sensations. Interestingly, putative gain-of-function mutations have been identified in patients with enhanced sensitivity to pain (94, 95) and patients with loss-of-pain sensations (96). Gain-of-function mutations in Nav1.7 have been identified in patients with severe neuropathic pain sensations such as PEPD and erythromelalgia (22, 97, 98). Conversely, loss-of-function mutations in Nav1.7 are associated with complete insensitivity to pain (99, 100).

However, it is unclear if Nav1.7 is crucial to all pain sensations, especially in adults. Loss of Nav1.7 from birth could predispose individuals to a complete inability to sense pain throughout life. Interestingly, animals with loss of Nav1.7 in sensory neurons do not exhibit a complete insensitivity to all pain conditions (101). This raises the possibility that specific pain conditions are independent of Nav1.7. For example, chemotherapeutic-induced pain does not appear to depend on classic nociceptors and the sensory selective isoforms Nav1.7, Nav1.8 or Nav1.9 (16, 26, 101). Instead, an atypical candidate has recently emerged, Nav1.6.

Nav1.6

Nav1.6 is an isoform that is not classically associated with sensitivity to pain, in part because its expression is restricted to peripheral sensory neurons (102-104). In addition to peripheral sensory neurons, Nav1.6 is also abundantly expressed in the adult mammalian brain and spinal cord (105). Expression has also been described in cardiomyocytes and non-excitable cells such as macrophages, microglia and Schwann cells (106-109), albeit at lower levels. Studies with Nav1.6 null mice suggest that it is important for proper neurological function and development. In particular, Nav1.6 null animals suffer from motor disorders and do not survive past three weeks (102). Mutations identified in Nav1.6 are associated with pathologies in which brain, heart and motor functions are altered (102, 107, 110-114). As such, until recently it has not been studied in

as much detail in the context of pain as other isoforms. For example, Nav1.6 is important for the development of persistent mechanical hypersensitivity mediated by localized chemogenic inflammation of the DRG, a proposed radicular pain model (115, 116). In the early stages of inflammation, increased Nav1.6 expression was positively correlated with increased spontaneous activity (14). Localized injection (near the DRG) of small interfering RNAs (siRNA) targeted to Nav1.6 in parallel with the induction of inflammation prevented the development of persistent mechanical hypersensitivity(14). Furthermore, knockdown of Nav1.6, but not Nav1.7, abolished early stage inflammation mediated increases in electrical activity(14). While resurgent and persistent currents where not examined in this study, the increased propensity of Nav1.6 to generate these currents potentially contributes to the increase electrical activity.

The role of Nav1.6 in nociception was also investigated in two rat models of neuropathic pain (spinal nerve ligation and chronic constriction injury). Localized knockdown (as previously described) of Nav1.6 prior and at the time of nerve ligation or injury greatly reduced mechanical, but not cold-dependent pain associated behaviors (15). Nav1.6 knockdown reduced the spontaneous firing and reduced the increased firing frequency in DRG neurons that is commonly observed in these models (117, 118). Interestingly, Nav1.6 knockdown also decreased abnormal neuronal outgrowth from sympathetic neurons into DRG neurons (15). It is not clear how these new sympathetic innervation in DRG neurons alter nociception. Studies suggest that sympathetic sprouting is

stimulated by ectopic activity in DRGs (119). Abnormal sympathetic contacts may in turn stimulate DRG neurons, forming a cycle that maintains chronic pain sensations (120-122). This hypothesis is supported by the fact that in these models sympathetic sprouting was highly co-localized to DRG neurons that expressed Nav1.6 (15). One possibility is that Nav1.6 mediates initial changes that may later contribute to the maintenance of chronic pain sensation and thus targeting Nav1.6 activity (such as resurgent currents) in early stages may be a viable strategy to prevent the development of neuropathic pain.

Pharmacological and genetic manipulation of Nav1.6 in a preclinical model of oxaliplatin suggest that it is a key factor in mediating oxaliplatin-induced increases in electrical activity (16, 26). Oxaliplatin is an anticancer drug used mainly to treat colorectal cancer. The acute stage of the neuropathy arises shortly after infusion and is observed with high incidence (123). Sensory, and in some cases motor symptoms, are aggravated or triggered by cold temperatures ((124)). One study showed that DRG nerve fibers from heterozygous knockout Nav1.6 mice exhibited a dampened cold dependent increase in activity to oxaliplatin exposure. DRG fibers from homozygous knockout Nav1.6 mice exhibited no increase in electrical activity to oxaliplatin exposure (26). At a behavioral level, Deuis et al, showed reversal of cold-triggered pain associated behaviors in an oxaliplatin mouse model by selectively inhibiting Nav1.6 and Nav1.1 with a high concentration GIIIA toxin(16). Consistent with these findings, Nav1.6 activity is altered in a cold dependent manner upon exposure to

oxaliplatin. While other mechanisms may also contribute to the acute painful neuropathy, Nav1.6 may prove to be a key target that would enable the patient to withstand higher doses or more frequent treatments of oxaliplatin (16, 26, 125-127).

The role of Nav1.6 is not clear in other pain pathologies. For example, in a histological study of a trigeminal nerve injury, Nav1.6 accumulates at the proximal site of the nerve injury particularly at remodeled nodes of Ranvier (128). The remodeled nodes exhibited demyelination resulting in widened gaps in the myelin sheath. The nodes of Ranvier are important for saltatory transmission of AP along the axon (129). If the nodal structure is disrupted this may result in slower nerve conduction. On the other hand, it is possible that increased expression of Nav1.6 promotes the generation of spontaneous action potentials and thus activation of nociceptive pathways. The contribution of these changes to trigeminal pain require further study.

Another pain pathology in which the role of Nav1.6 has been controversial is painful diabetic neuropathy. In animal model studies of type 1 diabetic neuropathy (early stage) where increased pain associated behavior was confirmed, Nav1.6 levels in DRG neurons have been reported to be both upregulated (130) and downregulated (131). In a Type 2 diabetes animal model, Nav1.6 is upregulated in early stages of diabetic neuropathy, which persisted, in the later stages of the disease. In the type 2 diabetes model, changes in pain-

associated behavior were positively correlated with increased Nav1.6 mRNA levels in DRG neurons (132). Further studies may provide a better understanding of the role of Nav1.6 in painful diabetic neuropathy (Type 1 or Type 2).

While there is compelling evidence for Nav1.6's role in some pain pathologies, broadly targeting Nav1.6 might result in many unwanted side effects. Therefore, targeting specific patterns of activity such as resurgent current and persistent currents might provide a more viable strategy. Auxiliary proteins that interact with Nav1.6 are potential modulators of channel activity and may result in more selective therapeutic strategies (133, 134).

Auxiliary proteins

Beta-subunits

Auxiliary subunits can associate in multiple ways with VGSCs resulting in a variety of heteromultimers that can impact VGSC properties. Beta (β)-subunits are the most commonly known auxiliary subunit (135, 136). To date four β-subunits (Navβ1–β4) have been identified. These subunits share some common features which include a single transmembrane domain, an intracellular C-terminal domain, and an extracellular N-terminal domain (135). β-subunits can associate with α subunits non-covalently (Navβ1, β3) or covalently (Navβ2, β4) (137). All β-subunits are expressed in DRG neurons although distribution can

vary between specific DRG sub-classes (133, 138). For example, Navβ4 (a subunit that has been associated with the generation of resurgent currents) is expressed at higher levels in the medium to large compared to the population of small diameter neurons (23, 138). In a similar manner Navβ1 is more abundant in medium to large population than in small diameter neurons and Navβ3 is more abundant in small diameter neurons than in the medium to large population of DRG neurons. Navβ2 is ubiquitously expressed throughout the different size classes (139).

β-subunits can alter the expression and biophysical properties of the channel such as gating, current density, persistent current and resurgent current (140). These effects can vary depending on the α-subunit expression, and cell background. For example, in small diameter neurons, deletion of Navβ2 decreased the expression of TTXS channels and increased the rate of activation and inactivation. However, TTXR channels were not significantly modulated (141). In contrast, Navβ1 deletion decreased the expression of Nav1.9 and shifted the voltage-dependence of inactivation for TTXS channels to positive potentials, which resulted in hyperexcitability of small diameter neurons (142). There is good evidence to support the potential role of β-subunits in pain sensations. For example, Navβ2 null mice exhibit reduced pain behavior responses after nerve injury (141). In contrast, upregulation of Navβ3 in sensory neurons has been associated with increased pain responses in different animal models (139, 143, 144). The role of Navβ4 in pain sensations has not been fully

explored and is one of the aims of this dissertation. Additionally, β-subunits can act as cell adhesion molecules (CAM) (145). As such, β-subunits may also be important for neuronal outgrowth(136, 146, 147). However, this potential role and implication to pain sensations has not been extensively studied in sensory neurons and will not be explored in this dissertation.

Fibroblast growth factor homologous factors

FHFs are intracellular signaling proteins expressed mainly in excitable cells. Contrary to their homologue counterparts (i.e. fibroblast growth factors), FHFs are neither secreted nor activate FGF-Receptors (148). While FHFs can interact with multiple partners including microtubules (149), kinases (150), scaffolding proteins (151, 152), nuclear factors (153) and calcium channels (154); their interaction with VGSCs (134, 148) qualifies them to be considered as VGSC auxiliary proteins. To date four FHF genes have been identified in vertebrate species (FHF1-4). Each FHF gene can result in multiple isoforms through alternative splicing and promoter usage resulting in distinct N-terminal sequences (155). Two commonly identified isoforms are FHF Type A (FHFA) and FHF Type B (FHFB). FHFBs are cytosolic. In contrast, FHFAs contain a bipartite nuclear localization signal that depending on the properties of the cell background may be active or silent (156). Both “A” and “B” isoforms of FHF have conserved core domains that enable them to bind to the C-terminus of sodium channels (157-160). FHF interaction with VGSC can alter the biophysical properties of

activation, inactivation and current density (148, 161). In particular, FHFs binding to the C-terminus of VGSC shifts the voltage-dependence of inactivation. For example, heterologous co-expression of FHF2 and FHF4 isoforms with Nav1.6 consistently shifted the voltage-dependence of inactivation to positive potentials, whereas, differential effects were observed in current density depending on isoform and cell background.

Adult DRG neurons can express a variety of FHF isoforms including FHF1, FHF2 and FHF4 (134, 162-165). FHF1 is present mainly as variant B (FHF1B), since FHF1A is downregulated in adult animals. FHF1 expression is found in membrane, cytosol and nucleus; therefore, the FHF1A nuclear signal is predicted to be active in DRG neurons. A potential interaction of FHF1B with Nav1.9 was identified. However, this interaction is not predicted to occur in sensory neurons since both proteins are not generally expressed together in the same population of DRG neurons (159, 164). FHF2 variants colocalize with Nav1.6 in different subpopulations of DRG neurons: FHF2A colocalizes with Nav1.6 in C-fibers, whereas, FHF2B colocalizes with Nav1.6 in A-fibers (162, 163). The FHF2A nuclear localization signal is predicted to be silent since expression is detected at the membrane and in the cytosol of DRG neurons, but not the nucleus. FHF3 expression has not been studied in sensory neurons in much detail (148). Overall, there has not been extensive research of FHF's contribution to pain pathologies. Two studies using cDNA arrays reported FHF2 cDNA levels were downregulated with no change in FHF1 and FHF4 after

peripheral nerve injury (165, 166). Which of the FHF2 isoforms contribute to this change and how these changes translate to changes in VGSC is not known. One possibility is modulation of resurgent currents since FHFs are proposed to modulate resurgent current generation in CNS neurons (167). Because of the gap in knowledge, modulation of resurgent current by FHF2 isoforms is one of the areas explored in this dissertation.

Overall, VGSCs subunits can form heteromultimeric complexes with a diverse combination of α subunits and auxiliary proteins. Although the focus of this dissertation is modulation of Nav1.6 currents by β-subunits and FHF isoforms, these proteins are not the only partners known to interact with VGSCs. Numerous other proteins have been identified that reportedly interact with α subunits including calmodulin, ankyrins, multiple protein kinases, Nedd4-2, CRMP2, syntrophin, contactin, annexin II light chain and KIF5 (to name a few) (168). The formation of the complexes depends on expression, colocalization and interaction between the sodium subunits and auxiliary proteins in a given cell type. As VGSC activity is modulated by interactions with auxiliary proteins, these interacting partners have the potential to be molecular regulators of excitability and nociception. In particular, we focus on how Navβ4 and FHF2 isoforms may regulate resurgent currents, VGSC inactivation and excitability of DRG neurons.

Intrinsic mechanisms of VGSC inactivation and contributions to nociception

There are several mechanisms by which VGSCs intrinsically inactivate, and major mechanisms include fast inactivation and slow inactivation (169, 170). Fast inactivation occurs within milliseconds of channel activation, as the intracellular loop between the DIII-DIV folds (inactivation particle) and occludes the cytoplasmic face of the pore (59). Recovery from fast inactivation (i.e. channel repriming) typically occurs within 10ms. Interestingly, the DIII-DIV intracellular loop is highly conserved among the nine different isoforms, including Nav1.9 despite its dramatically slower inactivation kinetics(171). VGSCs can undergo both closed-state and open-state fast inactivation, but it is not entirely clear if the mechanisms for these two are identical. Alterations in fast inactivation are believed to be important modulators of nociceptor activity and pain sensations (7). For example, recovery from inactivation is a limiting factor for sodium channel availability to respond to an additional stimulus. Indeed, local anesthetics that target sodium channel activity in peripheral fibers are believed to act largely by stabilizing fast inactivation of VGSCs in nociceptors (172).

In contrast to fast inactivation, slow inactivation is a gradual process that occurs on the time scale of seconds to minutes through conformational changes of the channel pore (169, 170). It is less clear to what extent slow inactivation contributes to alterations in nociception. Slow inactivation of Nav1.8 seems to

modulate the duration of the AP firing in nociceptive neurons in response to sustained stimulation (173). Interestingly, slow inactivation of TTX-S channels is enhanced by cold. Enhancement of slow inactivation would result in a reduction of available TTXS VGSC to respond to a given stimulus. Thus, enhancement of slow TTXS could contribute to the ability of tissue cooling to reduce some types of pain sensations. Conversely, a lack of cold sensitivity for Nav1.8 slow inactivation is believed to be crucial to cold-induced pain sensations (174). Since, Nav1.8 slow inactivation is insensitive, this isoform would remain available to generate the rising phase of the AP in a nociceptive neuron and conduct the impulse to the CNS.

Extrinsic mechanisms: Long-term inactivation and excitability

An alternate extrinsic mechanism of inactivation is long-term inactivation, which is mediated by FHFA variants through a sequence of amino acid residues in the N-terminus domain. Long-term inactivation is a distinct and competing mechanism to fast inactivation. For FHF2A, the long-term inactivation particle is proposed to be the 20 amino acid sequence: AAAIASSLIRQKRQARERE (175). This sequence is highly conserved between all FHFA isoforms. Binding of the long-term inactivation particle to the α subunit pore prolongs the recovery period of the VGSC from 10ms to 100-400ms (175). For example in a DRG-derived cell line (ND7/23), FHF2A expression causes accumulation of channel inactivation due to slowing of recovery from inactivation (163). Current clamp simulations

incorporating long-term inactivation parameters suggest that this mechanism decreases firing frequency (175). Simulation predictions were later confirmed with hippocampal neurons, which showed that FHFAs elevated AP voltage threshold and slowed AP frequency with each consecutive stimulus (176). Long-term inactivation induced by FHFAs is a recent finding and there are no reported studies examining whether it occurs in DRG neurons. However, based on CNS and heterologous cell expression systems studies we predict that increased long-term inactivation would greatly reduce neuronal excitability and firing frequency by favoring channels to remain inactive for longer periods of times. One of the aims of this dissertation is to examine if long-term inactivation regulates resurgent currents in DRG neurons and potentially modulate neuronal excitability.

Extrinsic mechanisms: Open-channel block and nociception

In addition to long-term inactivation, open channel-block is also an extrinsic competing mechanism with classic fast inactivation (177). Although binding of the open channel blocker initially terminates sodium current, rapid unbinding of the blocker at intermediate voltages (e.g., -40 mV) allows sodium current to be uncharacteristically generated during periods where the channel is usually refractory. This mechanism is known to produce atypical currents referred to as resurgent sodium currents. The present model for resurgent current generation proposes that the open channel blocker binds at positive voltages and unbinds upon membrane repolarization (Figure 2A-B) (178-180). Open channel

block bypasses fast inactivation, enabling the channel to recover faster and have a shorter refractory period (180). Therefore, resurgent currents are predicted to increase neuronal firing frequency through a more rapid channel recovery in conjunction with the depolarizing contribution during the repolarization phase of the action potential (17-19, 181, 182). The identity of the open channel blocker in sensory neurons is not completely clear. Thus, one of the aims of this dissertation is to determine the identity of the open channel blocker in sensory neurons. In particular, we examine the potential role of Navβ4.

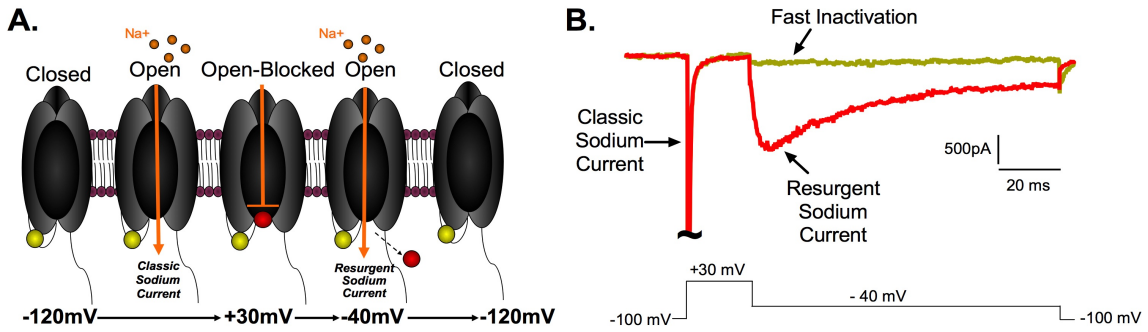

Figure 3: Resurgent currents: ***A***, Simplified Model of Resurgent Current State Transitions. As VGSC open upon depolarization (+30mV), the open channel blocker (represented as red sphere) competes with the intrinsic mechanism of inactivation (intracellular linker between DIII and DIV, represented by the yellow sphere). Binding of the open channel blocker terminates classic sodium current but prevents inactivation particle interaction; forcing the channel to remain in an open-blocked state. Membrane repolarization (-40mV) causes the blocker to unbind from the channel in the open-blocked state and resurgence of sodium conductance occurs (i.e.resurgent currents). Unbinding of the blocker allows channels to return to closed state directly or as they recover from classic inactivation. ***B***, Representative traces of a DRG neuron with resurgent sodium current (red) and no resurgent sodium current (yellow) due to channel fast inactivation with respective voltage command protocol.

Two types of resurgent currents have been identified in DRG neurons and are classified based on their kinetics (fast and slow; Figure 4). Nav1.6 is the main contributing isoform to fast resurgent currents (27). Under normal conditions fast

resurgent currents are observed in a ~50% of medium to large diameter neurons but not in small diameter neurons (19, 27). In contrast, slow resurgent currents are mediated by Nav1.8 and are mainly observed in a small-medium diameter neurons (25). The voltage-dependence of resurgent currents is different between these two currents; fast resurgent currents peak at -45mV, whereas slow resurgent currents peak at -25 mV (Figure 3B), likely reflecting differences in binding of the open channel blocker to the pores of Nav1.6 and Nav1.8.

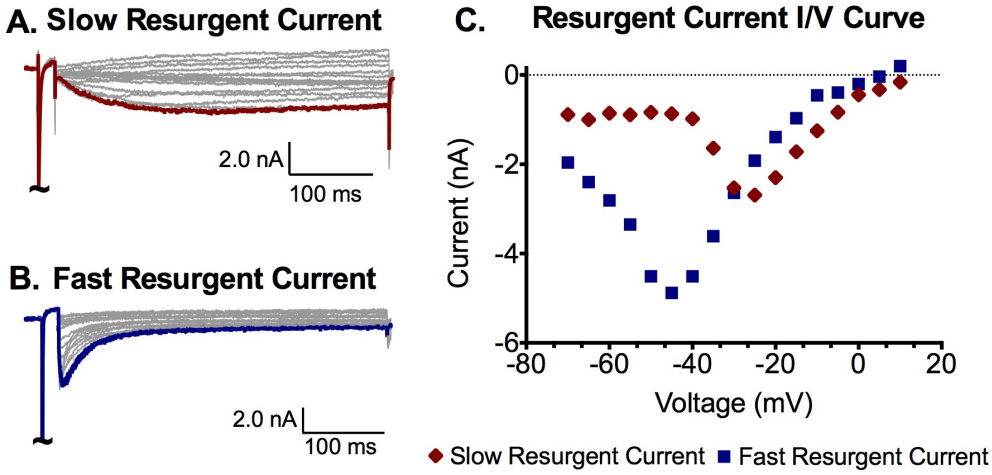

Figure 4: Slow and fast resurgent currents have different kinetic and voltage properties. ***A***, Representative trace of slow resurgent current and (***B***) fast resurgent current obtained from DRG neurons. Peak current amplitude for slow resurgent current is -25mV (red trace) and -45mV for fast resurgent current (blue trace). ***C***, Current-Voltage (I/V) curve for slow (red) and fast resurgent current (fast).

Studies of human VGSCs mutations are the first reported example of the potential contribution of resurgent currents to pain pathologies. Inherited and de-novo Nav1.7 mutations identified in patients that suffer from PEPD result in functional channels with altered inactivation properties and increased resurgent

currents (19, 21, 183-185). Recombinant expression of Nav1.7-PEPD mutant channels in sensory neurons results in hyperexcitability (22). Nav1.7 is an isoform that does not frequently generate robust resurgent currents in DRG neurons. However, PEPD mutations seem to increase the probability of binding of the open channel blocker due to delayed fast inactivation (i.e. voltage-dependence of inactivation shifted to positive potentials and in some cases accompanied by slowed rate of inactivation). DRG simulation studies of the Nav1.7-I1462T PEPD mutant showed that altered gating properties result in a decrease in the magnitude of the stimulus needed to elicit an action potential (rheobase). Interestingly, when increased resurgent currents were added into the model there was a substantial increase in the number of evoked action potentials. Therefore, resurgent currents were identified as a key factor that contributes to the increased firing frequency (19). The combined changes in rheobase and firing frequency are thought to contribute to painful sensations in PEPD patients.

Through a similar mechanism as seen with PEPD, increased resurgent currents may contribute to increased electrical activity of sensory neurons in non-inherited (acquired) pain pathologies. The first example is ATX-II induced pain. ATX-II is a VGSC site-3 neurotoxin isolated from the venom of sea anemone (Anemonia sulcata; (186)). Intradermal injection of ATX-II toxin into humans induces pain and itch that resembles those experienced by divers stung by the anemone, suggesting this component of the venom contributes to the pain

sensations perceived by the divers (23). Using the differential nerve block approach, A-type sensory fibers were identified to mediate the pain and itch sensations. In congruence with this observation, ATX-II increased TTXS resurgent and persistent currents in medium to large diameter neurons (associated with A-type fibers; see Table 1) but not small diameter neurons (23). Increased resurgent and persistent currents potentially increase the electrical activity in A-fibers. ATX-II's mechanism of action is likely due to direct interaction of the toxin with VGSCs. As a site-3 toxin ATX-II binds to the extracellular face of VGSCs and restricts DIVS4 voltage sensor movement (187). DIVS4 voltage sensor movement is important for the channel to change conformations that favor binding of the inactivation particle (188-190). Thus ATX-II indirectly impairs the fast inactivation process and potentially increases the binding probability of the open channel blocker (177). Other site-3 toxins from scorpions, sea anemones, and spiders may also induce painful sensations through a similar mechanism (191).

The second example is cooling aggravated oxaliplatin-induced acute painful neuropathy. As previously discussed, studies suggest Nav1.6 is a key factor in mediating oxaliplatin induced increases in electrical activity (16, 26). Consistent with these findings, fast resurgent currents and persistent currents increased in neurons from oxaliplatin treated animals as temperature decreased suggesting that this mechanism contributes to the cold aggravated painful episodes experienced by the patients. The increase in resurgent current and

persistent current is theoretically due to impaired fast inactivation, as evidenced by slower inactivation kinetics observed in medium to large diameter neurons exposed to oxaliplatin (26).

The third example is increased resurgent currents under inflammatory conditions. Several studies have shown that inflammatory mediators alter the firing properties of sensory neurons, which can result in hyperexcitability and contribute to persistent pain (192, 193). Inflammatory mediators can also increase the amplitude of fast and slow resurgent currents in sensory neurons (25). Both fast and slow resurgent currents likely contribute to hyperexcitability in inflammatory conditions. In particular, activation of Protein Kinase C (PKC) pathways (194, 195) is seen under inflammatory conditions and enhances Nav1.7 mediated resurgent currents in human embryonic kidney (HEK) (24).The phosphorylation site identified in this study is near the inactivation particle. Interestingly, this site is conserved in other isoforms (Nav1.1-Nav1.9), which may also be modulated by PKC. However, because modulation of VGSC activity can be cell background dependent and isoform dependent, further studies should explore if activation of this pathway results in the same effects as those seen with Nav1.7 in HEK cells.

Hypothesis and specific aims

While there is compelling evidence of the important role fast resurgent currents may play in nociception, our limited knowledge of how they are modulated in peripheral sensory neurons hinders our capability to target these currents. The goal of this dissertation is to address the gap in our knowledge and identify resurgent current modulators that may yield novel therapeutic targets. In particular, we focus on Nav1.6 mediated currents because they are the main carrier of fast resurgent currents. In addition, Nav1.6 activity is implicated in several pain pathologies, as previously discussed.

The first question we addressed was: what is the identity of the open channel blocker that mediates resurgent currents? Evidence from CNS studies suggest that it is part of the Navβ4 subunit (180, 196, 197). The Navβ4 subunit was initially identified because the cytoplasmic C-terminus contains positively charged and hydrophobic residues that have the necessary properties to act as the voltage dependent open channel blocker (180, 198). Based on this observation, a synthetic β4 peptide was designed from the C-terminus of Navβ4 (β4 peptide: KKLITFILKKTREKKKECLV; (180, 199)). The synthetic β4-peptide can reconstitute resurgent currents in cerebellar granule neurons and other cell lines that do not exhibit endogenous resurgent current. However, the role of Navβ4 is not fully understood since heterologous expression of full length Navβ4 is not sufficient to recapitulate resurgent current generation (183, 197, 200-202).

Interestingly, in DRG neurons, the incorporation of the β4 peptide into the intracellular recording solution evokes resurgent currents in neurons that do not endogenously generate them (23). In DRG neurons that endogenously generate resurgent currents, the synthetic peptide increased resurgent current amplitude (25). Therefore, we hypothesized that Navβ4 is likely the open channel blocker in sensory neurons. Thus, the first aim of this dissertation was to determine if Navβ4 regulates fast resurgent currents in DRG neurons.

The results from the first aim suggested that Navβ4 is a positive regulator of Nav1.6 resurgent currents and neuronal excitability (203). Therefore, we next explored the role of Navβ4 in pain associated behavior. In some preclinical pain models including a model of radicular pain produced by localized inflammation of the DRG (LID), abnormal spontaneous activity of sensory neurons is observed as an early event, and plays a key role in initiation and maintenance of hypersensitivity (119, 121, 204-209). In the radicular pain model spontaneous activity consists of high frequency bursting that occurs predominantly in myelinated neurons. Interestingly, in vivo knockdown of Nav1.6 strongly reduced mechanical hypersensitivity as well as spontaneous activity and repetitive firing of myelinated neurons (14). The propensity of Nav1.6 to generate persistent and resurgent currents is likely key to spontaneous and repetitive firing observed in this model. In particular, resurgent currents generated are proposed to increase the firing frequency of neurons (17-19, 182, 210). Therefore, we hypothesized that Navβ4 would be a key mediator for resurgent currents, repetitive firing and

mechanical hypersensitivity induced by inflammation in sensory neurons. As such, the second aim of this dissertation was to examine the effects of Navβ4 knockdown on resurgent currents, firing frequency, and pain associated behavior in the LID radicular pain model.

We next addressed the question: is there a negative determinant that is preventing resurgent currents from being generated in some DRG neurons? As previously discussed, resurgent currents are normally observed in a subpopulation of medium and large diameter DRG neurons that express Nav1.6 (27). The factors that permit Nav1.6 to produce resurgent current in some cells, but not in others, have not yet been identified. We hypothesized a potential mechanism for the regulation of fast resurgent currents by integrating long-term inactivation and the resurgent current model. FHFA mediated long-term inactivation is proposed to compete with VGSC's fast inactivation and in a similar manner, open channel block also competes with fast inactivation (177). Based on these observations, we propose long-term inactivation and open channel block likely compete with each other as suggested by Goldfarb (Figure 5) (211). In a HEK cell line stabling expressing Nav1.5, addition of long-term inactivation peptide reduced β4-peptide mediated resurgent currents supporting the possibility that these particles compete with each other (176). FHF2A is capable of mediating long-term inactivation and has been shown to interact with Nav1.6. FHF2A predominantly co-localizes with Nav1.6 in small diameter neurons, a subpopulation of DRG neurons that does not usually generate resurgent currents

(163). Therefore, we hypothesized FHF2A limits fast resurgent current generation in sensory neurons.

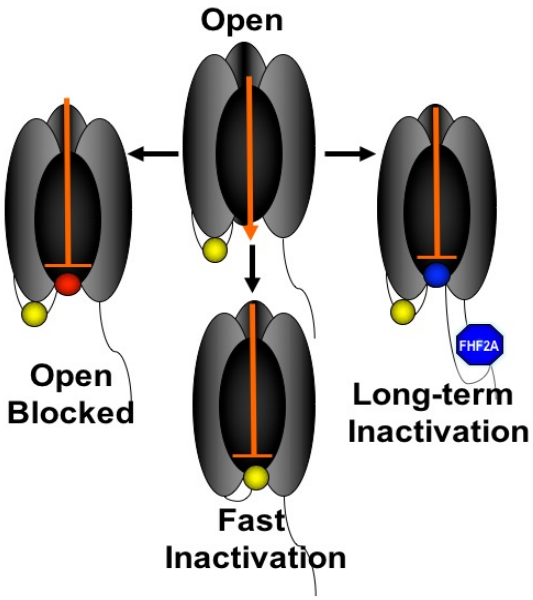

Figure 5: Schematic representation of fast Inactivation, long-term inactivation, and open channel block as competing mechanisms for the open channel state. Intrinsic fast inactivation is represented by the yellow sphere. Long-term inactivation particle is represented as a blue sphere part of the N-terminus of the FHFA protein represented as a blue octagon. Open channel blocker is represented as a red sphere.

In contrast, FHF2B does not mediate long-term inactivation, but may alter voltage-dependence and the kinetics of inactivation that may favor open channel block (148). For example, FHF4B in Purkinje neurons increased resurgent currents by slowing the rate of inactivation and shifting the voltage-dependence of inactivation to positive potentials. Thus increasing the probability of the endogenous open channel blocker to bind (167). In a similar manner, co-expression of FHF2B in several cell lines shifted the voltage-dependence of Nav1.6 to positive potentials (160, 162). Because FHF2B lacks the ability to

mediate long-term inactivation, but may retain the capability to “delay” fast inactivation, we hypothesized that FHF2B enhances the generation of resurgent currents in DRG neurons. Therefore, the third aim of this dissertation was to determine if FHF2A and FHF2B functionally regulate Nav1.6 currents, including resurgent currents in sensory neurons**.**

Overall, this dissertation focuses on Nav1.6 mediated resurgent sodium currents and the molecular determinants that potentially regulate them. The results of this research suggest that Navβ4 and FHF2B are positive regulators, whereas, FHF2A is a negative determinant of fast resurgent currents generation. The results of our work could help identify potential approaches for the study and treatment of hyperexcitability associated with increased resurgent currents such as PEPD and oxaliplatin acute-painful neuropathy among many others.

***Partial content of this chapter was adapted from a book chapter published in Elsevier. ***

Barbosa C, Cummins TR. Unusual voltage-gated sodium currents as targets for pain. In: Noskov S, French R, Simon S, editors. Sodium channels across phyla and function: Elsevier; 2016.

PART I: $Na_V\beta4$ REGULATES FAST RESURGENT SODIUM CURRENTS AND EXCITABILITY IN SENSORY NEURONS

Summary

Resurgent currents are proposed to enable high frequency firing and increased resurgent currents in sensory neurons are associated with pain pathologies. While Nav1.6 has been identified as the main carrier of fast resurgent currents, our understanding of the mechanisms that contribute to resurgent current generation is limited. Specifically, the open channel blocker in sensory neurons has not been identified. Previous studies suggest that Navβ4 mediates resurgent currents in CNS neurons. The goal of this study was to determine whether Navβ4 regulates resurgent currents in DRG neurons. Our immunocytochemistry studies show that Navβ4 expression is highly correlated with Nav1.6 expression predominantly in medium to large diameter rat DRG neurons. Navβ4 knockdown decreased endogenous fast resurgent currents in medium to large diameter neurons as measured with whole cell voltage clamp. Using a reduced expression system in DRG neurons, we isolated recombinant human Nav1.6 sodium currents in rat DRG neurons and found that overexpression of Navβ4 enhanced Nav1.6 resurgent currents. By contrast neither overexpression of Navβ2 nor overexpression of a Navβ4-mutant, predicted to be an inactive form of Navβ4, enhanced Nav1.6 resurgent current generation. DRG neurons transfected with wild-type Navβ4 exhibited increased

excitability with increases in both spontaneous activity and evoked activity. Thus, Navβ4 overexpression enhanced resurgent currents and excitability, whereas knockdown or expression of mutant Navβ4 decreased resurgent current generation. This study identified Navβ4 as an important regulator of resurgent currents and excitability in sensory neurons. As such, Navβ4 may be a potential target for the manipulation of neuronal excitability and pain sensations.

Materials and Methods

cDNA constructs

These studies used cDNA constructs of sodium channel β subunits, Navβ2 and Navβ4, which were tagged at the C-terminus to verify expression**.** To generate the rat Navβ4 C-terminal tagged construct, an ApaI restriction enzyme site was introduced into pCMV6 vector before the stop codon (Origene clone, RR210027) using Quickchange XL II Site Directed Mutagenesis kit (Agilent Technologies). The open reading frame for Navβ4 protein (NP_001008880.1) between ApaI and EcoRI was cut and inserted into mVenus N1 or pmTurquoise2 N1. Vectors, mVenus N1 and pmTurquoise2 N1, were gifts from Dr. Richard Day at Indiana University School of Medicine (Indianapolis, IN). Two constructs were generated using this approach: Navβ4-Turquoise and Navβ4-Venus. A predicted inactive form of Navβ4-tagged (Navβ4-Mt) was generated by converting lysines at position 192-193 and 197-199 to alanine using Quickchange XL II Site

Directed Mutagenesis kit. To generate the rat Navβ2-tagged construct, cDNA encoding for rat Navβ2 protein (NP_037009.1) was codon-optimized and synthesized. The *SCN2B* open reading frame was cut with NheI–AgeI and inserted into mVenus N1 vector.

To generate the Nav1.6r construct, *SCN8A* gene encoding for human Nav1.6 protein (NP_055006.1) was codon-optimized and synthesized. The open reading frame was cut with KpnI-XbaI and inserted into pcDNA3.1 vector. The resulting construct was modified by converting tyrosine 371 to serine to confer high resistance to TTX as previously described (212, 213). To isolate Nav1.6r currents, Nav1.8 was knocked down with a Nav1.8 shRNA-IRES-dsRED construct. The Nav1.8 shRNA-IRES-dsRED construct is a vector plasmid (pIRES2-dsRed) that encodes for the Nav1.8 shRNA sequence (targeting sequence, GATGAGGTCGCTGCTAAGG (214)) and an internal ribosome entry site for the translation of fluorescent protein marker dsRed (IRES-dsRED) as previously described in (19).

Cell culture

Adult rat DRG ganglia were harvested, dissociated and cultured as previously described in (19, 70, 212). Briefly, adult male Sprague Dawley rats were rendered unconscious by CO_2 exposure and decapitated. The spinal column was removed and dorsal root ganglia were harvested from the lumbar

region up to the cervical region. Excised ganglia were digested in Dulbecco' modified Eagle's Medium (DMEM, Fisher Scientific) containing collagenase (1.25mg/mL) and neutral protease (0.78mg/mL) for 45 minutes at 37°C. Ganglia were mechanically dissociated with sequentially smaller pasteur pipettes in 10% Fetal Bovine Serum (FBS, Hyclone) DMEM (Invitrogen). Glass coverslips coated with poly-D-lysine and laminin were loaded with dissociated cell suspension. After 10 minutes, cells settled and 10% FBS DMEM was added. For knockdown experiments, L4 and L5 ipsilateral dorsal root ganglia were excised from rats injected with non-targeting control or β4siRNA (see below). The above dissociation protocol and culture was followed with the exception of the digestion time, which was decreased, to 28 minutes. Cells were maintained at 37°C in a humidified 95% air and 5% CO_2 incubator. Media was changed every two days. For experiments longer than two days, such as isolated recordings of Nav1.6r from DRG neurons, 10% FBS DMEM was supplemented with mitotic inhibitors: 5-fluoro-2-deoxyuridine (50μM, Sigma Aldrich) and uridine (150μM, Sigma Aldrich). Indiana University School of Medicine Institutional Animal Care and Use Committee approved the animal protocols described.

Procedure for in vivo injection of siRNA near the DRG

siRNA ''smartpool'' consisting of four different siRNA constructs combined into 1 reagent directed against rat Navβ4 subunit (Gene ID: 315611) and non-targeting control siRNA were purchased from Dharmacon. Catalog numbers

were M-101002-01 (directed against Navβ4) and D-001210-02 (n.t. control, directed against firefly luciferase). The non-targeting control siRNAs are reported to: 1) not target any known rat genes, 2) have a minimum of four mismatches to all human, mouse and nontargeted rat genes, and 3) have minimal targeting confirmed by genome wide microarray analysis as stated by manufacturer. The four siRNA sequences directed against Navβ4 were: construct 1, GGAUCGUGAAGAAUGAUAA; construct 2, UCCAAGUGGUUGAUAAAUU; construct 3, GCAAUACUCAGGCGAGAUG; construct 4, AAACAACUCUGCUACGAUC. siRNAs were prepared for transfection using cationic linear polyethylenimine-based reagents (in vivo JetPEI, Polyplus Transfection, distributed by VWR Scientific). Aliquots of 3μL containing siRNA/Jet Pei mixture (80pmol of siRNA) were injected into each L4 and L5 DRG on one side, through a small glass needle inserted close to the DRG as previously described by (14). Three days post-injection L4 and L5 dorsal root ganglia were harvested. 16-30 hours after culture a fraction of the DRG neurons were examined by immunocytochemistry to verify knockdown and another fraction was used for whole cell patch clamp (see next sections for more details). Indiana University School of Medicine Institutional Animal Care and Use Committee approved the experimental procedure described.

Immunocytochemistry

The expression patterns of Nav1.6 and Navβ4 were studied in dissociated cultures of DRG neurons. DRG neurons were fixed after 24 hours in culture with 4% paraformaldehyde (0.1M phosphate buffer, pH 7.4) for 20 minutes and washed in phosphate buffered saline (PBS) three times. Cells were permeabilized in 1% Triton X-100 in PBS for 20 minutes at room temperature (~22°C), washed in PBS three times, blocked for 2 hours (10% normal goat serum, 0.1% Triton X-100 in PBS) at room temperature and washed an additional three times in PBS. Cells were then incubated in primary antibodies diluted in blocking solution overnight at 4°C. Primary antibodies used were anti-Nav1.6 clone K87A/10 (1:200, AB_2184197, UC Davis/NIH NeuroMab Facility) and polyclonal anti-Navβ4 antibody (1:500, #Ab80539, Abcam). After three washes, cells were incubated with secondary antibodies in blocking solution for 2 hours at room temperature. Secondary antibodies used were Alexa Fluor® 488 Goat Anti-Rabbit IgG and Alexa Fluor® 594 Goat Anti-Mouse IgG (Molecular Probes, Life Technologies) at 1:2000 concentration. Coverslips were mounted in Prolong Gold Antifade (Molecular Probes) and DRG neurons imaged using Axio Observer Z1 Widefield Microscope with a 20X objective (ZEISS Microscopy). Images were analyzed using Axio Vision software (Version 4.8.2, ZEISS Microscopy. Each cell was delineated as a region of interest and correlation was determined using the colocalization module of the software. The analysis yielded the Pearson correlation coefficient between Nav1.6 and Navβ4 fluorescence

signal and area for each cell. The data were grouped into small diameter neurons (<400μm^2) and medium to large diameter neurons (>400μm^2). The Pearson correlation coefficient was compared between small and medium to large neurons using Student's t-test. It is important to note that due to the limitations of this approach, the Pearson correlation values do not specifically represent colocalization of the proteins but rather describe the population of cells that co-express Navβ4 and Nav1.6. Additionally, images were analyzed using NIS Elements Advance Research (Nikon®) software and mean intensity for Navβ4 and Nav1.6 staining signal was determined for each cell by defining the region of interest. The data were grouped into small diameter neurons (<400μm^2) and medium to large diameter neurons (>400μm^2). The mean intensity Navβ4 and Nav1.6 staining signal was compared between small and medium to large neurons using Student's t-test.

To verify knockdown of Navβ4 protein, L4 and L5 ipsilateral DRG harvested and cultured from rats injected with non-targeting control and β4-siRNA three days after injection were examined. DRG neurons were fixed, permeabilized, blocked and treated with primary anti-Navβ4 antibody (1:500 dilution) and secondary antibody goat Alexa Fluor® 488 Goat Anti-Rabbit IgG (1:1000 dilution; Molecular Probe, Life Technologies). Coverslips were then mounted and imaged with a Nikon Eclipse TE2000-E confocal microscope with a 20X objective. Corrected Total Cell Fluorescence (CTCF) was calculated in Excel

(Microsoft) by applying measurements obtained from NIS Elements Advance Research (Nikon®) software using the following equations adapted from (215):

Equation 1

$$CTCF = \frac{Integrated}{Density} - (Area\ of\ selected\ cell\ X\ Mean\ fluorescence\ of\ background\ readings)$$

Equation 2

$$Integrated\ Density = (Mean\ Intensity\ Value\ X\ Area\ of\ the\ cell)$$

Quantification experiments were carried out independently at least three times; more than 250 cells were counted for each condition.

Nav1.6r currents in DRG neurons

The goal of these experiments was to study the modulation of Nav1.6 by β subunits: Navβ4 and Navβ2. DRG neurons express a variety of sodium channels, therefore, Nav1.6 current properties needed to be isolated. In order to achieve this we expressed a Nav1.6 construct resistant to TTX (i.e. Nav1.6r) as described in the cDNA constructs section. Endogenous TTXS currents were pharmacologically inhibited with the addition of 500nM TTX to the extracellular recording solution. DRG neurons can also endogenously express TTXR sodium currents: Nav1.8 and Nav1.9 (70, 75, 171). Nav1.8 currents are greatly decreased in culture (19, 216); additionally Nav1.8 was further decreased by co-

transfecting a Nav1.8 shRNA-IRES-dsRED construct to minimize contamination of Nav1.8 currents in the recordings. Nav1.9 currents are not observed under the culture and recordings conditions used (217, 218). β subunits studied, Navβ4-WT, Navβ4-Mt and Navβ2, were tagged at the C-terminus with fluorescent protein (mVenus or pmTurquoise2) to verify expression as described in the cDNA constructs section. No difference was observed between modulation of the biophysical properties of human Nav1.6r by co-expression of Navβ4-Turquoise compared to Navβ4-Venus, thus, these constructs were used interchangeably in experiments. As a negative control, fluorescent proteins (mVenus or pmTurquoise 2) were co-transfected instead of the tagged beta subunits. No difference was observed between modulation of the biophysical properties of human Nav1.6r by co-expression of pmTurquoise2 compared to mVenus, thus these constructs were used interchangeably in experiments. The Helios Gene Gun (Bio-Rad Laboratories) was used to transiently transfect DRG neurons as previously described in (212, 218-220). DRG neurons were co-transfected 36-48 hours after dissociation with: Nav1.6r, Nav1.8shRNA-IRES-dsRED, and tagged β subunit or control (tag only) DNA at a 2:1:1 ratio. DRG neurons that were positive for 1.8shRNA (indicated by dsRed fluorescence) and β subunit expression (indicated by Turquoise or Venus fluorescence) were selected for whole cell patch clamp. In the cells expressing Nav1.6r that were used in the final voltage clamp analysis, the peak recombinant current amplitude averaged 21.2 ± 1.7nA (n=94). Cells that expressed Navβ4 or Navβ2 localized only to intracellular compartments (based on fluorescence localization) were excluded. Cells with

residual Nav1.8 current greater than 3% of the peak current of Nav1.6r were excluded. Nav1.8 contamination can be determined for each individual cell expressing recombinant current by examining the voltage-dependence of steady-state fast inactivation. The midpoint of inactivation for Nav1.8 is much more depolarized compared to Nav1.6. The curve of the voltage-dependence of inactivation was used to determine absolute and relative amplitude for Nav1.8 and Nav1.6r (19). Whole cell patch clamp recordings in voltage clamp and current clamp mode were obtained 2-3.5 days after transfection. As an observational note, DRG neurons that were biolistically transfected were generally considered small diameter neurons based on their membrane capacitance (14.9 ± 0.6pF, n=123).

Electrophysiology

Whole cell patch clamp recordings were conducted in voltage clamp or current clamp mode at room temperature (~22°C) using a HEKA EPC-10USB. Data were acquired on a Windows-based Intel 2 Core using Patchmaster program (version 2X65; HEKA Elektronik). Fire polished glass electrodes (0.7-1.1MΩ) were fabricated using a P-97 puller (Sutter), and tips were coated with dental wax to minimize capacitive artifacts and enhance series resistance compensation. The offset potential was zeroed prior to seal formation. Capacitive transients were canceled using computer controlled circuitry; C-fast for pipette capacitance correction and C-slow for cell capacitance compensation. Voltage

errors were minimized by series resistance compensation >75%. Membrane currents were sampled at 20KHz and filtered online at 10KHz. Leak currents were linearly cancelled by P/-5 subtraction (pulse/number).

For voltage clamp recordings, the electrode solution consisted of 140mM CsF, 10mM NaCl, 1.1mM EGTA, and 10mM HEPES (adjusted to pH 7.3 with CsOH). The extracellular bathing solution contained 130mM NaCl, 30mM TEA chloride, 1mM $MgCl_2$, 3mM KCl, 1mM CaCl2, 0.05mM CdCl2, 10mM HEPES and 10mM D-glucose (adjusted pH 7.3 with NaOH). Recording solutions were adjusted using D-glucose to maintain physiological osmolarity values (310 mOsm for internal solution and 320 mOsm for external solution). Whole cell currents in voltage clamp mode were not recorded before 4 minutes after whole cell configuration for Nav1.6r isolation and before 2 minutes after whole cell configuration for endogenous sodium currents. Cells were held at a potential of -100mV.

Current-voltage (I/V) relationships were determined by steps of 50ms, from -100 to + 80mV, in 5mV increments. The voltage-dependence of activation (m_∞) was determined from sodium currents elicited with I/V protocol from voltages of -100mV to 0mV. Conductance (*G*) values were calculated at each test potential (V_m) using the following equation, $G = \frac{I}{(V_m - V_r)}$. V_r is the voltage at which the direction sodium influx reverses. The reversal potential was quantified for each neuron Goldman-Hodgkin-Katz equation (221). Data were then

normalized to the peak conductance, plotted as a function of voltage and fitted using single-phase Boltzmann distribution equation, $\frac{G}{G_{max}} = \left(\frac{1}{1+e^{\left(V_m - V_{1/2}\right)/k}} \right)$. The midpoint voltage of activation ($V_{1/2}$) and slope factor (k) were obtained for each cell.

Steady-state fast inactivation (h_∞) was assayed with 500ms pre-pulses from -130 to 5mV (in 5mV increments) followed by a 20ms test pulse to -20mV to assess channel availability. Currents at each pre-pulse were normalized to the peak current. Data of normalized currents as a function of voltage was fitted with the single phase Boltzmann distribution, $\frac{I}{I_{max}} = \left(\frac{1}{1+e^{\left(V_m - V_{1/2}\right)/k}} \right)$, from which the midpoint voltage of inactivation ($V_{1/2}$) and slope factor (k) were obtained for each cell. V_m corresponded to the prepulse voltage. Additionally, current densities were estimated for each individual recording by dividing the peak transient currents obtained from h_∞ by the membrane capacitance. For endogenous current recordings, the fast component of the sodium currents was isolated by pre-pulse subtraction of the slow component as previously described in (88). Current densities were estimated for each individual recording by dividing the peak transient currents obtained from h_∞ protocol by the membrane capacitance. Comparison of values for inactivation, activation and current density were done using ANOVA and post-hoc Bonferroni test.

For current clamp recordings, the goal was to study the activity mediated by Nav1.6r under control and Navβ4 overexpression conditions. Thus, transfected Nav1.6r was isolated by silencing the function of other voltage-gated sodium channels with TTX and Nav1.8-shRNA as described above. The pipette solution contained 140mM KCl, 0.5mM EGTA, 5mM HEPES and 3mM Mg-ATP (adjusted pH 7.3 with KOH). The extracellular solution contained 140mM NaCl, 3mM KCl, 2mM $MgCl_2$, 2mM $CaCl_2$, 10mM HEPES and 500nM TTX (adjusted pH 7.3 with NaOH). Recording solutions were adjusted using D-glucose to maintain physiological osmolarity values. Recording were obtained from the DRG neuron resting potential. No current was injected to hold the cell at a specific voltage. A cell was classified as spontaneously active if spontaneous firing was maintained for 3 or more minutes. DRG neurons that were not spontaneously active were examined for evoked activity with a series of current injections from -200pA to 1.2nA in 100pA increments. For evoked activity, the maximum number of action potentials elicited from each cell was determined as the maximum action potentials elicited from current injections from 0 to 1.2nA. For non-spontaneous neurons rheobase was determined as the minimum current injection needed to elicit an action potential response and input resistance (R) was estimated from the membrane potential (ΔV) change at -200pA current injection (I) using the equation: V=IR.

Comparison of current clamp parameters examined was done using Student t-test. Voltage and current clamp data were analyzed using Origin

(version 8, OriginLab), Fitmaster (v2X65, HEKA Electronik), Excel (Microsoft) and Prism (version 6, GraphPad) software programs.

Resurgent currents and analysis

Cells were assayed with a step protocol that initially depolarized the membrane to +30mV for 20ms from the holding potential, followed by repolarizing voltage steps from +15mV to -85 for 100ms in -5mV increments to test for resurgent currents; cells were then returned to their holding potential. Resurgent currents display unique characteristics of slow onset and slow decay along with a non-monotonic I/V relationship. Currents that did not meet these characteristics were classified as negative for resurgent currents. Based on these criteria, the percentage of DRG that were positive/negative for detectable resurgent current was quantified for each condition. The Chi-square test (X^2 test) was then used to compare distributions between conditions. Resurgent current amplitudes were measured from the leak-subtracted baseline to the peak after 3.0ms into the repolarizing pulse to avoid contamination from tail currents. Relative resurgent currents were calculated by dividing peak resurgent current by the peak transient current and expressed as a percentage of the peak transient current. The peak transient current was determined as the peak from the h_∞ protocol. For endogenous resurgent current recordings, the peak transient of the h_∞ protocol was determined after subtraction of the slow component using pre-pulse subtraction (88). For population data, relative resurgent currents were

plotted as a function of voltage. Student's t test was used to examine the statistical significance of relative resurgent current amplitude between groups.

Results

Navβ4 and Nav1.6 expression are correlated in DRG neurons.

The goal of our study was to determine if Navβ4 regulates fast resurgent currents in DRG neurons. Therefore, we examined the expression pattern of Navβ4 in rat DRG neurons and its correlation with Nav1.6 expression pattern. Immunostaining of DRG neurons in dissociated cultures shows that the Navβ4 signal is present in all size classes. However, the mean intensity of staining was three-fold higher in medium to large diameter neurons than in small diameter neurons (mean intensity $p<0.0001$: medium to large diameter, 49.5 ± 2 Arbitrary Units (AU), n=260; small diameter 17.4 ± 0.5AU, n=557). These medium to large diameter neurons, with estimated cross sectional area >400μm^2, most likely give rise to Aδ and Aβ fibers. Our results are consistent with previous studies, which found Navβ4 mRNA levels to be higher in medium to large diameter neurons relative to small diameter neurons (23, 138). Similarly, the Nav1.6 signal is observed in all size classes but exhibits more pronounced immunostaining in medium to large diameter neurons, consistent with previous observations (13, 222). The mean intensity of staining was more than two-fold higher in medium to large diameter neurons than in small diameter neurons (mean intensity

p<0.0001: medium to large diameter, 62.5 ± 2AU, n=260; small diameter 26.94 ± 1AU, n=557). Representative images are shown in Figure 6A-C. Co-expression of the two signals (Navβ4-green and Nav1.6-red) in neurons was quantified using the Pearson correlation coefficient method. Using this approach, we found that medium to large diameter neurons have a stronger correlation between Nav1.6 and Navβ4 expression than small diameter neurons (Figure 6D-E, Pearson correlation coefficient p<0.0001: medium to large diameter, 0.81 ± 0.01, n=344; small diameter, 0.18 ± 0.02, n=348).

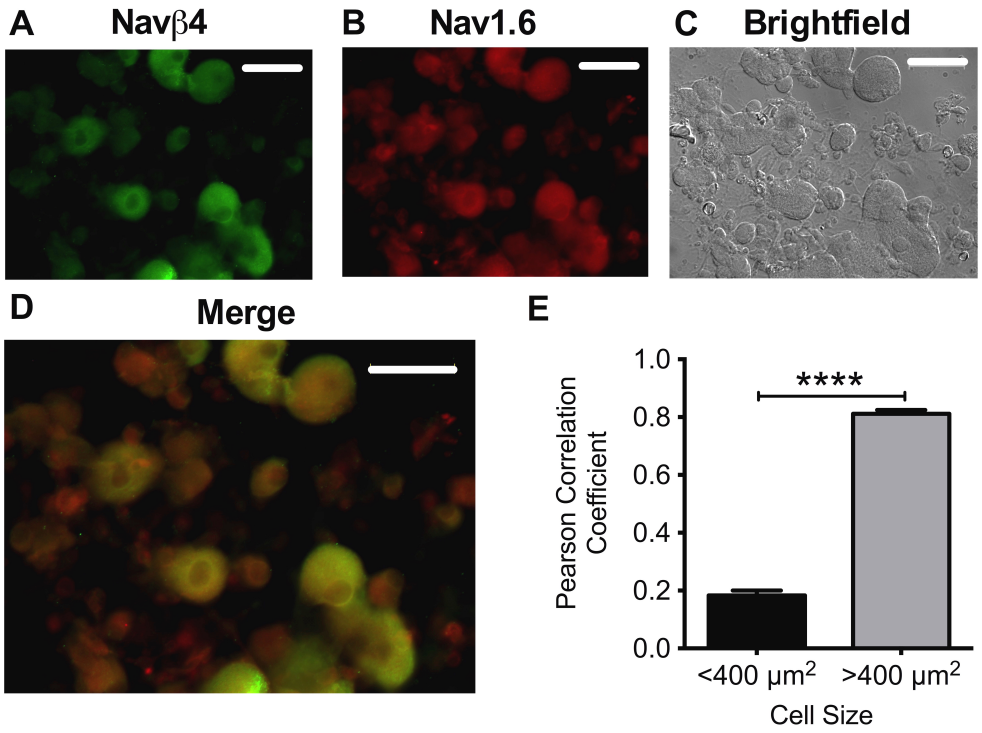

Figure 6: Expression of Nav1.6 and Navβ4 in DRG neurons. Examples of immunocytochemical staining of Navβ4 and Nav1.6 in primary cultured DRG neurons are shown in ***A*** and ***B***. Navβ4 signal is shown in green and Nav1.6 signal is shown in red with corresponding brightfield (DIC) image shown in ***C***. Merged image (***D***) shows that some DRG neurons but not all express both Nav1.6 and Navβ4. ***E,*** Strong co-expression of Nav1.6 and Navβ4 signal is mainly observed in medium to large diameter neurons (>400um^2, n=344), but not small diameter neurons (<400um^2, n=347) as indicated by the Pearson correlation coefficient. Asterisks (****) represent p <0.0001 obtained from Student's t-test. Scale bar 50μm.

Navβ4 knockdown reduces resurgent current generation.

We next investigated if Navβ4 functionally regulates endogenous fast resurgent current generation in DRG neurons. In order to address this question we used an *in vivo* knockdown approach (223). Animals received localized injections (near L4 and L5 DRG) of Navβ4-siRNAs (β4-siRNA) or non-targeting control siRNAs (n.t. control) mixed with the transfection reagent JetPEI (see Methods). Three days post injection, DRG neurons were grown in culture. After 16-36 hours in culture, DRG neurons were examined by immunocytochemistry to verify knockdown and subjected to whole cell patch clamp recordings to assess sodium current properties. Representative images of Navβ4 staining in n.t. control and β4-siRNA groups are shown in Figure 7A-B. Navβ4 levels were reduced in the β4-siRNA group by approximately 50% compared to n.t. control (Figure 7C, corrected total cell fluorescence $p<0.0001$: β4siRNA, 1.3 ± 0.10X10^7AU, n=352; n.t. control group, 2.5 ± 0.15 X10^7AU, n=264).

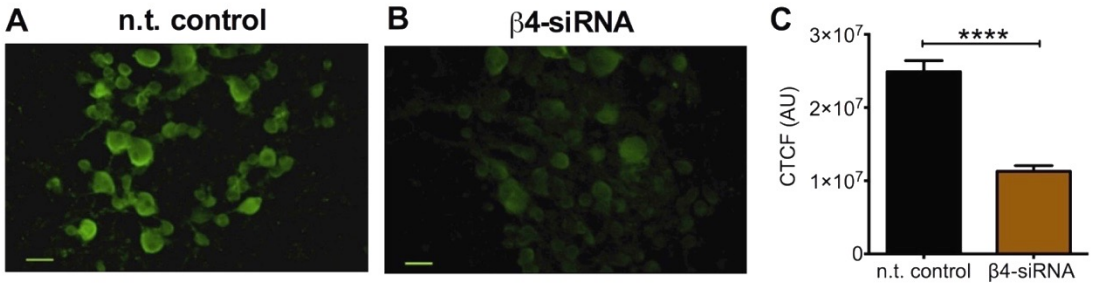

Figure 7: In vivo knockdown decreases Navβ4 expression levels. Representative images of immunocytochemical staining of Navβ4 in primary cultured DRG neurons from rats injected with non-targeting siRNA (n.t. control, ***A***) or Navβ4-siRNA (β4-siRNA, ***B***) 72 hours post injection. ***C***, Corrected Total Cell Fluorescence (CTFC) is significantly decreased in DRG neurons from rats injected with β4-siRNA (n=352 from 3 rats, $p<0.0001$) compared with n.t. control (n=264 from 3 rats). Scale bar 50μm. Asterisks (****) represent $p<0.0001$ obtained from Student's t-test.

Endogenous sodium currents were recorded from medium to large diameter DRG neurons cultured from rats treated with β4-siRNA or n.t. control. Small diameter neurons were excluded because these neurons do not endogenously generate fast resurgent current under normal conditions (23, 27), possibly reflecting the weak correlation of Nav1.6 and Navβ4 expression (Figure 5). Cell size was assessed by measurement of total membrane capacitance. In the 39 cells examined, the average cell capacitance was 60.2 ± 2.9pF and cell capacitance was not different between the groups. Capacitance is linearly correlated to the surface area of cell (224). We estimate that the average cell diameter was 60.2 μm, assuming a spherical morphology (34, 225). Therefore, the DRG neurons examined were considered as part of the large diameter population (226).

In order to determine relative changes in fast resurgent currents (which are TTXS) and exclude potential effects due to changes in TTXS channel density, resurgent current amplitudes were normalized to the TTXS peak transient current amplitudes. Resurgent currents were examined using a two-step pulse protocol described in the Methods section. Figures 8A and 8B show representative traces of endogenous fast resurgent current obtained from each group. β4-siRNA treatment significantly reduced the fraction of neurons positive for the fast resurgent current relative to n.t. control (Figure 8C, X^2 test, $p<0.05$). In the β4-siRNA group, 7 out of 20 neurons (35%) generated fast resurgent current, whereas in the n.t. control group, 15 out of 19 (79%) neurons exhibited

fast resurgent current. Moreover, the average amplitude of the fast resurgent current (expressed as a percentage of peak transient TTXS current) was significantly decreased in the β4-siRNA group compared to control (Figure 8D, n.t. control 1.79 ± 0.36%, n=19; β4siRNA 0.60 ± 0.28%, n=20).

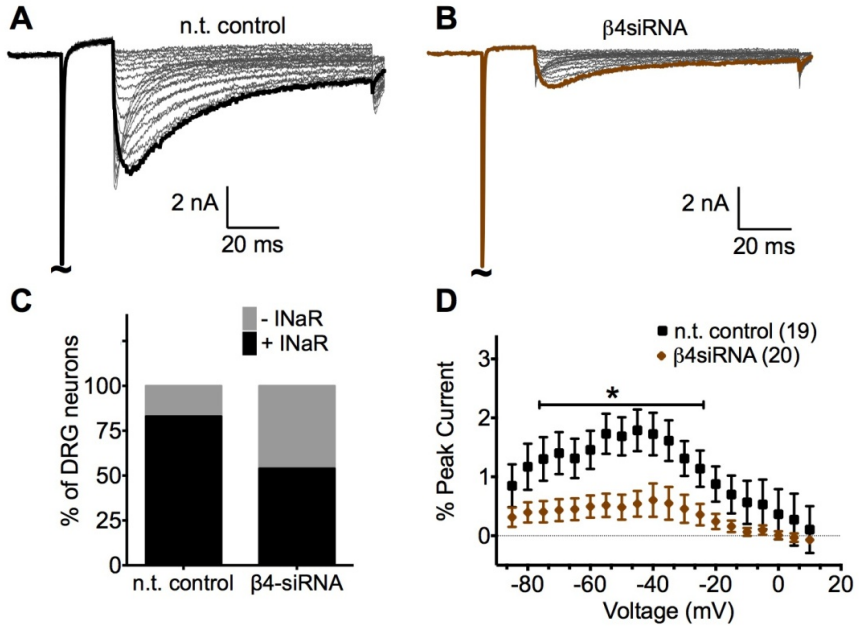

Figure 8: Navβ4 knockdown reduces endogenous fast resurgent current. Representative traces of endogenous fast resurgent currents obtained from medium to large diameter DRG neurons cultured from rats injected with n.t. control (***A***) or β4siRNA (***B)***. Peak resurgent current traces are highlighted with black (n.t. control) and brown (β4siRNA). ***C***, Compared with n.t. control, β4siRNA significantly decreased the percentage of DRG neurons that generated resurgent currents ($p<0.0005$, X^2 test). ***D***, Compared to control (black squares, n=19), Navβ4 knockdown (brown diamonds, n=20) significantly decreased resurgent current amplitude in a range of voltages. (*, $p<0.05$ obtained from Student's t-test). Summary data are mean ± SEM.

Navβ4 may also alter the voltage-dependence of activation and inactivation of VGSCs (135). For example, in cerebellar granule neurons Navβ4 knockdown shifted the voltage-dependence of inactivation to more negative potentials, whereas, activation was unchanged (197). In contrast, in heterologous expression systems, Navβ4 co-expression shifts the voltage-dependence of

activation to negative potentials but no change in inactivation is observed (198, 200, 227). Modulation by Navβ4 seems to be cell background specific. In the endogenous sodium current recordings obtained, activation was not studied due to contamination with TTXR currents that cannot be readily subtracted. However, using pre-pulse subtraction, we isolated the TTXS component of the sodium currents recorded with the steady-state inactivation protocol and compared the voltage-dependence of inactivation between groups. Navβ4 knockdown slightly shifted the voltage-dependence of inactivation to more hyperpolarized potentials. This apparent shift did not quite reach significance (Figure 9A. midpoint voltage of inactivation, p=0.052; n.t. control -67.7 ± 2.4mV, n=18; β4-siRNA -73.6 ± 2.6mV, n=20). The peak current density of transient currents, which can contain both fast (TTXS) and slow (TTXR) sodium currents, was not significantly different. However, when the TTXS component was isolated by prepulse subtraction, there was a 32% reduction in the peak current density with β4-siRNA treatment (Figure 9B-C).

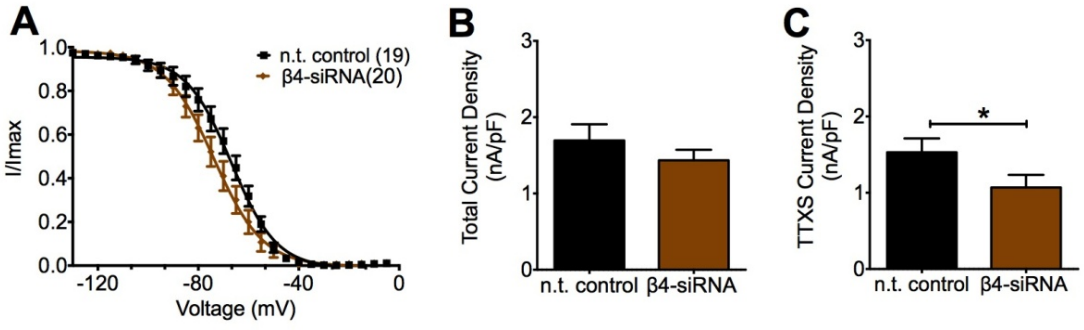

Figure 9: Inactivation properties and peak current of endogenous sodium current in control and β4-siRNA groups. ***A***, Voltage-dependence of steady-state inactivation in β4-siRNA group (brown diamonds) and n.t. control (black squares). **B**, Total peak current density is not different between non-targeting control (n=19) and β4-siRNA (n=20). ***C***, After pre-pulse subtraction the (TTXS) fast component was isolated from total peak current density. TTXS peak current density was significantly decreased in β4-siRNA relative to n.t. control (*, $p<0.05$ obtained from Student's t-test). Summary data are mean ± SEM.

Navβ4 increases Nav1.6r resurgent currents whereas Navβ2 does not.

Using recombinant expression in DRG neurons grown in culture, we studied the effects of overexpression of Navβ4 and Navβ2 on Nav1.6 mediated fast resurgent currents. Navβ4 is most homologous to Navβ2, with 35% identity (198). While they are structurally similar, Navβ2 has been proposed to lack the appropriate properties to enable open channel block (180, 199). Therefore, we hypothesized that Navβ4 overexpression would increase fast resurgent current, whereas Navβ2 would not. Interestingly, both subunits contain a free cysteine that is likely to form a disulfide bond with the α subunit (228-230). While it is not known if Navβ2 and Navβ4 compete for the same cysteine on the α subunit, if they do compete, then Navβ2 would be predicted to decrease fast resurgent current.

Dissociated DRG neuronal cultures were co-transfected with recombinant human Nav1.6 and either wild-type (WT) Navβ4 or Navβ2. We used a Nav1.6 construct (Nav1.6r) that has been mutated to be resistant to TTX (213). This allows 500nM TTX to be used to block endogenous TTXS currents without blocking Nav1.6r currents, enabling pharmacological isolation of Nav1.6r mediated fast resurgent currents (19) (see Methods section). β subunit constructs were tagged with a fluorescent protein (Venus or Turquoise) at the C-terminus to verify expression. As a control, Nav1.6r was co-expressed with fluorescent protein (corresponding to the tag). In addition, Nav1.8 was knocked

down with co-transfection of a Nav1.8 shRNA-IRES-dsRED construct to minimize contamination by Nav1.8 currents (19, 218) (see Methods section). Whole cell patch clamp recordings were obtained 2-3.5 days post-transfection.

Representative traces of Nav1.6r resurgent currents recorded with co-transfection of control (fluorescent tag), Navβ4-WT and Navβ2-WT are shown in Figure 10A-C. The percentage of transfected cells exhibiting fast resurgent current increased significantly with Navβ4-WT overexpression (Figure 10D, X^2-test, $p<0.0001$). For the Navβ4-WT group, 24 out 24 cells (100%) generated fast resurgent current, whereas in the control group 20 out of 36 cells (56%) exhibited identifiable fast resurgent currents. No difference in resurgent current frequency was observed between Navβ2 (7 out of 17 cells, 41%) and control. Overexpression of Navβ4-WT also resulted in a three-fold increase in fast resurgent current amplitude relative to control (Figure 10E, $p<0.0001$; control 0.84 ± 0.2%, n=36; Navβ4-WT 2.94 ± 0.3%, n=24). In contrast, there was no difference in fast resurgent current amplitude between the Navβ2-WT group and control (0.7 ± 0.2%, n=17).

Nav1.6r transient current recordings were analyzed for potential alterations in activation, steady-state fast inactivation and current density. Overexpression of Navβ4-WT caused a significant decrease in current density, a depolarizing shift in inactivation and no change in activation relative to control. T

Navβ2-WT overexpression only altered the slope of the voltage-dependence of activation and inactivation relative to control (Figure 11 and Table 2).

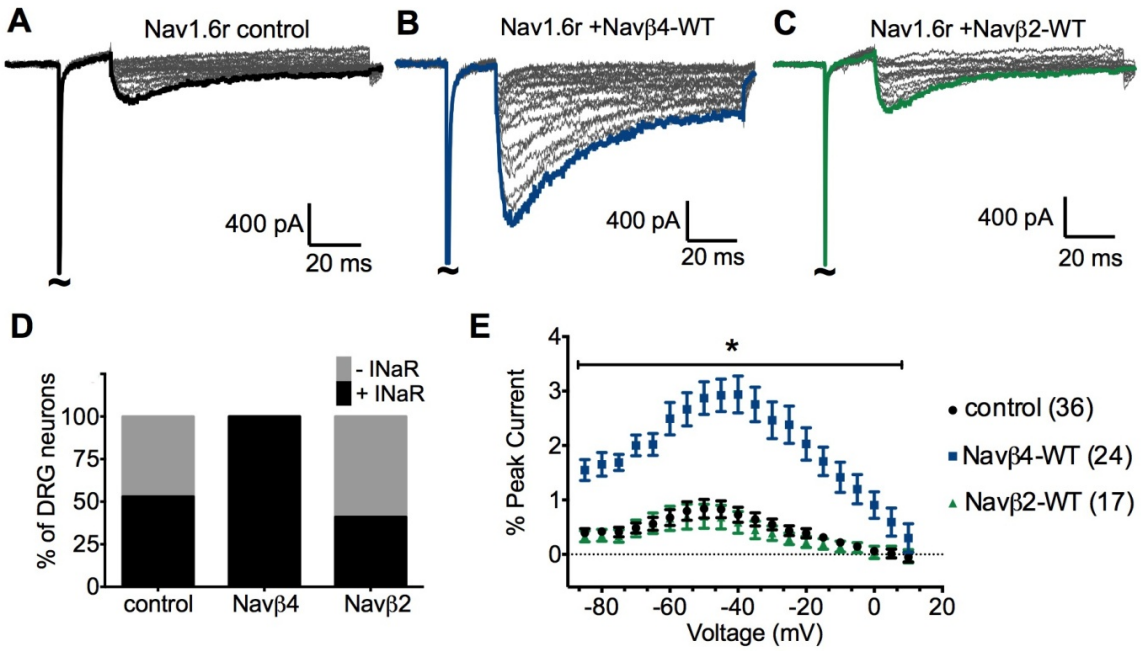

Figure 10: Overexpression of Navβ4-WT of DRG neuron increases Nav1.6r resurgent currents whereas Navβ2-WT does not. DRG neurons were transfected with Nav1.6r and Navβ4-WT, Navβ2-WT or fluorescent protein tag (control). β subunits were tagged with fluorescent protein to monitor expression. Representative traces were obtained from transfected DRG neurons and peak resurgent currents are highlighted for control (***A***, black), Navβ4-WT (***B***, blue), and Navβ2-WT (***C***, green). ***D***, Overexpression of Navβ4-WT significantly increased the percentage of DRG neurons that generated resurgent current compared to control ($p<0.0001$, χ^2 test). The percentage of DRG neurons that generated resurgent currents was not different between Navβ2-WT and control groups. ***E***, Compared to control (black circles, n=36), overexpression of Navβ4-WT (blue squares, n=24) increased resurgent current amplitude. Navβ2-WT (green triangles, n=17) did not alter resurgent current amplitude relative to control. Note that resurgent currents were normalized to peak transient currents and plotted as a function of voltage. Summary data are mean ± SEM.

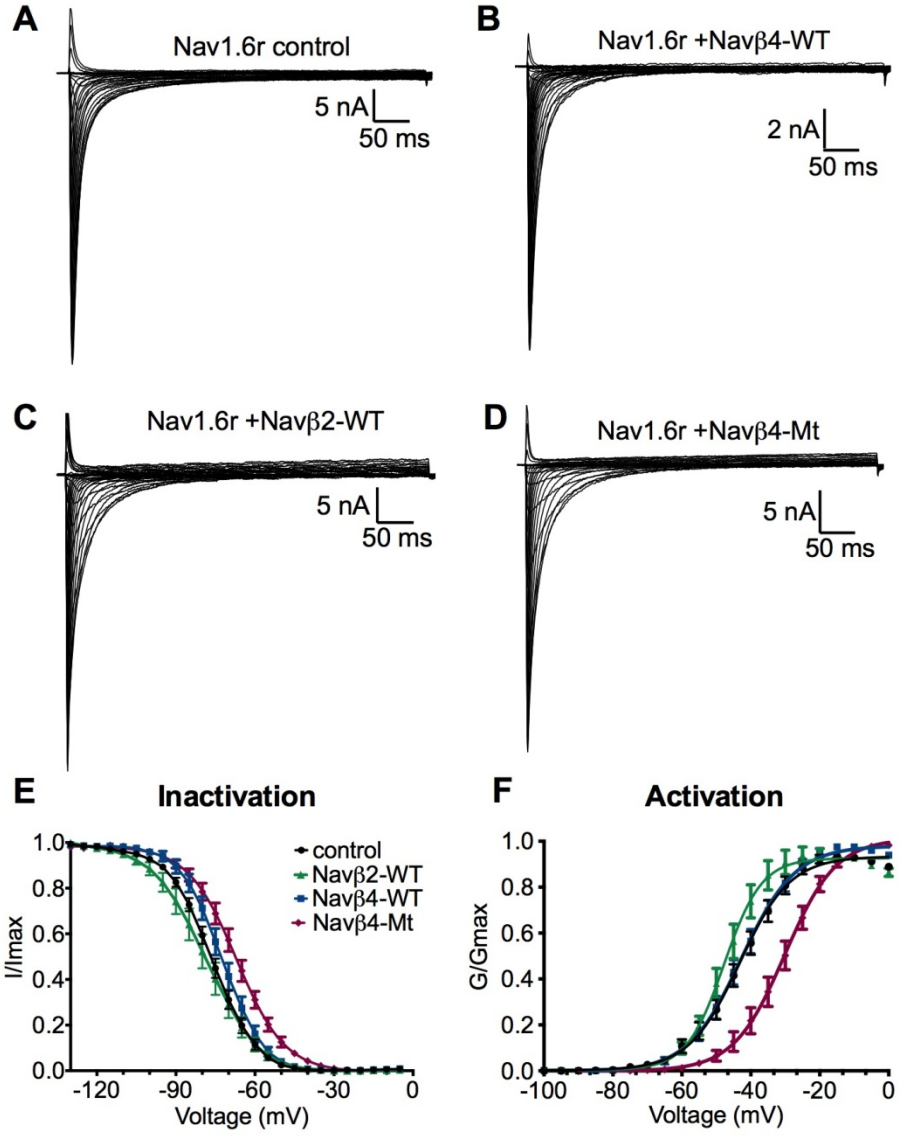

Figure 11: Biophysical properties of Nav1.6r transient current with β subunit co-expression. Representative traces of Nav1.6r transient current recordings with co-expression of fluorescent tag (control, ***A***, black circles), Navβ4-WT (***B***, blue squares), Navβ2-WT (***C***, green triangles) and Navβ4-Mt (***D***, purple diamonds). ***E***, Navβ4-WT and Navβ4-Mt co-expression significantly shift the voltage-dependence of steady-state fast inactivation to depolarizing potentials relative to control whereas Navβ2-WT does not. Navβ4-Mt shifted significantly the voltage-dependence of inactivation to more depolarized potentials relative to Navβ4-WT. ***F***, Navβ4-Mt co-expression shifts the voltage-dependence of activation of Nav1.6r to depolarized potentials relative to control and Navβ4-WT. Navβ2 and Navβ4-WT do not significantly alter the voltage-dependence of activation relative to control. Table 1 contains the values for Boltzmann fit for steady-state fast inactivation, activation and corresponding comparisons.

	Activation		Inactivation		Current Density (nA/pF)
	$V_{1/2}$ (mV)	k	$V_{1/2}$ (mV)	k	
Control	-41.1 ± 1.7	5.3 ± 0.3	-76.2 ± 1.3	6.2 ± 0.1	2.1 ± 0.4
n	34	34	35	35	36
Navβ2	-46.0 ± 2.5	4.2 ± 0.3*	-77.1 ± 2.5	7.2 ± 0.2$^{\#}$	2.3 ± 0.4
n	15	15	15	15	15
Navβ4-WT	-42.4 ± 1.8	5.9 ± 0.4	-72.3 ± 1.8*	6.0 ± 0.1	1.0 ± 0.2 *
n	24	24	21	21	24
Navβ4-Mt	-30.5 ± 1.9$^{\#,\dagger}$	5.7 ± 0.3	-67.1 ± 1.7$^{\#,\dagger}$	8.3 ± 0.5$^{\#,\dagger}$	1.3 ± 0.3
n	16	16	16	16	16

Table 2: Parameters of human Nav1.6r transient currents with β subunit co-expression. Abbreviations are; k, slope factor and $V_{1/2}$, midpoint voltage of activation or inactivation. Groups were compared to control using Student t-test. *p<0.05 (vs. control); $^{\#}$p<0.0005 (vs. control); † p<0.0005 (vs. Navβ4). Data are mean ± SEM and n is the number of cells from which recordings were obtained.

Navβ4 C-terminus is important for the regulation of Nav1.6r resurgent currents

We next investigated if the C-terminal region proposed to act as an open channel blocker (Amino Acids: 184-203; β4 peptide) (180, 183, 197) was important for Navβ4-WT positive regulation of fast resurgent currents in DRG neurons. While the β4-peptide can recapitulate resurgent currents in various cell types (199), the role of this region has not been studied in full length Navβ4. Therefore, we generated a mutant Navβ4 (Navβ4-Mt) in which five lysine residues at positions 192-193 and 197-199 were converted to alanine (Figure 12A). These residues were chosen because the positive charges at these positions are highly conserved between Navβ4 of different species and have been shown to be important for β4-peptide open channel blocker activity (180, 199). Based on peptide studies, we predicted that the C-terminus of Navβ4-Mt would not be able to bind to the sodium channel pore and therefore would not facilitate the generation of fast resurgent current.

In contrast to Navβ4-WT, overexpression of Navβ4-Mt did not enhance fast resurgent current generation. Figure 12B, shows a comparison of representative traces of Nav1.6r resurgent currents recorded after co-transfection of Navβ4-Mt, control (fluorescent tag) and Navβ4-WT**.** Overexpression of Navβ4-Mt decreased the percentage of resurgent current positive neurons (Figure 12C: % of fast resurgent current positive neurons, Navβ4-Mt, 31%, X^2-test, $p<0.0001$) relative to Navβ4-WT group but was not significantly different from control

(p=0.053). Similarly, fast resurgent current amplitude was significantly decreased relative to Navβ4-WT (Figure 12D, p<0.0001; Navβ4-Mt 0.61 ± 0.3%, n=16) but was not significantly different compared to control. Surprisingly, analysis of transient current recordings revealed that Navβ4-Mt overexpression shifted the voltage-dependence of steady-state fast inactivation and activation to positive potentials relative to Navβ4-WT and control (Figure 11 and Table 2).

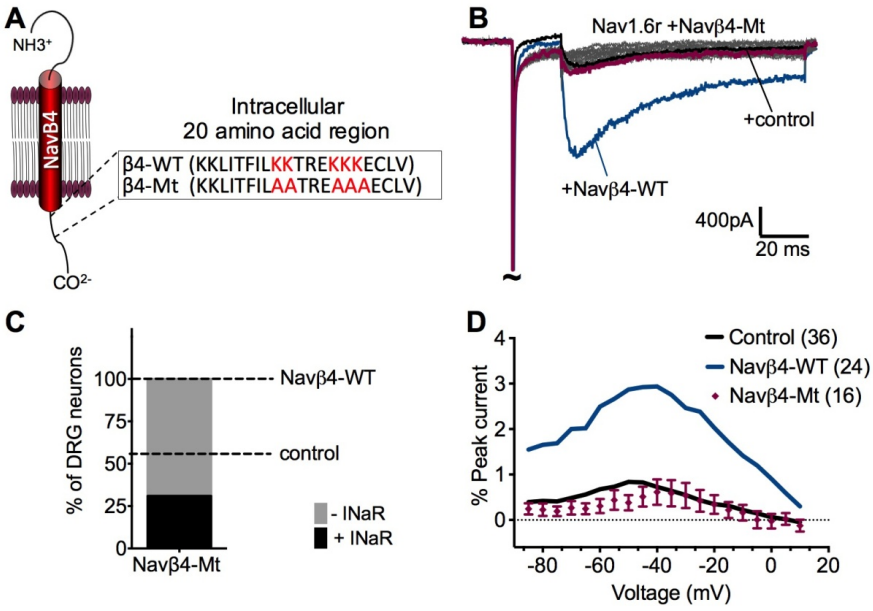

Figure 12: Navβ4 C-terminus is important for positive regulation of resurgent currents. ***A***, Illustration of Navβ4 subunit, which consists of an extracellular immunoglobulin-like domain, a single transmembrane domain, and a cytoplasmic domain. The cytoplasmic domain contains the β4 peptide sequence (amino acids 183-203) proposed to mediate resurgent currents. ***Inset***, highlights the 20 amino acids segment sequence of the cytoplasmic domainl of Navβ4 corresponding to residues 183-203 of the rat protein. Red lettering indicates five lysine residues corresponding to Navβ4-WT (β4-WT) sequence in C-terminal region that were neutralized to alanine to generate a predicted inactive form of Navβ4 (Navβ4-Mt). ***B***, Representative trace obtained from transfected DRG neurons with Nav1.6r and Navβ4-Mt. Navβ4-Mt peak resurgent current is highlighted in purple. For comparison representative trace of peak resurgent current obtained from Navβ4-WT group is highlighted in blue and control is highlighted in black. ***C***, Overexpression of Navβ4-Mt significantly decreased the percentage of DRG neurons that generated resurgent current compared to Navβ4-WT (p<0.0001, X^2 test) but not significantly different to control. ***D***, Resurgent current amplitude in Navβ4-Mt group (purple circles, n=16) was significantly decreased compared to Navβ4-WT (blue line) but not different to control. Note that resurgent currents were normalized to peak transient currents and plotted as a function of voltage. Navβ4-WT and control data are plotted as a line of the average for reference. Navβ4-Mt summary data are mean ± SEM.

Navβ4 expression increases excitability of DRG neurons

Our data demonstrate that Navβ4-WT overexpression increased Nav1.6r resurgent currents DRG neurons. Therefore, we used this as an opportunity to study the impact of increased fast resurgent current on DRG neuronal excitability. DRG neurons were co-transfected with Nav1.6r and either the fluorescent tag (control) or Navβ4-WT. Current clamp experiments were conducted on transfected neurons using Nav1.8 shRNA and TTX to block endogenous sodium currents. This approach allowed us to examine Nav1.6r dependent neuronal excitability. Spontaneous activity was observed in the Navβ4-WT group but not in the control neurons (Figure 13A-B). Four out of 15 cells (27%) transfected with Navβ4-WT were spontaneously active while zero of 15 control cells (0%) were spontaneously active. Thus, overexpression of Navβ4-WT significantly increased spontaneous activity (X^2 test, $p<0.05$). In cells that did not exhibit spontaneous activity, neuronal excitability was examined by a series of 1s current injections (-200pA up to 1.2nA in 100pA increments) from their resting membrane potentials. Representative membrane responses to current injections (evoked activity at rheobase) in control and Navβ4-WT transfected neurons are shown in Figure 13C. Navβ4 overexpression significantly increased the maximum number of evoked action potentials (Figure 13D: Navβ4-WT 4.5 ± 1.8, n=11; control 1.2 ± 0.1, n=15, $p<0.05$). The maximum number of evoked action potentials was defined as the maximum number of action potentials elicited at a given current injection from -200pA to 1.2nA for each cell. The

number of evoked action potentials was also significantly greater with Navβ4 overexpression when measured specifically at rheobase, and at 2X and 3X rheobase compared to control (Figure 14). In cells that we examined for evoked activity no significant change was observed in resting membrane potential, input resistance or rheobase (Table 3).

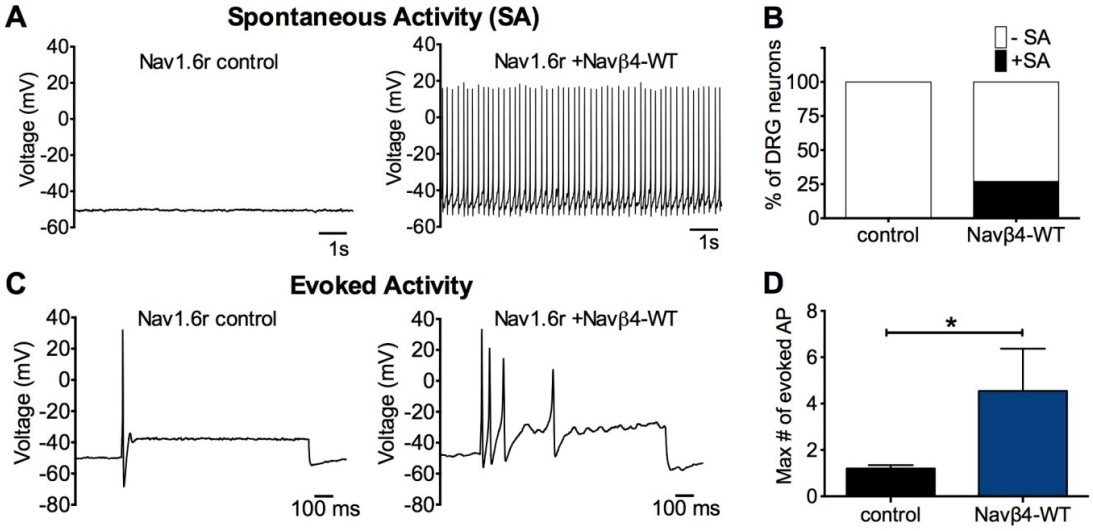

Figure 13: Overexpression of Navβ4-WT increases excitability of DRG neurons. DRG neurons co-transfected with Nav1.6r and fluorescent probe tag (control) or Navβ4-WT were examined under current clamp conditions. 500nM TTX was included in the bath solution to block endogenous TTXS channels and Nav1.8 was knocked-down with shRNA. ***A***, Representative traces of spontaneous activity recorded in control (left panel) and Navβ4 (right panel) groups. ***B***, Overexpression of Navβ4 (n=14) increased the percentage of neurons that were spontaneously active ($p<0.05$, Fisher's exact test) compared to control (n=15). Cells that were not spontaneously active were examined for evoked activity. A series of one second depolarizing current steps (0pA up 1.2nA in 100pA increments) were injected into transfected DRG neurons from their resting membrane potentials. ***C***, Representative membrane responses to current injections at rheobase in control (left panel) and Navβ4-WT (right panel). ***D***, Compared with control, Navβ4-WT overexpression significantly increased the maximum number of evoked action potential. The maximum number of evoked action potentials was defined as the maximum number of action potentials elicited at a give current injection from -200pA to 1.2nA for each cell. Data are mean ± SEM. *$p<0.05$, Student's t-test

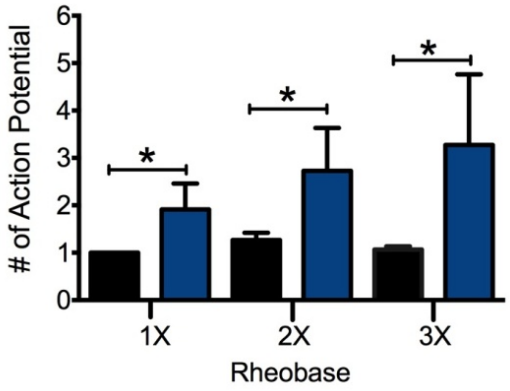

Figure 14: Navβ4 increased evoked action potentials in response to a range of stimuli intensities. Non-spontaneous cells were stimulated with 1X, 2X and 3X rheobase current injections. Compared to control (black, n=15), Navβ4-WT (blue, n=11) overexpression significantly increased the maximum number of evoked action potential at 1X, 2X and 3X rheobase. Data are mean ± SEM. *p<0.05, Student's t-test

Parameters	Control	Navβ4
Resting Membrane Potential (mV)	-47.3 ± 1.8	-48.8 ± 2.4
n	15	11
Input Resistance (MΩ)	236 ± 40	345 ± 62
n	15	11
Rheobase (pA)	287 ± 37	227 ± 38
n	15	11

Table 3: Measured excitability parameters of non-spontaneously active cells in control and Navβ4-WT groups. No significant difference was observed when groups were compared using Student's t-test.

Discussion

In this study we tested the hypothesis that Navβ4 is key to the generation of fast resurgent sodium currents in DRG sensory neurons. Five principle findings support the conclusion that Navβ4 is the primary open channel blocker underlying sensory neuron fast resurgent currents. First, Navβ4 antibody staining is highly correlated with Nav1.6 antibody staining, and this relationship is predominantly observed in medium to large neurons where endogenous fast resurgent currents are typically observed. Second, Navβ4 knockdown substantially attenuates endogenous fast resurgent sodium currents in medium to large diameter sensory neurons. Third, co-expressing Navβ4 with recombinant Nav1.6r channels in cultured sensory neurons resulted in a 3-fold increase in Nav1.6r resurgent current amplitude relative to control. Fourth, co-expressing the closely related Navβ2 with recombinant Nav1.6r channels in cultured sensory neurons did not increase Nav1.6r resurgent current amplitude relative to control. Fifth, co-expressing a mutant Navβ4 with recombinant Nav1.6r channels in cultured sensory neurons also did not increase Nav1.6r resurgent current amplitude relative to control, although other channel properties were altered. In addition, co-expressing the wild-type Navβ4 with recombinant Nav1.6r channels in cultured sensory neurons substantially increased neuronal excitability, indicating that resurgent sodium currents are important regulators of sensory neuron action potential activity.

Sensory neurons express multiple isoforms of the voltage-gated sodium channel, including TTXS and TTXR channels. In a previous study, fast resurgent sodium currents were observed in 44% of mouse sensory neurons with larger diameter somas, but were not observed in neurons from Nav1.6-knockout mice (27). In the current study, we observed a high degree of association between Nav1.6 and Navβ4 antibody staining in medium to large diameter rat neurons, 79% of which generated fast resurgent currents. Although the immunocytochemistry we performed demonstrates that expression of Nav1.6 and Navβ4 is highly correlated in medium to large diameter neurons, it cannot determine if these subunits interact. All of the neurons co-transfected with Navβ4 and Nav1.6r channels generated fast resurgent sodium currents, supporting the hypothesis that Nav1.6 and Navβ4 interact and suggesting that expression of Navβ4 might be sufficient for fast resurgent sodium current generation in DRG sensory neurons expressing Nav1.6. However, it is important to point out that the neurons typically transfected and recorded from in our sensory neuron expression system experiments are almost always small diameter sensory neurons; larger diameter neurons do not survive the culturing and transfection procedure very well. It is possible, and even likely, that in some neuronal populations there are other factors that limit the ability of Navβ4 to generate resurgent sodium currents (176).

Navβ2 co-expressed with Nav1.6r did not result in increased resurgent sodium currents. Although the percentage of transfected Navβ2 cells that

generated fast resurgent sodium currents seemed slightly lower than that of control neurons, this difference was not significant (nor was the resurgent current amplitude significantly different). Both Navβ4 and Navβ2 are thought to form a disulfide linkage with sodium channel α subunits and because of this it has been proposed that a given α subunit may associate with either Navβ4 or Navβ2, but not both (231). Although Navβ2 overexpression did not significantly reduce fast resurgent current amplitude, this does not necessarily indicate that Navβ4 and Navβ2 can simultaneously associate with α subunits. One possibility is that Navβ2 may poorly associate with Nav1.6r channels. Another possibility is that the expression of Navβ2 was not high enough to compete with endogenous Navβ4 (although expression of Navβ2 was visually confirmed with a fluorescent tag). Interestingly, expression of a mutant Navβ4 also did not reduce the baseline resurgent current amplitude significantly. However, this construct shifted the voltage-dependence of Nav1.6r channel activation and inactivation, indicating it does associate with Nav1.6r channels. This raises the possibility that there might be another open channel blocker, at least in small diameter sensory neurons, that could contribute to fast resurgent current generation independent of Navβ4 association.

Although Nav1.6 appears to be the predominant generator of fast TTXS resurgent currents in sensory neurons, it is not the only isoform that can generate resurgent sodium currents (19, 232, 233). Nav1.7 is not an efficient generator of resurgent sodium currents (19) despite having similar kinetics of open-state

inactivation to Nav1.6 (212), but mutations identified in patients with PEPD can substantially increase Nav1.7 resurgent currents (19, 24, 183). Nav1.8 channels can also generate resurgent sodium currents in DRG sensory neurons (25). Nav1.8 resurgent currents are much slower and are resistant to TTX. Although we did not examine slow TTXR resurgent currents in this study, it is likely that Navβ4 plays an important role in these currents, as inclusion of a 14-mer peptide corresponding to the proximal portion of the Navβ4 cytoplasmic C-terminus (the first 14 amino acids highlighted in Figure 12A) significantly enhanced slow TTXR resurgent currents in DRG neurons (25).

Resurgent currents are likely to be an important determinant of sensory neuron excitability. Overexpression of Navβ4 with Nav1.6r substantially enhanced both spontaneous and evoked firing in sensory neurons compared to neurons transfected with Nav1.6r and the fluorescent tag. It is important to note that the activity of endogenous sodium channels was blocked in these experiments, so the increased excitability most likely reflects enhanced Nav1.6r activity. Overexpression of wild-type Navβ4 increased resurgent current amplitude by 3-fold and shifted the voltage-dependence of inactivation by +4 mV. Based on the small magnitude of the shift in the voltage-dependence of inactivation, we predict that the 3-fold increase in resurgent currents was the major factor in the increased evoked action potential firing that we observed. Although the mutant Navβ4 did not enhance resurgent currents, it induced a pronounced shift in activation that precluded its use in the current clamp

experiments. The increased spontaneous activity observed with overexpression of wild-type Navβ4 is intriguing, but as resurgent currents are predicted to have their pronounced impact during the repolarization phase of action potentials, it is not entirely clear how the increased spontaneous activity might result from enhanced resurgent current activity. One possibility is that, in addition to enhancing resurgent currents, Navβ4 might also increase persistent sodium currents associated with Nav1.6. Although we did not examine persistent currents in this set of experiments, our work with Navβ4 knockdown in the localized inflammation of the DRG pain model (see Part II) suggests that indeed Navβ4 plays a role in modulating persistent currents. Alternatively, Navβ4 may alter other targets that contribute to spontaneous activity. For example, Navβ1 has been reported to modulate voltage-gated potassium channels in CNS neurons (234, 235). Voltage gated potassium channels are major contributors to the action potential waveform and can thus substantially modulate the excitability of neurons (236). Although we did not see a significant change in resting membrane potential or input resistance in non-spontaneously active cells, it is possible that spontaneously active neurons did exhibit these changes. Further studies would be needed to elucidate if Navβ4 modulates potassium channels in DRG neurons.

Enhanced Nav1.6 resurgent currents have been proposed to underlie the sensory neuronal excitability associated with oxaliplatin and sea anemone toxin ATX-II induced pain sensations (23, 26). Furthermore, an inflammatory mediators

applied to cultured DRG neurons increased both TTXS and TTXR resurgent currents, suggesting that resurgent currents can also play a role in inflammatory pain (25). Inflammatory mediators can increase the activity of multiple kinases and phosphorylation is known to enhance resurgent current generation (24, 237). It will be interesting to determine if chronic oxaliplatin treatment and/or chronic inflammation can induce an upregulation of Navβ4 in sensory neurons.

Nav1.6 and Navβ4 expression is highly correlated in medium to large diameter neurons. Navβ4 overexpression enhanced resurgent currents and excitability, whereas knockdown or expression of mutant Navβ4 decreased resurgent current generation. Overall, our data suggest that Navβ4 is a major contributor to fast resurgent current generation, particularly in larger diameter neurons. Although it is not clear what sensory modalities are most impacted by fast resurgent sodium currents, Navβ4 is likely to be an important determinant of sensory neuronal hyperexcitability and thus could represent an important target for the development of novel therapeutics.

***The content of this chapter was adapted from a published manuscript in Molecular Pain. ***

Barbosa C, Tan ZY, Wang R, Xie W, Strong JA, Patel RR, Vasko MR, Zhang JM, Cummins TR. Navbeta4 regulates fast resurgent sodium currents and excitability in sensory neurons. Mol Pain. 2015;11:60. doi: 10.1186/s12990-015-0063-9. PubMed PMID: 26408173; PMCID: PMC4582632.

PART II: UPREGULATION OF THE SODIUM CHANNEL $Na_V\beta4$ SUBUNIT AND ITS CONTRIBUTIONS TO MECHANICAL HYPERSENSITIVITY AND NEURONAL HYPEREXCITABILITY IN A RAT MODEL OF RADICULAR PAIN INDUCED BY LOCAL DRG INFLAMMATION

Special Acknowledgement: This study was a collaboration between Dr. Jun-Ming Zhang's laboratory at University of Cincinnati and Dr. Theodore Cummins' laboratory at Indiana University. Dr. Judith Strong and Dr. Wenrui Xie carried out the surgical procedures, behavioral tests, immunohistochemical assays, Western blotting and microelectrode experiments. C Barbosa and Dr. Zhiyong Tan carried out the surgical procedures, patch clamp experiments, immunocytochemical assays and corroborated mechanical hypersensitivity effects of LID and Navβ4 knockdown. The results were published in PAIN. Dr. Strong produced the initial draft of the manuscript, which was subsequently edited and revised by all collaborators. This part of the dissertation is adapted from the published study.

Summary

High frequency spontaneous firing in myelinated sensory neurons plays a key role in initiating pain behaviors in several different models, including a radicular model in which the rat lumbar DRG are locally inflamed. Sodium channel isoform Nav1.6, the main carrier of fast resurgent currents, contributes to pain behaviors and spontaneous activity in this radicular pain model. Resurgent

currents are generated by an alternate mechanism of inactivation that blocks the channel in the open conformation. As the blocking particle disengages during membrane repolarization, atypical sodium influx is generated and may promote high frequency firing. Our previous study suggests the regulatory Navβ4 subunit is likely the endogenous blocker in DRG neurons. Therefore, we used in-vivo siRNA mediated knockdown of Navβ4 to examine its role in this radicular pain model induced by localized inflammation. Navβ4 siRNA, but not control siRNA reduced persistent mechanical hypersensitivity induced by inflammation. Microelectrode recordings in isolated whole DRG showed that Navβ4-siRNA blocked inflammation induced increases in spontaneous activity of Aβ neurons, reduced repetitive firing and attenuated other measures of excitability. Navβ4 was preferentially expressed in larger diameter cells; inflammation of the DRG increased Navβ4 expression and this was reversed by Navβ4-siRNA, based on immunohistochemistry and Western blotting. Patch clamp recordings of TTXS currents in acutely cultured medium diameter DRG neurons showed that DRG inflammation increased transient and fast resurgent sodium currents; effects reduced by Navβ4-siRNA. Based on our findings, Navβ4 may prove to be a novel target for pain conditions that depend on hyperexcitability of myelinated neurons expressing Nav1.6.

Materials and Methods

Procedure for in vivo injection of siRNA near the DRG

The experimental protocol was approved by the Institutional Animal Care and Use Committees of the University of Cincinnati and Indiana University School of Medicine. Experiments were conducted in accordance with the National Institutes of Health Guide for the Care and Use of Laboratory Animals. Adult Sprague Dawley rats (Harlan, Indianapolis, USA) of both sexes were used as indicated.

siRNAs directed against rat Navβ4 subunit (Scn4b; gene ID 315611) and non-targeting control were designed by and purchased from Dharmacon/ThermoFisher (Lafayette, CO). The Navβ4-siRNA was siGENOME™ siRNA consisting of a "smartpool" of four different siRNA constructs combined into one reagent. Catalog numbers were M-101002-01 (directed against Navβ4) and D-001210-02 (non-targeting control directed against firefly luciferase, screened to have minimal off-target effects and at least 4 mismatches with all known human, mouse and rat genes according to the manufacturer). The sequences for the Navβ4-siRNA were: AAACAACUCUGCUACGAUC, GCAAUACUCAGGCGAGAUG, UCCAAGUGGUUGAUAAAUU and GGAUCGUGAAGAAUGAUAA. Aliquots of 3 μL containing 80pmoles of siRNA mixed with cationic linear polyethylenimine (PEI) based transfection reagent ("in

vivo JetPEI", Polyplus Transfection, distributed by WVR Scientific, USA) at a nitrogen/phosphorus ratio of 8 were injected near each L4 and L5 DRG on one side, through a small glass needle inserted close to the DRG through a small hole cut into the overlying membrane, as previously described (223). The siRNA was injected just prior to DRG inflammation in experiments using both procedures.

The surgical procedures for local inflammation of the DRG (LID) were performed as previously described (238). The L5 DRG was inflamed by depositing the immune activator zymosan (2mg/mL, 10μL, in incomplete Freund's adjuvant) over the L5 DRG via a small needle inserted into the L5 intervertebral foramen. For animals used for electrophysiological and microscopy experiments the L4 DRG was also inflamed. Naive or Sham operated animals were used as a control. Sham operated animal underwent the above procedure with the exception of zymosan injection.

Behavioral testing

Mechanical sensitivity was tested by applying a series of von Frey filaments to the heel region of the paws, using the up-and-down method (239). A cutoff value of 15 grams was assigned to animals that did not respond to the highest filament strength. A wisp of cotton pulled up from, but still attached to a cotton swab was stroked mediolaterally across the plantar surface of the

hindpaws to score the presence or absence of a brisk withdrawal response to a normally innocuous mechanical stimulus (light touch-evoked tactile allodynia). This stimulus does not evoke a response in normal animals. Cold sensitivity was scored as withdrawal responses to a drop of acetone applied to the ventral surface of the hind paw. When observed, responses to acetone or light brush strokes consisted of several rapid flicks of the paw and/or licking and shaking of the paw; walking movements were not scored as positive responses. Hypersensitivity to thermal (heat) stimuli was not examined because we have previously observed that this behavior is minimally affected in this model (116). True blinding of the experimenter to the siRNA type injected was found to be difficult due to the large effect size; however, a subset of behavioral experiments was conducted with the experimenter blind to the siRNA type, as indicated.

Electrophysiology

Microelectrode current clamp recordings in whole DRG: Intracellular recording in current clamp mode was performed at 36-37°C using microelectrodes on sensory neurons near the dorsal surface of an acutely isolated whole DRG preparation, as previously described (238). This preparation allows neurons to be recorded without enzymatic dissociation, with the surrounding satellite glia cells and neighboring neurons intact (117, 118) but does not allow voltage clamp of sodium currents. DRG were continuously perfused with artificial cerebrospinal fluid (in mM: NaCl 130, KCl 3.5, NaH2PO4

1.25, NaHCO3 24, Dextrose 10, MgCl2 1.2, CaCl2 1.2, 16 HEPES, pH=7.3, bubbled with 95% O2/ 5% CO2). Cells were classified by conduction velocity (stimulation of attached dorsal root) as follows: <1.2 m/s, C; ≥7.5 m/s, Aβ; between 1.2 and 7.5 m/s, Aδ (240). Excitability parameters were analyzed as described previously in (15). Briefly, after measurement of any stable spontaneous activity, action potential parameters were measured during the smallest depolarizing current that could evoke an action potential (rheobase). Longer suprathreshold current steps were then applied to determine the maximum number of action potentials that could be evoked, and whether subthreshold membrane oscillations (with characteristic frequencies in the range of 100–200Hz) could be evoked.

Patch clamp recordings of sodium currents: Adult rat DRG ganglia were dissociated and grown in culture as previously described (19, 25). Transient, persistent, and resurgent sodium currents were recorded from neurons after 14–28 hours in primary culture. Neurons were dissociated from sham or inflamed (after 3 days) L4 and L5 DRGs or 3 days after siRNA injection and DRG inflammation. The extracellular solution consisted of (in mM): 130 NaCl, 30 TEA chloride, 1 MgCl2, 3 KCl, 1 CaCl2, 0.05 CdCl2, 10 HEPES, and 10 Dextrose, pH 7.3. The pipette solution contained (in mM) 140 CsF, 10 NaCl, 1.1 EGTA, and 10 HEPES, pH 7.3. Resurgent currents were recorded using a two-voltage step protocol. A 20ms, +30mV voltage pulse was first used to inactivate transient sodium currents. This was followed by a series of repolarizing pulses to elicit

resurgent currents. The repolarizing pulses were 450ms long, from +5 to -85mV in 5mV steps. Resurgent currents were measured as the peak inward current elicited during the repolarizing step. Persistent currents were measured during the last 20ms of the 450ms repolarization pulses. Transient current amplitudes were measured using a steady-state inactivation protocol that depolarized the membrane to 0mV from 500ms pre-holding at voltage levels from -130 to -5mV, with an increment of 5mV. Peak transient currents were measured from the pre-holding level of -110 mV. Peak transient, resurgent and persistent currents were normalized to cell capacitance and expressed as current density. Voltage-dependence of inactivation and activation of the transient current was determined as in reference (19); values of $V_{1/2}$ (voltages at which activation or inactivation was half maximal) are reported. Cells used for recording had diameters of 35–45μm. The median capacitance was 53.8pF with 25th–75th percentile falling in the range 45–65pF.

Immunohistochemistry

DRG sections were cut at 40μm on a cryostat after fixation in 4% paraformaldehyde in 0.1M Phosphate Buffer and 4% sucrose. The primary Navβ4 antibody was from Alomone (Jerusalem, Israel, catalog ASC-044) used at a dilution of 1:150. The secondary antibody conjugated to Alexa Fluor 594 (Invitrogen, Carlsbad, CA) was used at a dilution of 1:1000. Images from multiple sections of each DRG were captured under an Olympus BX61 fluorescent

microscope using Slidebook 4.1 imaging acquisition software (Intelligent Imaging Innovation, Denver, CO). To measure the expression of Navβ4 in the DRG neurons, the summed intensities of the Navβ4 signal were measured and normalized by the cellular area in each analyzed section to give an intensity ratio. In all immunohistochemical experiments, data from at least four animals were included to control for interanimal variability. For experiments examining the effect of Navβ4 knockdown on Nav1.6 expression, the procedure was the same as described above except that the polyclonal antibody against Nav1.6 was used (Alomone; catalog ASC-009, used at 1:100 dilution). For quantification of immunohistochemical data, sections from different experimental groups were examined in a side-by-side protocol with identical display parameters.

Immunocytochemistry

To verify knockdown of Navβ4 protein in dissociated DRG cultures under the conditions used for patch clamp measurements of sodium currents, L4/L5 ipsilateral LID DRG ganglia were harvested and cultured from rats injected with non-targeting control or Navβ4-siRNA three days after siRNA injection and DRG inflammation. DRG neurons were fixed after 24 hours in culture with 4% paraformaldehyde (0.1M phosphate buffer, pH 7.4) for 20 minutes and washed in phosphate buffered saline (PBS) three times. Cells were permeabilized in 1% Triton X-100 in PBS for 20 minutes at room temperature (~22 °C), washed in PBS three times, blocked for 2 hours (10% normal goat serum, 0.1% Triton X-

100 in PBS) at room temperature and washed an additional three times in PBS. Cells were then incubated with primary antibody against Navβ4 (#Ab80539, Abcam, Cambridge, MA, USA) diluted 1:500 in blocking solution at 4°C overnight. After three washes, cells were incubated with secondary antibody diluted in blocking solution 1:1000 (Alexa Fluor® 488 Goat Anti-Rabbit IgG, Molecular Probes, Life Technologies, Grand Island, NY, USA) for 2 hours at room temperature. Coverslips were mounted unto microscope slides with Prolong Gold Antifade (Molecular Probes). Cells were imaged with Nikon Eclipse TE2000-E microscope. Images were analyzed with NIS Elements Advance (Nikon®) software.

Western blot analysis of Navβ4

DRGs were isolated and homogenized in ice-cold lysis buffer (50mM Tris pH 7.4, 5mM EDTA pH 8), 1% Triton X-100 and protease inhibitor cocktail (Complete, EDTA-free, Roche, Life Sciences, Indianapolis IN USA) followed by centrifugation at 57,000 x g at 4°C for 60 minutes. Samples (20μg of total protein per lane) were subjected to sodium dodecyl sulfate polyacrylamide gel electrophoresis (SDS-PAGE) running in NuPAGE MES SDS running buffer (Invitrogen). Reducing conditions were used to break covalent bonds to the α subunits (198, 228). Electrophoresis was followed by electrophoretic transfer to nitrocellulose membrane (Bio-Rad, Hercules, CA, USA) in Tris-glycine-SDS transfer buffer. Nonspecific binding sites were blocked with 5% nonfat dry milk in

Tween (Bio-Rad; 0.1%)–phosphate-buffered saline at room temperature for 1 hour. The rabbit antibodies to Navβ4 (1:400, Alomone) and to β-Actin (1:2000, Abcam) were applied to the blot followed by incubation with immunopure peroxidase conjugated goat anti-rabbit IgG (H+L) (1:20,000, Pierce, Rockford, IL). The signal was detected using a ChemiDoc-It system controlled by VisionWorksLS software version 7 (UVP, Upland, CA). After background subtraction, signals in the Navβ4 band were normalized to the intensity of the β actin bands.

Data analysis

Behavioral time course data were analyzed using two-way repeated measures ANOVA with Bonferroni post-hoc test to determine on which days experimental groups differed. For electrophysiological, Western blot, and immunohistochemical data, comparison of values between different experimental groups was done using nonparametric methods for data that did not show a normal distribution based on the D'Agostino and Pearson omnibus normality test. The statistical test used in each case is indicated in the text, or figure legend. Significance was ascribed for $p<0.05$. Levels of significance are indicated by the number of symbols, e.g., *, p=0.01 to <0.05; **, p=0.001 to 0.01; ***, $p<0.001$. Data are presented as the mean ± S.E.M.

RESULTS

Navβ4 knockdown reduces mechanical hypersensitivity in the DRG inflammation model

Previous studies have shown that local inflammation of the L5 DRG (LID) causes pronounced mechanical hypersensitivity in the ipsilateral hindpaw as measured by the von Frey test. LID also produces mechanical allodynia as measured by the withdrawal responses to stroking the paw with a light cotton wisp; and cold allodynia as measured by increased withdrawal to acetone stimuli (116, 238, 241). These behaviors are observed as early as postoperative day (POD)1. The mechanical hypersensitivity is maintained for at least 4 weeks at which point the other behaviors are beginning to resolve. In the present study, similar results were obtained when non-targeting (n.t.) control siRNA was injected into the L4 and L5 DRG just prior to DRG inflammation (Figure 15). In the control group, the von Frey threshold differed from baseline on all tested days. However, in animals injected with siRNA directed against Navβ4, the ipsilateral mechanical hypersensitivity (von Frey test) was significantly reduced compared to control siRNA on all days tested, and differed from baseline only on POD1. The ipsilateral mechanical allodynia responses (cotton wisp test) were also significantly reduced from the control siRNA group on most days (Figure 15B), and were significantly different from baseline only on POD1. In contrast, cold allodynia (acetone test) induced by DRG inflammation was not significantly

reduced by Navβ4-siRNA, either ipsilaterally (Figure 15C) or contralaterally. As previously reported in this model (14, 238), contralateral von Frey threshold reductions in the control siRNA group were very modest, with the lowest average value observed on any day being 11 grams. In the Navβ4-siRNA group, contralateral thresholds differed from baseline only on POD1. No animals in either group showed contralateral responses to the mechanical allodynia test on any day (data not shown). As shown in Figure 15, Navβ4-siRNA had no effect on baseline behaviors prior to implementation of the pain model; however, the tests used reached cut-off values and would not have detected increased thresholds.

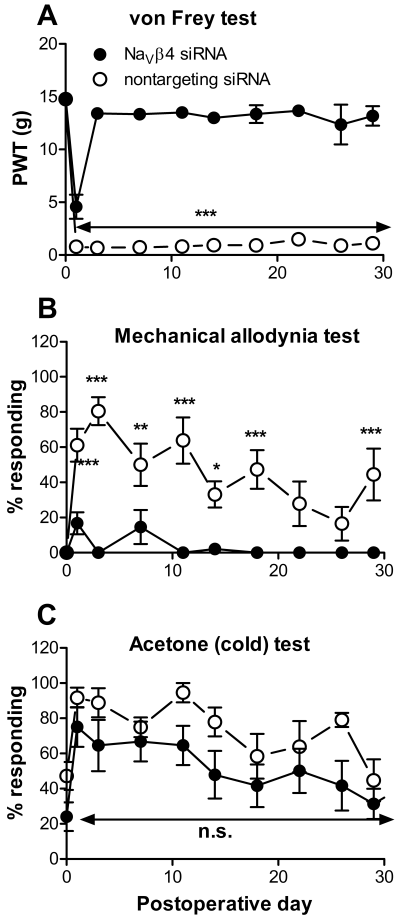

Figure 15: Effects of Navβ4 knockdown on pain behaviors elicited by local inflammation of the L5 DRG. Baseline measurements plotted on post operative day (POD) 0 are the average of 2 measurements made 3-5 days prior to inflammation of the L5 DRG and injection of siRNA directed against Navβ4 or non-targeting control siRNA on POD0. The behavioral data was obtained from the ipsilateral paw of the animals. ***A***, Mechanical threshold measured by the von Frey test was significantly reduced for the duration of the experiment in the n.t. injected animals. In Navβ4-siRNA injected animals the threshold differed from the n.t. animals on all days except baseline. ***B***, Mechanical allodynia, measured as withdrawal to stroking the paw with a fine cotton wisp, was never observed prior to DRG inflammation (average baseline plotted on POD0), was increased by DRG inflammation in n.t. siRNA injected animals, and was significantly less on most days in Navβ4-siRNA injected animals. In Navβ4-siRNA injected animals the decreased threshold was significantly different from baseline only on POD1; in n.t injected animals the decreased threshold differed significantly from baseline on all POD except POD 14 and 22. ***C***, Cold allodynia, measured as withdrawal to a drop of acetone placed on the paw, was increased by DRG inflammation but not significantly affected by Navβ4-siRNA. N=6 n.t. and 8 Navβ4-siRNA injected male rats. *, $p<0.05$; **, $p<0.01$; ***, $p<0.001$, significant difference between the two groups (two-way repeated measures ANOVA with Bonferroni posttest). Differences from baseline on later POD within each group discussed above were tested using one-way ANOVA with Dunnett's posttest. The data presented in the figure were not obtained with blinding of the experimenter; however, the findings about the initial time course of pain behaviors were confirmed in a separate experiment in which the experimenter was blinded to the siRNA status of the animals, n=4 per group, data not shown.

Immunohistochemistry and Western blotting confirm Navβ4 knockdown by siRNA and upregulation by DRG inflammation

Immunohistochemical staining for Navβ4 was performed in DRG sections from normal animals, and on POD4 after DRG inflammation and injection of non-targeting or Navβ4-siRNA. The immunohistochemical staining of Navβ4 showed that DRG inflammation upregulated Navβ4 and this upregulation was blocked by Navβ4-siRNA (Figure 16A-D) This result was confirmed by Western blotting (Figure 16E). A representative Western blot is shown in Figure 16F. Navβ4 protein signal (24kDa) was normalized to actin protein signal (42kDa). In a separate set of immunohistochemical experiments, examination of sections from both normal and inflamed DRGs showed that Navβ4 was not as highly expressed in the cells with the smallest cross-sectional areas. The average cell area of Navβ4-positive cells was larger than that of Navβ4-negative cells in both conditions, and there were no striking changes in the cell size distribution after DRG inflammation. The inflammation-induced increase in staining for Navβ4 seemed to be primarily due to an increase in the intensity per cell rather than an increase in the percentage of cells expressing Navβ4; 62% of all cells scored in normal DRG were Navβ4-positive (61.5% ± 2.2%, based on average values from 4 animals), while 67% of all cells scored in inflamed DRG were Navβ4-postive (67.7% ± 3.4%, based on average values from 4 animals). This apparent increase in percentage was not significant when analyzed based on the average animal values ($p=0.17$, t-test) and could not account for the overall 64%

increased average intensity in inflamed compared to normal DRG shown in Figure 16D. Navβ4 has also been observed in peripheral axons and nodes (228). The data in Figure 16A-D were obtained from cellular regions of the DRG sections, however, Navβ4 was also observed in axonal regions, albeit at lower intensities. These regions also showed increased staining after DRG inflammation and reduced staining after Navβ4-siRNA injection (data not shown).

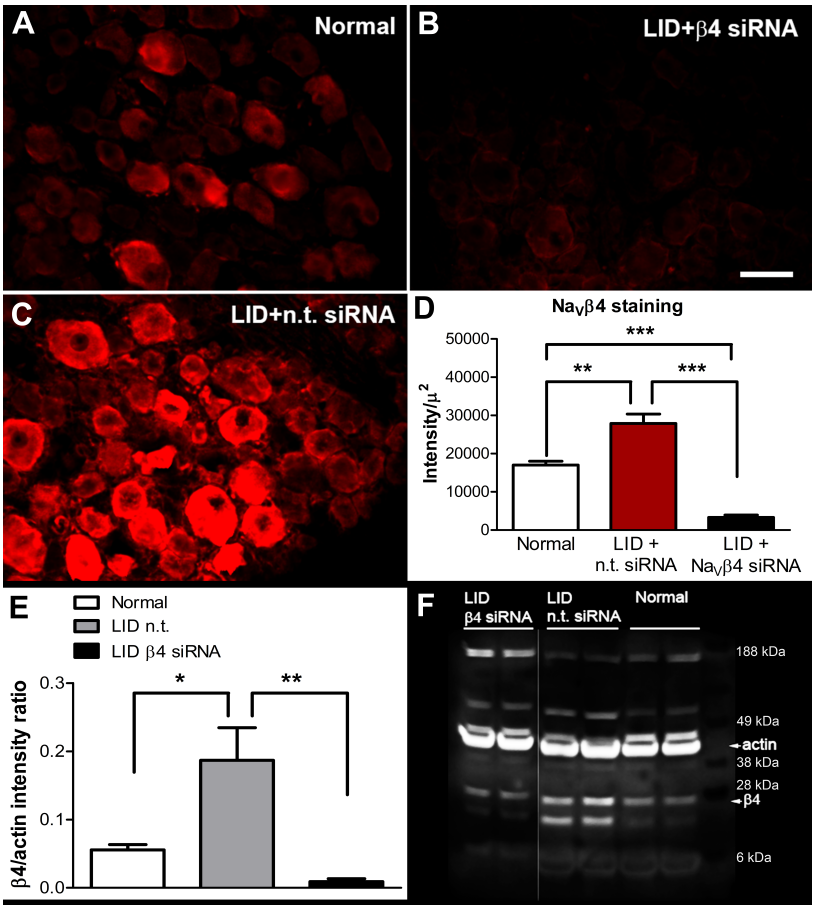

Figure 16: Immunohistochemical and Western blot detection of Navβ4. Sample sections stained for Navβ4 are shown from normal DRG (***A***), and DRG 4 days after DRG inflammation ("LID") and injection of either Navβ4 (β4 siRNA,***B***) or non-targeting (n.t.) siRNA (***C***). Scale bar, 50μm. ***D***, summary data of Navβ4 intensity normalized to cellular area in DRG sections. **, p<0.01; ***, p<0.001significant difference between the indicated groups (one-way ANOVA with Tukey's posttest). n=4 animals per group, 19 to 34 sections per animal. Graph and statistical analysis are based on the animal averages. ***E***, Summary data of the ratio of Navβ4 intensity to actin intensity from Western blot analysis of the same 3 experimental groups. Actin always appeared as a double band and both lanes were included in the actin measurement. *, p<0.05; **, p<0.01; significant difference between the indicated groups, one-way ANOVA with Tukey's posttest. n=6 samples per group. ***F***, Two sample lanes from each experimental group. Some intervening lanes from a different experiment run on the same gel have been removed. Male and female animals were used for these experiments.

$Na_V\beta4$ knockdown reduces $Na_V1.6$ expression

The Navβ subunits can also regulate localization and trafficking of the α subunits. We therefore examined the effect of Navβ4-siRNA on expression of Nav1.6 in DRG sections. DRG were inflamed and injected with siRNA directed against Navβ4 or the non-targeting (n.t.) control construct. Four days later DRGs were fixed and sectioned and stained for Nav1.6. As shown in the examples in Figure 17, the expression of Nav1.6 was higher in n.t. siRNA injected DRG (Figure 17A-C) than in Navβ4-siRNA injected DRG (Figure 17D-F). Summary data from 4 animals per group, 104 sections per animal, showed that Nav1.6 was 1.6 ± 0.18 times higher in n.t. siRNA injected DRG than in Navβ4-siRNA injected DRG (ratio t-test based on animal averages, p=0.002).

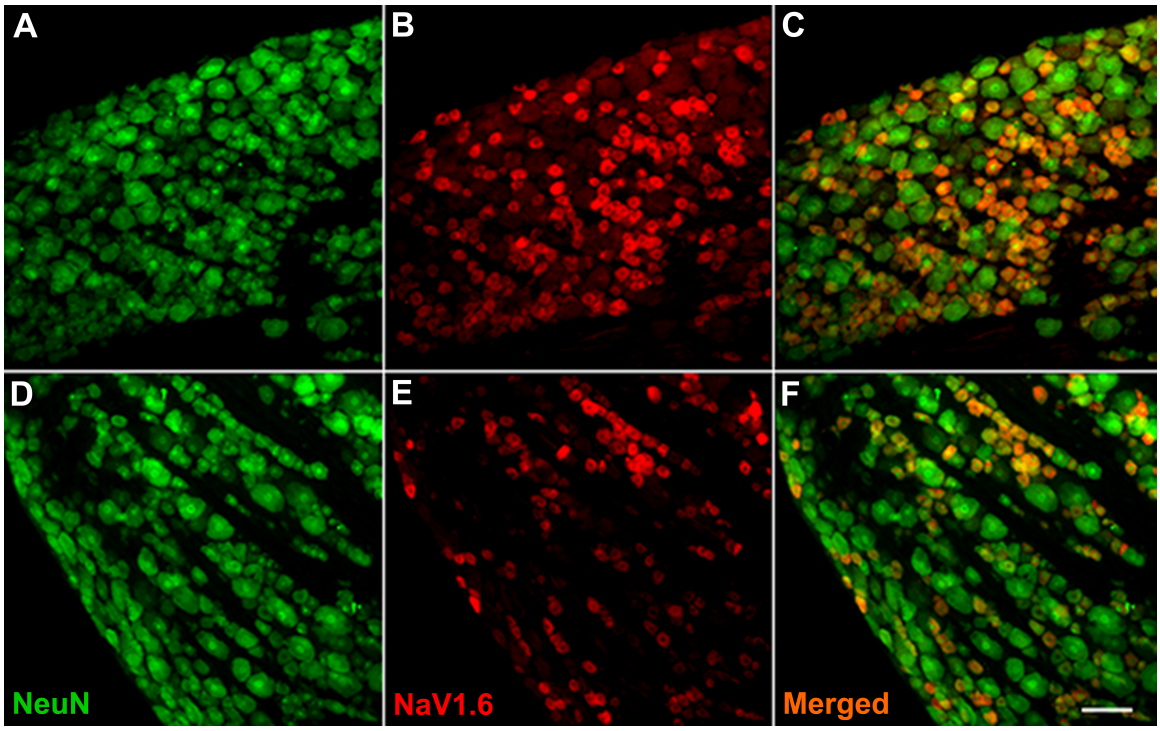

Figure 17: Effect of Navβ4-siRNA on immunohistochemical detection of Nav1.6 in DRG sections. Sample sections are shown from DRG 4 days after DRG inflammation and injection of either non-targeting siRNA (***A***, ***B***, ***C***) or Navβ4-siRNA (***D***, ***E***, ***F***). Scale bar, 100μm.

Navβ4 knockdown reduces hyperexcitability induced by DRG inflammation in Aβ sensory neurons.

It had been previously shown by our colleagues that DRG inflammation leads to marked neuronal hyperexcitability and spontaneous activity of myelinated Aβ neurons in the inflamed DRG, as measured on POD 3-4 in the isolated whole DRG preparation with sharp electrode recording Methods (238). In addition, it was also shown that injecting siRNA directed against Nav1.6 restored many of these hyperexcitability parameters towards normal values(14). In our collaboration, we observed a similar reduction of inflammation-induced hyperexcitability of Aβ myelinated cells by injecting Navβ4-siRNA at the time of DRG inflammation (Figure 18). Spontaneous activity induced by DRG inflammation was restored to normal levels by the Navβ4-siRNA. The LID-induced decrease in rheobase was partially normalized by the Navβ4-siRNA (Figure 18B); a similar result was observed when spontaneously active cells, with rheobase defined as zero, were excluded from the calculation (data not shown). The observed changes in rheobase did not reflect changes in input resistance (16.3 ± 0.1 MΩ, 16.0 ± 0.7 MΩ, and 17.0 ± 0.7MΩ in normal + n.t. siRNA, LID + Navβ4-siRNA , and LID + n.t. siRNA, respectively; no significant differences between groups per Kruskal-Wallis test with Dunn's post-test). DRG inflammation caused a small depolarization of the resting membrane potential (from -66.2 ± 0.5 mV to -62.1 ± 0.7mV) that was partially normalized by Navβ4-siRNA (to -64.1 ± 0.5mV; Figure 18D). Action potential duration was slightly increased by LID but

not affected by Navβ4-siRNA (Figure 18C). Action potential threshold did not differ between the three groups. Parameters particularly associated with resurgent and persistent currents, such as the ability to fire repetitively or show subthreshold membrane oscillations in response to long suprathreshold current injections, were also increased by DRG inflammation and largely normalized by Navβ4 knockdown (Figure 18E-F). The number of Aδ cells observed in these experiments was relatively small (26 in the control group, only 8 in the LID + non-targeting siRNA group, and 45 in the LID + Navβ4-siRNA group); few significant differences in the electrophysiological parameters were observed and none of the Aδ cells showed spontaneous activity (data not shown). In contrast, excitability parameters of C cells were much less affected by DRG inflammation or Navβ4-siRNA. Spontaneous activity was low or zero in DRG neurons treated with Navβ4-siRNA or non-targeting siRNA and there were no significant differences between the groups. Rheobase, membrane potential, and the ability to fire repetitively were not affected by DRG inflammation or by Navβ4-siRNA (data shown in (242)).

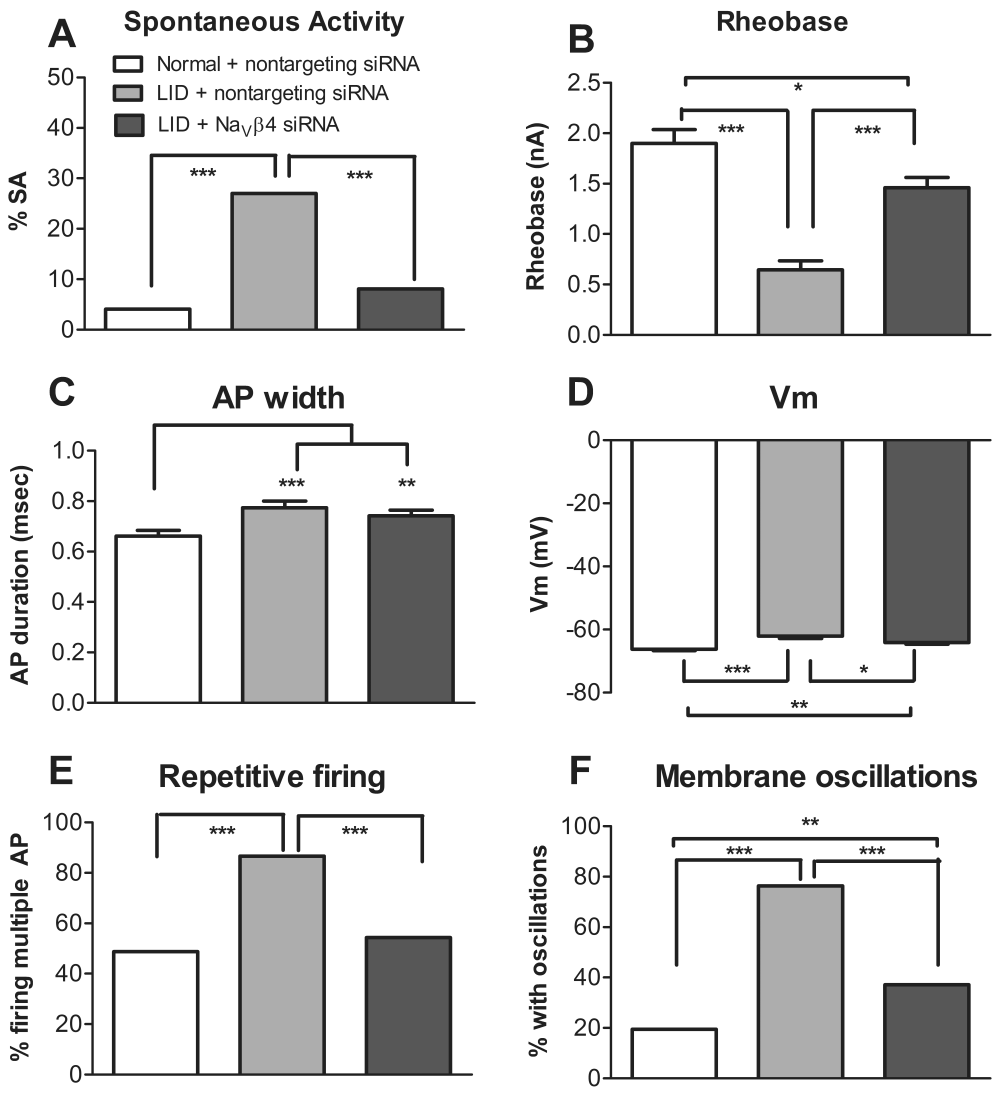

Figure 18: Navβ4 knockdown reduces hyperexcitability of myelinated Aβ cells induced by DRG inflammation. L4/L5 DRGs were injected in vivo with either Navβ4 or non-targeting siRNA and inflamed ("LID"). For comparison normal DRGs were injected with non-targeting siRNA but not inflamed. Four days later DRGs were isolated for in vitro whole DRG microelectrode recording. Data are from myelinated Aβ cells based on dorsal root conduction velocity. ***A***, Incidence of spontaneous activity was increased by LID and normalized by Navβ4 knockdown. ***B***, Rheobase was reduced by LID and partially normalized by Navβ4 knockdown. ***C***, Action potential duration was modestly increased by LID but not affected by Navβ4-siRNA. ***D***, Resting membrane potential was depolarized by LID and partially normalized by Navβ4-siRNA. Responses to longer suprathreshold current injections showed that the percentage of cells that could be induced to fire repetitively (> 2 action potentials; ***E***) or demonstrate subthreshold oscillations (***F***) was significantly increased by LID and partially normalized by Navβ4-siRNA. *, $p<0.05$; **, $p<0.01$; ***, $p<0.001$; significant difference between groups, X^2 test (***A, E, F***); Kruskal-Wallis test with Dunn's multiple comparison posttest (***B, C***); ANOVA with Bonferroni's posttest (***D***). n=123 normal + n.t. siRNA cells from 4 female rats, n=74 LID + n.t. siRNA cells from 3 female rats, and n=172 LID + Navβ4-siRNA cells from 6 female rats.

DRG inflammation increases transient and resurgent TTXS sodium currents in medium diameter cells in vitro.

We next examined the effects of DRG inflammation and Navβ4 knockdown on resurgent sodium currents, since these currents are thought to facilitate high frequency repetitive firing. Transient, resurgent, and persistent sodium currents were recorded in acutely isolated, medium to large diameter (35 to 45μm) neurons from DRGs from sham operated animals or DRGs isolated 3 days after DRG inflammation. Medium to large sized DRG neurons with 35 to 45μm diameter were chosen to ensure a better quality of recording and better voltage control. DRG neurons with a diameter greater than 45μm were not examined. In addition, previous microelectrode studies have shown that spontaneous activity occurs primarily in Aβ cells towards the smaller end of the diameter distribution (238). Previous patch clamp studies showed that medium to large diameter neurons have a high likelihood of expressing Nav1.6, the main carrier of TTXS resurgent current in DRG neurons (27). Cells were classified as having predominantly TTXS current (based on fast current kinetics and a single component in their steady-state inactivation curves) or mixed TTXS and TTXR currents, as previously described (88, 243). Because previous studies with this model showed that spontaneous activity and hyperexcitability are predominantly observed in Aβ cells and are TTXS (238), we focused on the subset of cells that predominantly express TTXS currents. In addition, cells with predominantly TTXS current have previously been observed to be the ones to express TTXS

resurgent currents (25). Excluding cells with mixed TTXR and TTXS sodium currents also most likely excluded most cells with Aδ conduction velocities as measured in vivo (84), even though those would otherwise be expected to be enriched in the size range examined. In those cells with predominantly TTXS current, both peak transient and peak resurgent current densities were increased by DRG inflammation (Figure 19). The ratio of resurgent to transient current increased from 0.034 ± 0.002 in control cells to 0.041 ± 0.002 in inflamed cells (p=0.02, Mann-Whitney test). The persistent current density was 4.0 ± 0.63pA/pF in control cells vs. 5.7 ± 0.61pA/pF in cells from inflamed DRG (p=0.055, Mann-Whitney test). The ratio of persistent to transient current was 0.003 ± 0.0005 in control cells and 0.003 ± 0.0004 in cells from inflamed DRG (p=0.46, t- test).

Cells from inflamed DRG also had a negative shift in the voltage-dependence of activation of the transient current ($V_{1/2}$ of -46.4 ± 0.9mV compared to -41.8 ± 1.6mV in control cells; p=0.03, t-test). There was also a small shift in steady-state inactivation (~2.5mV) which may not have had a major impact on channel availability ($V_{1/2}$=-57.3 ± 0.8mV in LID cells vs. -59.9 ± 0.8mV in control cells, p=0.04, t test).

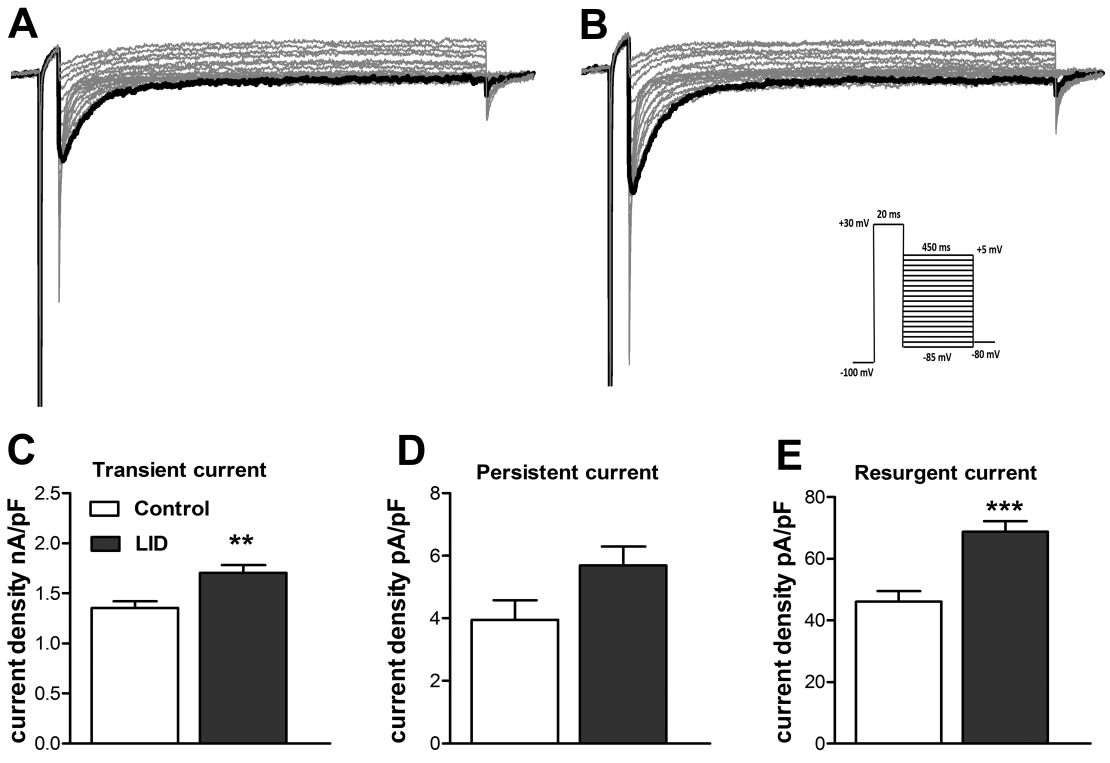

Figure 19: TTXS resurgent and transient currents are increased by DRG inflammation. Sodium currents were recorded in acutely cultured medium to large diameter DRG neurons from sham operated animals (control) or animals with localized inflammation of the DRG (LID) at POD3. Data are from medium to large diameter cells that expressed only TTXS sodium current. Representative traces of resurgent current recordings are shown for control (***A***) and LID (***B***) cultured DRG neurons. The much larger transient current during the 20 mV pre-pulse (inset: voltage protocol) is off-scale. ***C-E***, Summary data shows both peak transient current (***C***) and resurgent current (***E***) densities were higher in cells from inflamed DRG (n=15 cells from 3 male rats) compared to sham control DRG (n=20 cells from 3 male rats). Increase in persistent current (***D***) did not reach significance (p=0.055, Mann-Whitney test). **, p<0.01; ***, p<0.001; significantly different from sham control (***C***, t-test; E, Mann-Whitney test).

Navβ4 knockdown in vivo preferentially reduces TTXS persistent and resurgent currents in medium to large diameter neurons cultured from inflamed DRG

In a separate set of experiments, transient, resurgent, and persistent sodium currents were recorded in acutely isolated, medium to large (35 to 45μm) diameter neurons from cultured DRGs isolated 3 days after in vivo DRG inflammation and injection of either non-targeting control or Navβ4-siRNA. Cells having only TTXS currents were chosen to study based on the same criteria and reasons described above. In those cells, densities of both resurgent currents and persistent currents were reduced by the Navβ4-siRNA (Figure 20). The ratio of resurgent to transient current was also significantly lower in Navβ4-siRNA treated cells (0.048 ± 0.003 with n.t. siRNA vs. 0.033 ± 0.002 with Navβ4-siRNA, p=0.0003, Mann-Whitney test). In addition, the ratio of persistent to transient current was lower (0.0034 ± 0.0003 in n.t. siRNA group vs. 0.0023 ± 0.0003, p=0.0005, Mann-Whitney test). Navβ4 knockdown also resulted in a depolarizing shift in the voltage-dependence of activation of the transient current (from $V_{1/2}$ of -48.2 ± 1.9 to -42.4 ± 1.2mV, p=0.01, t-test). There was no significant difference between the 2 groups in the voltage-dependence of inactivation.

Knockdown of Navβ4 under the experimental conditions used for the patch clamp recordings was confirmed with immunostaining of cultured neurons (Figure 21). To parallel the protocol used for the patch clamp experiments, siRNA (non-targeting or Navβ4 directed) was injected in vivo at the time of DRG

inflammation; DRGs were isolated and dissociated 3 days later, and cultured cells were fixed and stained after 24 hours in culture.

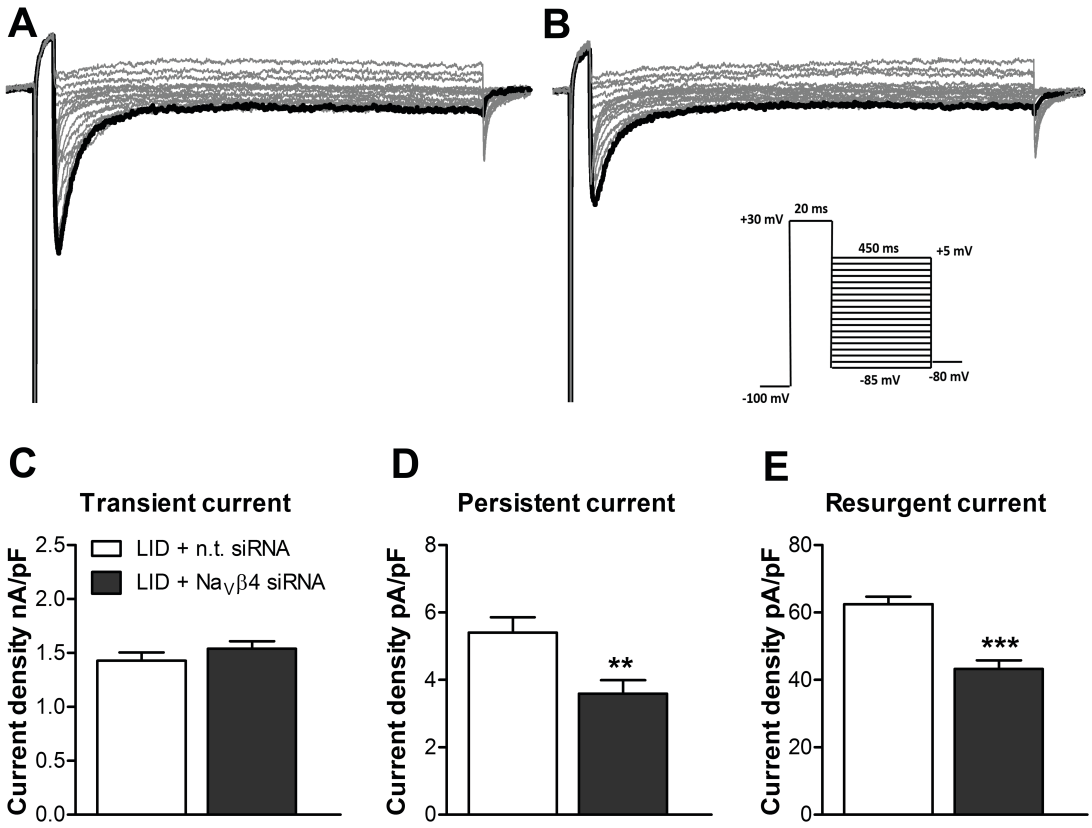

Figure 20: Navβ4 knockdown in vivo reduces TTXS persistent and resurgent currents in medium to large diameter neurons cultured from inflamed DRG. Sodium currents were recorded in acutely cultured medium to large diameter DRG neurons from LID animals injected with non-targeting (n.t.) or Navβ4-siRNA. Data are from neurons that expressed only TTX-sensitive current. Representative traces of resurgent current recordings are shown for LID +n.t. siRNA (***A***) and LID + Navβ4-siRNA (***B***) groups. The much larger transient current during the 20 mV pre-pulse (inset: voltage protocol) is off-scale. ***C***-***E***: Summary data shows both persistent current (***D***) and resurgent current (***E***) densities were reduced in LID + Navβ4-siRNA (n=31 from 5 males rats) group relative to LID + n.t.siRNA (n=25 from 5 males rats). No difference was observed in transient current density. **, $p<0.01$, ***, $p<0.001$, significantly different from n.t. siRNA group (***D***, Mann-Whitney test; ***E***, t-test).

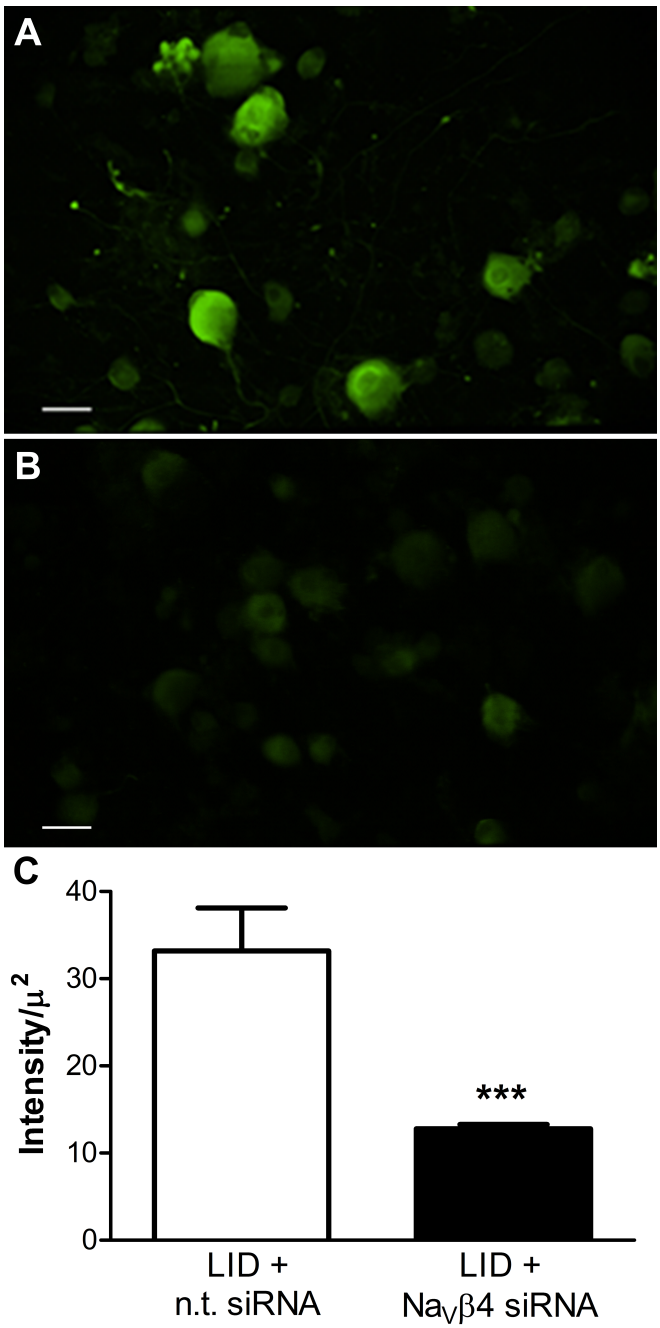

Figure 21: Immunocytochemical detection of Navβ4 in cultured DRG cells. DRG neurons were obtained under the same conditions as for the electrophysiological experiments in Figure 20. L4/L5 DRG were isolated at POD3 and cultured for 24 hours before fixation and staining. Representative images of DRG neurons cultured from LID animals injected with n.t. siRNA (***A***) or Navβ4-siRNA (***B***). Scale bars are 50μm. ***C***, Summary data of intensity per cell area shows decreased Navβ4 staining for LID + Navβ4 (n=1164 from 4 male rats) cultured DRG neurons relative to LID + n.t siRNA (n=1132 from 3 male rats). ***, significant difference between the groups ($p<0.001$), t test. Intensity units are not comparable to Figure 16D because different microscopes and analysis programs were used.

Discussion

In this collaborative study we investigated the effects of Navβ4 knockdown on pain associated behaviors, DRG neuronal excitability and sodium currents. Knockdown of Navβ4 via intraganglionic siRNA injection prevented the development of persistent mechanical hypersensitivity after local inflammation of the DRG and reduced inflammation induced increases in neuronal excitability Navβ4 expression was upregulated on POD 3-4 in DRG neurons from LID animals. At this time point, POD 3-4, DRG inflammation increased TTXS resurgent and transient currents in medium to large diameter neurons. Navβ4 knockdown selectively reduced the inflammation induced increase of resurgent currents and persistent currents but did not alter transient current density.

β-subunits can be expressed in nonneuronal cells and have effects independent of the Navα subunits (136, 244). However, our immunohistochemical data in DRG sections and cultured neurons show that the majority of DRG neurons express Navβ4. The behavioral effects of Navβ4 knockdown in the lumbar DRG are also strikingly similar to those of Nav1.6 knockdown (14). The only difference between Navβ4 and Nav1.6 knockdown was at POD1. At this time point, Navβ4 knockdown effect on von Frey responding was only partially reversed but the Nav1.6 knockdown effect is a complete reversal to baseline level. Both Navβ4 and Nav1.6 knockdown reduce mechanical pain behaviors for the duration of the experiment (at least 4 weeks).

As it is unlikely that the single siRNA injection was effective for this long, we interpret this to mean that an early period of spontaneous activity is required to initiate long lasting pain behaviors, consistent with other studies in this and other rat pain models (15, 119, 238).

We propose two mechanisms that may contribute to the observed behavioral and electrophysiological effects of Navβ4 knockdown and reduction of spontaneous activity in myelinated Aβ cells: (1) reduction of Nav1.6 expression; and (2) reduction of resurgent and persistent current, mitigating their upregulation by DRG inflammation. The first potential mechanism reflects that, in addition to their roles regulating electrophysiological properties of the pore-forming α subunits, Navβ subunits have been shown to regulate trafficking to the membrane, subcellular localization, and even gene expression of α subunits (136, 228, 244). In the PNS, Navβ4 is enriched at the nodes of Ranvier, particularly at nodes in large diameter axons. In the CNS, Navβ4 may be localized at the axon initial segment, unmyelinated axons or at the nodes of Ranvier depending on the cell type and region (228). Navβ4 co-expression did not increase peak Nav1.6 current in a heterologous expression system (227) though not all aspects of sodium channel function are captured in such systems. While we did detect a reduction in Nav1.6 immunohistochemistry with Navβ4 knockdown relative to control siRNA, we did not see a reduction in TTXS current density in corresponding patch clamp experiments, which were conducted on a defined subset of neurons. In our previous study with large diameter neurons in

the higher end of the cell size spectrum (~60 μm; see Part I), we did detect a small reduction in TTXS current density with Navβ4 knockdown. The β subunit background may be different between these two populations (35-45 μm vs. 60 μm). Therefore, by knocking down Navβ4 other beta subunits may compensate depending on the cell background. It is also possible that not all the Nav1.6 protein visualized by immunohistochemistry was necessarily functional membrane-localized channels; conversely the patch clamp experiments may not reflect changes in axonal current densities. The staining for Nav1.6 was diffuse and did not appear restricted to the membrane. However, we did not use thin sections to specifically address this question but other studies have shown a similar pattern (13, 222, 245). Details of possible Navβ4 effects on α subunit trafficking and expression require further study. In particular, studies with other β subunits suggest two potential pathways that may regulate trafficking and expression (244). Navβs are part of the immunoglobulin CAM superfamily and the extracellular domain is essential for CAM activity (198, 246). Therefore, one way Navβs may regulate VGSC localization is through interactions with the extracellular matrix or other CAMs. On the other hand, Navβ subunits have been reported to interact with cytoskeletal proteins such as Ankyrin which may regulate expression and localization of VGSCs (228, 247, 248).

The second proposed mechanism to explain the impact of Navβ4 knockdown focuses on alterations in sodium channel gating properties. The electrophysiological parameters that seem to best correlate with mechanical

hypersensitivity is the incidence of high-frequency spontaneous activity in Aβ neurons. Increased resurgent and persistent currents can facilitate such high frequency spontaneous activity, and Navβ4 knockdown effects on these currents may have contributed to our electrophysiological and behavioral findings. The decrease in resurgent and persistent currents in voltage clamp experiments in response to Navβ4-siRNA was not due to a decrease in total TTXS current (which was unaffected by the siRNA); both the absolute values and the ratios of resurgent-to-transient and persistent-to-transient current were significantly reduced by Navβ4 knockdown. Navβ4 knockdown also decreased persistent sodium currents in cerebellar granule neurons (197). Consistent with known properties of persistent currents, we observed that DRG inflammation depolarized the resting membrane potential of Aβ neurons, an effect that was partially reversed by Navβ4 knockdown. Although other sodium channel α subunit isoforms can generate resurgent currents when the cytoplasmic terminal peptide of Navβ4 is introduced, in vivo, fast TTXS resurgent currents in most (though not all) of the neurons studied to date seem likely to be the result of Navβ4 in association with Nav1.6, in both central and DRG neurons (27, 182, 228, 249). The upregulation of Navβ4 in the DRG inflammation model is a plausible mechanism for facilitating the high frequency repetitive firing seen in spontaneously active Aβ neurons. In our experimental conditions knockdown of either Navβ4 or Nav1.6 had relatively minor effects on evoked single action potentials, and no effect on action potential duration, but pronounced effects on spontaneous activity or repetitive firing capability. Our results suggest that the

latter two electrophysiological parameters best correlate with mechanical hypersensitivity.

Changes in the voltage-dependence of sodium channel activation and inactivation can also contribute to altered excitability. Previous studies examining the impact of Navβ4 on recombinant Nav1.6 channels expressed in heterologous cells such as HEK293 cells indicate that Navβ4 can induce negative shifts in the voltage-dependence of activation (by almost -10 mV) and, to a lesser extent, steady-state inactivation (227). We observed a hyperpolarizing shift in activation with inflammation of the DRG; this is likely to enhance spontaneous firing in sensory neurons. Navβ4 knockdown also induced a +6 mV shift in the voltage-dependence of activation, supporting the notion that Navβ4 subunits modify Nav1.6 voltage-dependence of activation. In our previous study (see Part I), co-expression of rat Navβ4 with human Nav1.6 did not produce a change in activation in small diameter neurons (203). A possible explanation for this discrepancy is that inflammation may trigger additional mechanisms (e.g., activating kinase pathways) that endow Navβ4 to mediate this enhanced activity. The effect may depend on neuronal background (e.g., small diameter vs. medium diameter neurons). An alternative possibility is that the small species differences between human Nav1.6 and rat Nav1.6 account for this effect. Interestingly, co-expression of Navβ4 with mouse Nav1.6 which is more similar to rat Nav1.6 than human, did produce a similar shift in activation (data not shown).

Our results with the LID model confirm work in the previous section showing that Navβ4 is primarily expressed in larger sensory neurons and extend it by showing that it plays a key role in mediating resurgent currents in inflamed, hypersensitive sensory neurons (23, 198, 203). In this study, the patch clamp experiments on sodium currents were conducted on medium diameter neurons expressing only TTXS sodium currents. This focus was dictated by our collaborators' previous work showing that spontaneous activity in this model is sensitive to TTX and largely observed in cells at the smaller end of the size range for Aβ neurons(238). By excluding cells expressing both TTXR and TTXS currents, we most likely eliminated many Aδ neurons (84). TTXR resurgent sodium currents mediated by Nav1.8 and enhanced by the Navβ4 cytoplasmic terminus have also been observed in DRG neurons (25). These resurgent currents activate over an order of magnitude more slowly than those mediated by Nav1.6; e.g. at -20mV the times to peak are 130ms for TTXR resurgent current currents compared to 3.5ms for TTXS resurgent currents. Thus, it is not clear if these TTXR currents could facilitate the high frequency firing observed in the LID model, in which the interspike interval is commonly less than 10ms. Nav1.8 has recently been found to be upregulated in myelinated Aβ neurons by peripheral inflammation (CFA paw injection) (250) and therefore a possible role of Nav1.8 in our model remains to be investigated. Arguing against Nav1.8 playing a predominant role in our model are the observations that peripheral inflammation with CFA and local DRG inflammation yield DRG gene expression changes with almost no overlap (251), and the reduction of pain associated behaviors and

spontaneous activity by Nav1.6 knockdown in the LID model (14). In addition, preliminary experiments from our collaborators in the Zhang lab using protocols similar to the current study showed no effect of Nav1.8 knockdown on pain associated behaviors induced by DRG inflammation through POD 4.

In conclusion, although $Na_V1.6$ has not generally been considered a good therapeutic target for pain, due to its widespread distribution and key role in the node of Ranvier, our results suggest that targeting the persistent and resurgent currents generated by this channel (which appear to depend on Navβ4) might be a promising approach.

***The content of this chapter was adapted from a manuscript published in PAIN. ***

Xie W, Tan ZY, Barbosa C, Strong JA, Cummins TR, Zhang JM. Upregulation of the sodium channel Navbeta4 subunit and its contributions to mechanical hypersensitivity and neuronal hyperexcitability in a rat model of radicular pain induced by local DRG inflammation. Pain. 2015. doi: 10.1097/j.pain.0000000000000453. PubMed PMID: 26785322.

PART III: FHF2 ISOFORMS DIFFERENTIALLY REGULATE $Na_V1.6$-MEDIATED RESURGENT SODIUM CURRENTS IN DORSAL ROOT GANGLION NEURONS.

Summary

The sodium channel subtype Nav1.6 as well as the Nav1.6-mediated resurgent currents have been implicated in several pain pathologies. However, our knowledge of how fast resurgent currents are modulated in DRG neurons is limited. This study explored the potential regulation of Nav1.6-mediated resurgent currents by isoforms of Fibroblast growth Factor Homologous factor 2 (FHF2) in an effort to address the gap in our knowledge of resurgent current modulation. FHF2 isoforms colocalize with Nav1.6 in peripheral sensory neurons. Heterologous expression of FHF2 isoforms suggests that these proteins differentially regulate inactivation of VGSCs. In particular, FHF2A mediates long-term inactivation (175), a mechanism proposed to compete with the open channel blocker mechanism that mediates resurgent currents. On the other hand, FHF2B lacks the ability to mediate long-term inactivation and may delay inactivation, favoring open channel block. Based on these observations, we hypothesized that FHF2A limits the generation of resurgent current, whereas, FHF2B enhances resurgent currents. Overall, our results suggest that FHF2A negatively regulated fast resurgent current by enhancing long-term inactivation and delaying recovery. In contrast, FHF2B positively regulated resurgent current

and did not alter long-term inactivation. Chimeric constructs of FHF2A and Navβ4 (likely the main open channel blocker in DRG neurons; see Part I) exhibited differential effects on resurgent currents suggesting that specific regions within FHF2A and Navβ4 have opposing regulatory functions. Interestingly, FHFAs and FHF2B isoforms were differentially regulated in a radicular pain model in a manner that likely contributes to enhanced resurgent currents. As such, these findings suggest that FHF2A and FHF2B regulate resurgent current in DRG neurons and may contribute to hyperexcitability associated with some pain pathologies.

Materials and Methods

cDNA constructs

These studies used cDNA constructs of the sodium channel auxiliary subunits, FHF2A, FHF2B and chimeric constructs of FHF2A and Navβ4. All constructs were tagged at the C-terminus with photostable monomeric Turquoise2 (pmTurquoise2) to verify expression. To generate the FHF2A and FHF2B tagged constructs, the coding sequence corresponding to mouse FHF2A (National Center for Biotechnology Information database (252) reference number: NP_034330.2) and human FHF2B (NP_378668.1) were synthesized and purchased from Genscript (Piscataway, NJ). Mouse FHF2A protein is 99.56% identical to human FHF2A (NP_004105.1) and is predicted to be 100%

identical to rat FHF2A (NC_005120.4). Human FHF2B protein is 99.48% identical to mouse (NP_001277344.1) and rat FHF2B (NP_445880.1). The FHF2A sequence was cut from a pUC57 vector and inserted into the pmTurquoise2-N1 vector with HindIII/KpnI restriction enzymes. The FHF2B sequence was cut from pcDNA3.1 (+) vector and inserted into pmTurquoise2-N1 vector with HindIII/BamHI restriction enzymes. The sequences were moved in-frame by site directed mutagenesis (Quickchange XL II Site Directed Mutagenesis kit, Agilent Technologies).

The chimeric constructs of FHF2A and Navβ4 were designed by replacing the long-term inactivation particle sequence (AAAIASSLIRQKRQARAREREK, 20 amino acids (175)) with the Navβ4 open channel blocker sequence (KKLITFILKKTREKKKECLV, 20 amino acids (199)) to generate the F2A(β4) construct. Conversely, the open channel blocker sequence in rat Navβ4 (NP_001008880.1) was replaced with the long-term inactivation particle of FHF2A to generate the (β4)F2A construct. The full chimeric sequences were synthesized and purchased from Genscript (Piscataway, NJ). The F2A(β4) and (β4)F2A sequences were cut from the pUC57 vector and sub-cloned into pmTurquoise-N1 with NheI/XhoI restriction enzymes. To move the sequences in frame with the fluorescent protein, the stop codon was mutated to a glycine residue using site-directed mutagenesis.

To study Nav1.6 in isolation from endogenous TTXS channels we used a

Nav1.6 TTXR construct previously described in (181). Briefly, the sequence corresponding to human Nav1.6 protein (NP_055006.1) was codon-optimized and purchased from Genscript (Piscataway, NJ). The sequence was then sub-cloned into pcDNA3.1 (+) with KpnI/XbaI restriction enzymes. The Nav1.6 sequence was then modified with site directed mutagenesis to confer high resistance to TTX by converting tyrosine residue 371 to serine as previously described (212, 213). The resulting construct was named Nav1.6r. Additionally, we knocked down endogenous TTXR Nav1.8 channels with a small hairpin RNA (shRNA) plasmid to aid in the isolation of Nav1.6r currents. The Nav1.8 shRNA-IRES-dsRED plasmid encoded for Nav1.8 shRNA sequence (targeting sequence, GATGAGGTCGCTGCTAAG, (214) and an internal ribosome entry site for the translation of fluorescent protein marker dsRed (IRES-dsRED) as previously described (19, 203).

Cell culture

DRG neurons were obtained from adult male Sprague Dawley rats. Rats were euthanized by CO_2 exposure and secondary decapitation. The spinal column was then removed and DRG were harvested from the lumbar to cervical region. The nerve processes were cut from the excised ganglia. Ganglia were then digested in Dulbecco' modified Eagle's Medium (DMEM, Fisher Scientific) containing collagenase (1.25 mg/mL) and neutral protease (0.78mg/mL) for 45 minutes at 37°C. Subsequently, the digested ganglia were centrifuged at

1000rpm for five minutes. Digestion media was aspirated and replaced with 10% Fetal Bovine Serum (FBS, Hyclone) DMEM (Invitrogen) and ganglia were mechanically dissociated with sequentially smaller glass pipettes. Dissociated ganglia were spun again at 700 rpm for five minutes. Media was aspirated and replaced with fresh 10% FBS DMEM media. Aliquots of cell suspension (~100 μL) were loaded onto glass coverslips coated with poly-D-lysine and laminin. After 10 minutes, cells settled and 500uL of 10% FBS DMEM was added to each well. For electrophysiological experiments with transfected neurons, the 10% FBS DMEM media was supplemented with mitotic inhibitors, 5-fluoro-2-deoxyuridine (50uM, Sigma Aldrich) and uridine (150μM, Sigma Aldrich), to prevent overgrowth of the supporting cells. Cells obtained from dissociated DRG (neurons and supporting cells) grown in culture were maintained at 37°C in a humidified 95% air and 5% CO_2 incubator. Media was changed every two days.

For Localized Inflammation of the DRG (LID) experiments, the ipsilateral L4 and L5 DRG were excised from sham operated rats and inflammation-induced rats at post operative day 5. The above dissociation protocol and culture was followed with the exception of the digestion time, which was decreased to 28 minutes. Indiana University School of Medicine Institutional Animal Care and Use Committee approved the animal protocols described above.

Surgical procedure for localized inflammation of the DRG

Localized inflammation of the DRG was used as a model of radicular pain as previously discussed in (253) and described in (238). Adult male Sprague Dawley rats under isoflurane anesthesia were used for these procedures. After deep anesthesia was verified, an initial incision on the back near the spinal column was made from L3-S1 to expose and visualize the superficial area of the spine. Then, a second deeper incision was made on one side of the animal approximately 1mm from the center of the spine from L4 to S1. Paraspinal muscles near L4/L5 were carefully teased apart until the intervertebral foramen could be visualized using the transverse processes, ilium and dorsal/ventral ramus as guides. Aliquots of 10uL containing zymosan diluted in incomplete Freud's Adjuvant (2mg/mL) were injected near L4 and L5 DRG each, through a needle inserted close to the DRG through the intervertebral foramen. The needle was bent in a 90 degree angle ~2 mm from the tip for easier access and was left for two minutes after injection to prevent leakage. Sham operated animals were used as a control; the above procedure was followed with the exception of zymosan injection. Indiana University School of Medicine Institutional Animal Care and Use Committee approved the surgical procedure described.

Immunocytochemistry

To study the expression pattern of FHF2A and FHF2B after inflammation, the L4 and L5 ipsilateral DRG ganglia were harvested and dissociated from sham operated and inflammation induced animals at post operative day 5. DRG neurons were fixed after 24 hours in culture, permeabilized, blocked and treated with antibodies in the following manner: Cells were fixed with 4% paraformaldehyde (0.1M phosphate buffer, pH 7.4) for 20 minutes at room temperature, washed with phosphate buffered saline (PBS), permeabilized in 1% Triton X-100 in PBS for 20 minutes at room temperature, washed with PBS, blocked for 2 hours (10% normal goat serum, 0.1% Triton X-100 in PBS) at room temperature, washed with PBS, incubated in primary antibodies diluted in blocking solution overnight at 4°C, washed with PBS and incubated with secondary antibody in blocking solution for 2 hours at room temperature. Primary antibodies used were Anti-Pan-FHF-A (1:200, Clone N235/22, UC Davis/NIH NeuroMab Facility) and monoclonal Anti-FGF13/FHF2.B (1:200, Clone N225A/10, UC Davis/NIH NeuroMab Facility). Secondary antibody used was Alexa Fluor® 488 Goat Anti-Mouse IgG (Molecular Probes, Life Technologies) at 1:750 dilution. Coverslips were mounted on microscope slides with Prolong Gold Antifade (Molecular Probes). DRG neurons were imaged using an Axio Observer Z1 Widefield Microscope with a 20X objective (ZEISS Microscopy). Images were analyzed using NIS Elements Advance Research (Nikon®) software by defining each cell as a region of interest and quantifying the mean intensity signal for

FHF2A and FHF2B. The mean intensity signal was compared between sham and LID groups using Student's t-test. Quantification experiments were carried out independently at least five times; more than 1000 cells were counted for each condition.

Recombinant expression in DRG neurons

DRG neurons were transiently co-transfected with Nav1.6r, tagged auxiliary subunit and Nav1.8 shRNA-IRES-dsRED using the Helios Gene Gun (Bio-Rad Laboratories) 36-48 hours after dissociation in 2:1:1 ratio respectively. As a negative control, pmTurquoise 2 (tag only) was co-transfected instead of the auxiliary subunits. For peptide studies, only Nav1.6r and Nav1.8 shRNA-IRES-dsRED were co-transfected. Expression of the Nav1.6r construct with Nav1.8 shRNA allowed us to study the modulation of Nav1.6r by auxiliary subunits in isolation from endogenous channels as previously described (19, 203). Although endogenous TTXR Nav1.8 channels run down in culture (19, 216), by using the Nav1.8 shRNA-IRES-dsRED plasmid we further decreased Nav1.8 to minimize contamination. TTXR Nav1.9 currents are not observed under our recoding parameters as previously reported (217, 218). Endogenous TTXS channels were blocked with 500nM TTX.

Electrophysiology and data analysis

General Setup: Whole cell patch clamp recordings were obtained with a HEKA EPC-10USB amplifier. Data were acquired on a Windows-based Intel 2 Core computer using the Patchmaster program (version 2X65; HEKA Elektronik). Fire polished glass electrodes (0.7-1.1MΩ) were fabricated using a P-97 puller (Sutter), and tips were coated with dental wax to minimize capacitive artifacts and enhance series resistance compensation. The offset potential was zeroed prior to seal formation. Capacitive transients were canceled using computer-controlled circuitry; C-fast for pipette capacitance correction and C-slow for cell capacitance compensation. Voltage errors were minimized by series resistance compensation >75%. Membrane currents were sampled at 20KHz and filtered online at 10KHz. Leak currents were linearly cancelled by P/-5 subtraction (pulse/number). Whole cell patch clamp recordings in voltage clamp mode were obtained 2-3.5 days after transfection at room temperature (~22°C). Cells examined were selected based on fluorescence of Turquoise (corresponding to auxiliary subunit) and dsRed (corresponding to Nav1.8 shRNA) signal. For peptide studies, only the dsRed signal was used as selection criteria since no auxiliary subunits were co-transfected. Cells with residual Nav1.8 current greater than 3% of the peak current of Nav1.6r were excluded. Nav1.8 contamination was determined by examining the voltage-dependence of steady-state fast inactivation as described previously (203). Whole cell patch clamp recordings were started five minutes after the whole cell configuration was obtained.

Electrophysiology data were analyzed using the software programs Origin (version 8, OriginLab), Fitmaster (v2X65, HEKA Electronik), Excel (Microsoft) and final graphs were made in Prism (version 6, GraphPad).

Recording solutions: The electrode solution consisted of 140mM CsF, 10mM NaCl, 1.1mM EGTA, and 10mM HEPES (adjusted to pH 7.3 with CsOH). The extracellular bathing solution contained 130mM NaCl, 30mM TEA chloride, 1mM MgCl2, 3mM KCl, 1mM CaCl2, 0.05mM CdCl2, 10mM HEPES,10mM D-glucose and 500nM TTX (adjusted pH 7.3 with NaOH). Recording solutions were adjusted using D-glucose to maintain physiological values of osmolarity (310 mOsm for internal solution and 320 mOsm for external solution).

Peptide Experiments: To study the effects of FHF2A`s long-term inactivation particle, we used a FHF2A derived peptide corresponding to amino acids residues 2-21 as reported in (175). The peptide, FHFA, was modified with an N-terminal acetyl group and C-terminal hydroxyl group yielding the following sequence: Ac-AAAIASSLIRQKRQARE REK-OH (purchased from Biopeptides Co). The FHFA peptide was added to the electrode solution at a 1mM concentration. In the control group no peptide was added to the intracellular solution.

Steady-State Activation: Current-voltage (I/V) relationships were determined by steps of 50ms, from -100 to + 80mV, in 5mV increments. The

voltage-dependence of activation (m_∞) was determined from sodium currents elicited with I/V protocol from voltages of -100mV to 0mV. Conductance (*G*) values were calculated at each test potential (V_m) using the following equation, $G = \frac{I}{(V_m - V_r)}$. V_r is the voltage at which the direction sodium influx reverses. The reversal potential was quantified for each neuron Goldman-Hodgkin-Katz equation (221). Data were then normalized to the peak conductance, plotted as a function of voltage and fitted using single-phase Boltzmann distribution equation, $\frac{G}{G_{max}} = \left(\frac{1}{1+e^{\left(V_m - V_{1/2}\right)/k}} \right)$. The half-activating voltage ($V_{1/2}$) and slope factor (k) were obtained for each cell.

Steady-State Inactivation: Steady-state fast inactivation (h_∞) was assayed with 500ms pre-pulses from -130 to 5mV (in 5mV increments) followed by a 20ms test pulse to -20mV to assess channel availability. Currents at each pre-pulse were normalized to the peak current. Data of normalized currents as a function of voltage was fitted with the single phase Boltzmann distribution, $\frac{I}{I_{max}} = \left(\frac{1}{1+e^{\left(V_m - V_{1/2}\right)/k}} \right)$, from which the half-point of inactivation ($V_{1/2}$) and slope factor (k) were obtained for each cell. V_m corresponded to the prepulse voltage. Additionally, current densities were estimated for each individual recording by dividing the peak transient currents obtained from h_∞ by the membrane capacitance.

Recovery from Inactivation: Recovery from inactivation was assayed with a two-pulse protocol that depolarized the membrane to -20mV for 20ms from the holding potential (-100mV). The time between the pulses was increased by an additive 2^n factor, where n=sweep number. At each time point the peak current measured in the second pulse (I_2) was normalized to the peak current measured in the first pulse (I_1), yielding the fraction of sodium channels available. The fraction available ($\frac{I_2}{I_1}$) was plotted as a function of time (t) and fitted to a double exponential equation, $\frac{I_2}{I_1} = A_0 + A_{fast}e^{-t/\tau fast} + A_{slow}e^{-t/\tau slow}$, from which we obtained the recovery time constants for the fast (τfast) and slow component (τslow) and compared between groups.

Accumulation of long-term inactivation: Cells were assayed with a four-pulse protocol, as previously described (175), to measure long-term inactivation. Each pulse depolarized the membrane to -20mV for 16ms from a holding potential of -90mV with -90mV 40ms interpulse recovery phases between each depolarization pulse. Currents measured at each pulse were normalized to peak current to yield percentage of sodium channels available. The % of channels available was plotted as a function of depolarization cycle (i.e., pulse number).

Resurgent Current: Cells were assayed with a two-pulse protocol that initially depolarized the membrane to +30mV for 20ms from the holding potential (-100mV), followed by repolarizing voltage steps from +15mV to -85mV for 100ms in -5mV increments to test for resurgent currents; cells were then returned

to their holding potential (-100mV). Resurgent currents display unique characteristics of slow onset and slow decay along with a non-monotonic I/V relationship. Currents that did not meet these characteristic were classified as negative for resurgent currents. Based on these criteria, the percentage of DRG that were positive/negative for resurgent current was quantified for each condition. Resurgent current amplitudes were measured after 3.0ms into the repolarizing pulse to avoid contamination from tail currents. Peak resurgent current amplitude at each test potential was normalized to peak transient current (obtained from the h_∞ protocol) and expressed as a percentage of the peak transient current. Normalized resurgent current amplitude was plotted as a function of voltage.

Statistics

Data are presented as mean ± standard error of the mean (SEM). The data were tested for a Gaussian distribution fit with the D'Agostino & Pearson omnibus normality test. Data that fit a Gaussian distribution were compared with a parametric Student's t-test at a 95% level of confidence (α=0.05). Data that did not fit Gaussian distribution were compared with a non-parametric Mann-Whitney Test with 95% level of confidence (α=0.05). The Chi-square test (X^2 test) was used to compare the frequency distribution of neurons that were positive or negative for resurgent current at a 95% level of confidence (α=0.05).

Results

Biophysical properties of Nav1.6r with FHF2A and FHF2B

We first examined if, in DRG neurons, FHF2A could mediate the characteristic long-term inactivation that has been reported in other cells with FHFAs variants (163, 175). Primary cultures of DRG neurons were biolistically co-transfected with Nav1.6r and tagged-FHF2A or tagged-FHF2B. As a negative control, only the tag (pmTurquoise2; fluorescent protein) was transfected. Whole cell voltage clamp recordings of isolated Nav1.6r currents were obtained by pharmacological (addition of 500nM TTX) and genetic (Nav1.8shRNA) inhibition of endogenous DRG sodium currents. Long-term inactivation was measured using a four-pulse step protocol (see Methods). Representative traces obtained with this long-term inactivation assay are shown in Figure 22A for each group. Overexpression of FHF2A increased accumulation of Nav1.6r in long-term inactivated states, consistent with previous reports (163, 175). FHF2A progressively decreased Nav1.6r availability with each depolarization cycle relative to control (Figure 22B, minimum sodium channel availability $p<0.0001$: FHF2A 72 ± 3%, n=18; Control 90 ± 2%, n=28), whereas, FHF2B did not (FHF2B 91 ± 2%, n=13).

We also examined how FHF2A and FHF2B alter other biophysical properties of Nav1.6r in DRG neurons since in different cell backgrounds the

interaction of FHFs with VGSCs have been reported to alter current density, inactivation, activation and recovery (161). Using the current-voltage (I/V) protocol for steady state activation (see Methods) we quantified the peak current density and the voltage-dependence of activation. Overexpression of FHF2A or FHF2B did not alter peak current density of Nav1.6r relative to control (current density p=0.10 and p=0.18 respectively: FHF2A 2.9 ± 0.2nA/pF, n=25; FHF2B 1.6 ± 0.3nA/pF, n=16; control 2.0 ± 0.2nA/pF, n=11). FHF2A did shift the voltage-dependence of activation to positive potentials by ~10mV (Figure 21C), whereas FHF2B did not, relative to control (Table 4). Consistent with previous reports (157, 162, 163, 254), FHF2A and FHF2B shifted the voltage-dependence of inactivation to more depolarized potentials (Figure 22D). FHF2A slowed recovery from inactivation, whereas, FHF2B enhanced recovery from inactivation relative to control (Figure 22E). Table 4 shows a summary of recovery, inactivation, activation and current density data.

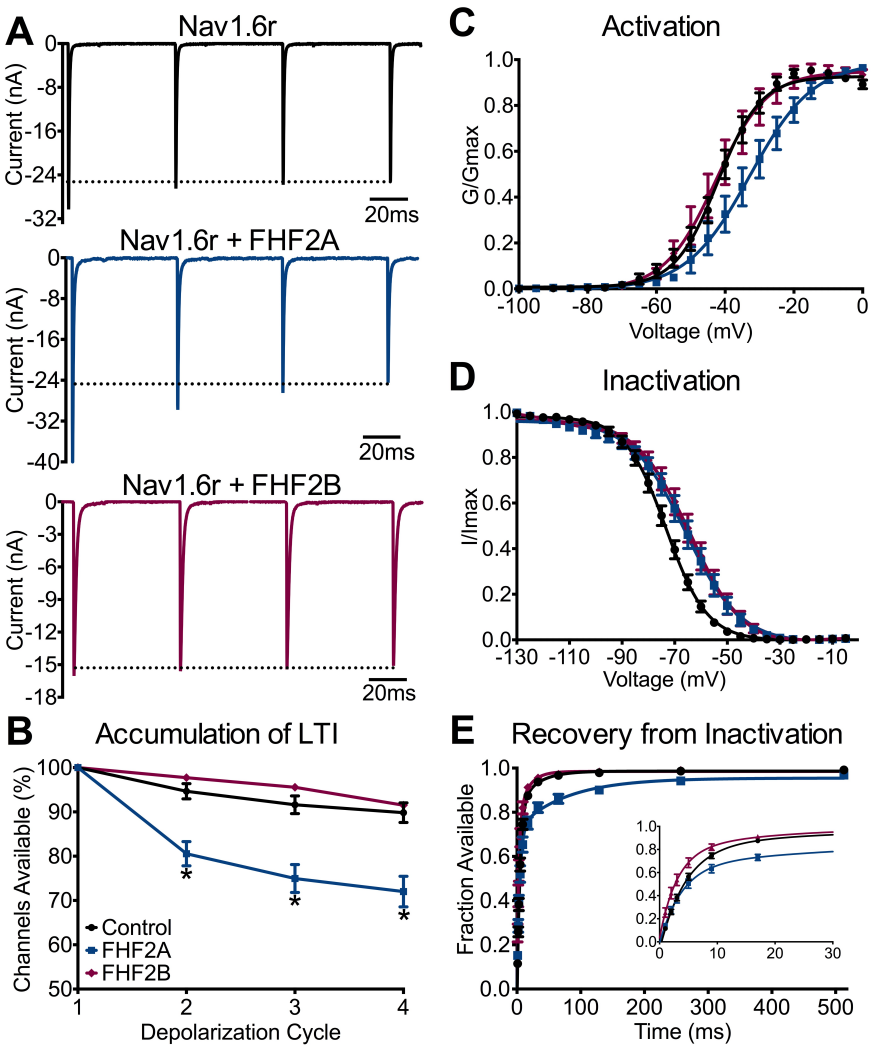

Figure 22: Biophysical properties of Nav1.6r modulated by FHF2A and FHF2B. DRG neurons were transfected with Nav1.6r and FHF2A, FHF2B or fluorescent protein tag (control). ***A***, Representative traces of cycle-dependent reduction as a measure of accumulation of long-term inactivation (LTI) for control (black), FHF2A (blue) and FHF2B (purple) groups. ***B***, The percentage of channels available as a function of depolarization cycle shows overexpression of FHF2A (n=19) increased accumulation of long-term relative to control (n=28), whereas, FHF2B (n=13) did not. ***C***, Normalized conductance (G/Gmax) as a function of voltage shows that FHF2A (blue squares, n=16) overexpression shifted the voltage-dependence of activation relative to control (black circles, n=25). No change is observed for FHF2B overexpression (purple diamonds, n=11) relative to control. ***D,*** Normalized current (I/Imax) as a function of voltage shows that voltage-dependence of inactivation was shifted to positive potentials in FHF2A (n=19) and FHF2B (n=13) groups relative to control (n=27). ***E***, Fraction of channels available as a function of time shows FHF2A (n=19) overexpression greatly slowed recovery from inactivation relative to control (n=15), whereas, FHF2B (Inset, n=12) enhanced channel recovery. Asterisks (*) represent $p < 0.0001$ obtained from Student's t-test. Data are mean ± SEM

	Activation		Inactivation		Recovery	
	$V_{1/2}$ (mV)	k	$V_{1/2}$ (mV)	k	τfast (ms)	τslow (ms)
Control	-41.0 ± 1.9	4.4 ± 0.4	-73.5 ± 1.4	6.7 ± 0.2	5.1 ± 0.5	29.0 ± 3.8
n	25	25	27	27	15	15
FHF2A	-32.5 ± 2.7*	5.2 ± 0.5	-65.6 ± 2.0*	8.0 ± 0.5	4.9 ± 0.8	141.1 ± 41†
n	16	16	19	19	19	19
FHF2B	-41.0 ± 3.4	4.9 ± 0.5	-64.8 ± 2.5*	8.1 ± 0.6	3.2 ± 0.6 *	17.7 ± 4.4
n	11	11	13	13	12	12

Table 4: Biophysical properties of Nav1.6r in control, FHF2A and FHF2B groups.
Abbreviations are: τ, time constant; k, slope factor of activation or inactivation curve; $V_{1/2}$, midpoint voltage of activation or inactivation curve. Groups were compared to control using Student's t-test (parametric) or Mann-Whitney U Test (non-parametric). *p<0.05 (vs. control); $^{\#}$p<0.005 (vs. control); † p<0.0001 (vs. control). Data are mean ± SEM and n is the number of cells from which recordings were obtained.

Differential modulation of fast resurgent currents by FHF2A and FHF2B

We next investigated the modulation of resurgent current by these FHF2 isoforms. To do so, we used a two-pulse protocol described in the Methods section. Resurgent current amplitudes were normalized to peak transient current (obtained from the steady-state inactivation protocol) and expressed as the percentage of the peak current. Representative traces of resurgent currents are shown in Figure 23A for each group. Overall FHF2A reduced the fraction of neurons positive for resurgent current (X^2 test $p<0.05$) whereas FHF2B did not, relative to control (Figure 23B). FHF2A also reduced resurgent current amplitude relative to control (Figure 23C Peak Resurgent Current Amplitude $p<0.005$: FHF2A 0.371 ± 0.21%, n=18; Control 1.14 ± 0.27%, n=29). FHF2B exhibited the opposite effect, doubling peak resurgent current amplitude relative to control ($p<0.05$: FHF2B 2.41 ± 0.22%, n=13).

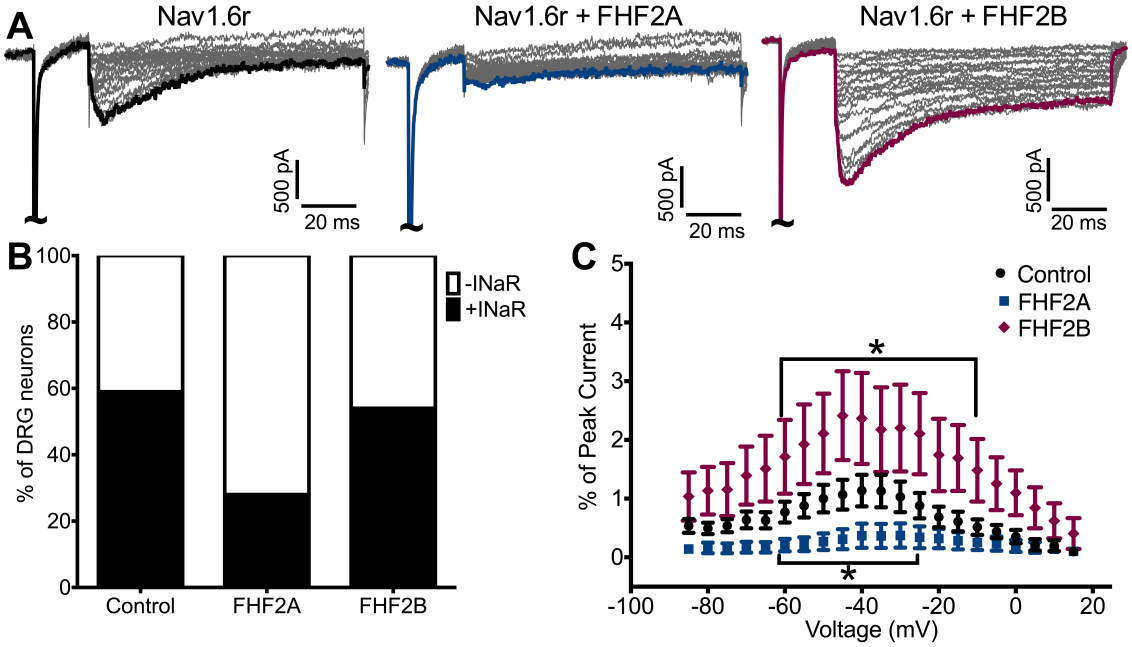

Figure 23: FHF2A and FHF2B differentially regulate fast resurgent currents. ***A***, Representative traces of Nav1.6r mediated resurgent currents obtained from cultured DRG neurons with corresponding peak resurgent currents highlighted for control (black), FHF2A overexpression (blue) and FHF2B overexpression (purple) conditions. ***B***, The distribution of resurgent current positive (+INaR)/resurgent current negative (-INaR) DRG neurons was not different with FHF2B (n=13) overexpression relative to control (n=29). FHF2A (n=18) overexpression significantly decreased the percentage of DRG neurons that generated resurgent currents relative to control ($p<0.0005$, X^2 test). ***C***, Normalized resurgent current amplitude as a function of voltage shows FHF2A overexpression (blue squares) decreased resurgent current amplitude in a range of voltages relative to control (black circles). In contrast, FHF2B overexpression (purple triangles) increased resurgent current amplitude in a range a voltages. Asterisks (*) represent $p<0.05$ (*vs* control) obtained from Student's t-test. Data are mean ± SEM.

FHFA peptide replicates long-term inactivation effects and reduces Nav1.6r resurgent currents

FHF2A has two known potential interactions that might contribute to Nav1.6r modulation: 1) binding to the C-terminus of sodium channels and 2) long-term inactivation particle binding (presumably to the inner pore region). We hypothesized that FHF2A's long-term inactivation particle is the main contributor for the observed negative regulation of fast resurgent currents. To explore this possibility, we used a peptide (FHFA) corresponding to amino acid residues 2-21 in the FHF2A protein, which was previously identified as the long-term inactivation particle (175). FHFA peptide (1mM) was added to the internal recording solution as described by Dover et al, 2010. DRG neurons were transfected with Nav1.6r and currents were isolated by pharmacological (500nM TTX) and genetic (Nav1.8shRNA) inhibition of endogenous sodium currents as described in the Methods. Voltage clamp recordings were obtained five minutes after dialysis of the internal solution in the presence or absence of the peptide. Using the protocols previously described we examined current density, activation, inactivation, recovery, long-term inactivation and resurgent currents. Representative traces of accumulation of long-term inactivation are shown in Figure 24A-B. Dialysis of the FHFA peptide greatly increased the accumulation of Nav1.6r in long-term inactivated state (Figure 24C, minimum sodium channel availability $p<0.0001$: +FHFA 29 ± 3%, n=15; -FHFA 84 ± 2%, n=16). Recovery from inactivation was significantly slowed in the +FHFA peptide group relative to

the -FHFA peptide group (Figure 24D and Table 5). Addition of the FHFA peptide did not alter Nav1.6r current density relative to control (current density p=0.08: +FHFA Peptide 1.7 ± 0.4nA/pF, n=16; -FHFA Peptide 0.9 ± 0.1nA/pF, n=14). The voltage-dependence of activation or voltage-dependence of inactivation, was not different between +FHFA peptide group and -FHFA peptide control (Table 5).

Representative traces of peak Nav1.6r resurgent currents are shown in Figure 24E. The amplitudes of the resurgent currents were normalized to peak sodium current and are expressed as the percentage of peak current. The +FHFA peptide group exhibited reduced resurgent current amplitudes relative to the -FHFA peptide group (Figure 24F, peak resurgent current $p<0.05$: +FHFA Peptide 0.88 ± 0.3, n=16; -FHFA Peptide 1.9 ± 0.6%, n=15). The fraction of resurgent current positive neurons was also greatly reduced in the +FHFA peptide group (X^2 test $p<0.005$: 20%, n=15) relative to control -FHFA peptide (69%, n= 16).

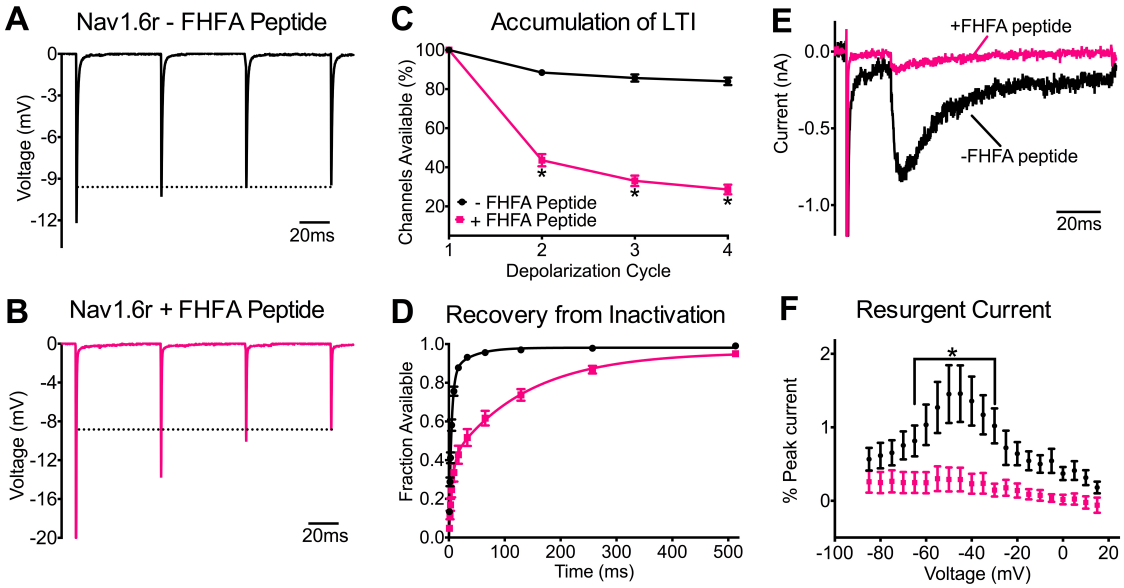

Figure 24: FHFA peptide exhibits long-term inactivation activity and recapitulates resurgent current reduction effects. Nav1.6r currents were isolated in DRG neurons and recordings were obtained in the presence (+) or absence (-) of FHFA peptide in the recording pipette. Representative traces of cycle-dependent reduction as a measure of accumulation of long-term inactivation (LTI) are shown for –FHFA peptide group (***A***, black) and +FHFA peptide group (***B***, pink). ***C,*** The percentage of channels available as a function of depolarization cycles shows that addition of the FHFA peptide (black circles, n=15) significantly increased accumulation of channels in long-term inactivated states relative to –FHFA peptide group (pink squares, n=14). ***D***, Recovery from inactivation was greatly slowed in +FHFA peptide group (n=15) relative to –FHFA peptide group (n=14). ***E***, Representative traces of Nav1.6r mediated resurgent currents with peak currents highlighted for -FHFA peptide (black) and +FHFA peptide (pink) groups. ***F,*** Compared to –FHFA peptide (black circles, n=15), addition of the FHFA peptide (pink squares, n=16) reduced resurgent current amplitude. Note resurgent currents were normalized to peak transient currents and plotted as a function of voltage. Asterisks (*) represent $p < 0.05$ obtained from Student's t-test. Data are mean ± SEM.

	Activation		Inactivation		Recovery	
	$V_{1/2}$ (mV)	k	$V_{1/2}$ (mV)	k	τfast (ms)	τslow (ms)
-FHFA	-39.0 ± 2.6	5.8 ± 0.6	- 71.2 ± 1.4	6.3 ± 0.3	5.1 ± 0.6	35.4 ± 7.8
n	16	16	16	16	16	16
+FHFA	-38.5 ± 2.6	6.5 ± 0.3	-75.1 ± 2.2	5.7 ± 0.3	7.0 ± 0.8*	139.5 ± 11†
n	14	14	15	15	15	15

Table 5: Biophysical properties of Nav1.6r with or without FHFA peptide. Abbreviations are: τ, time constant; k, slope factor of inactivation or activation curve; $V_{1/2}$, midpoint of activation or inactivation curve. Groups were compared using Mann-Whitney T-test or Student's T-test. *$p<0.05$;† $p<0.0001$. Data are mean ± SEM and n is the number of cells from which recordings were obtained.

Modulation of Nav1.6r by chimeric constructs of Navβ4 and FHF2A

The FHF2A long-term inactivation particle is potentially inhibiting fast resurgent currents by competing with the open channel blocker for the open channel state. Our previous reports suggest that Navβ4 is likely the main open channel blocker in DRG neurons (203). Therefore, we investigated if replacing the proposed open channel blocker sequence in Navβ4 with FHF2A's long-term inactivation sequence would transfer the long-term inactivation activity and reduce resurgent currents in DRG neurons. Conversely, we replaced the long-term inactivation sequence in FHF2A with the open channel blocker in the Navβ4 protein and hypothesized that this construct would increase resurgent current. The sequences were codon optimized and synthetically made (see Methods). The resulting chimeric constructs were named F2A(β4) for the FHF2A protein containing the Navβ4 open channel blocker sequence and β4(F2A) for the Navβ4 protein containing the FHF2A long-term inactivation sequence (Figure 25). Both constructs were tagged at the C-terminus with a fluorescent protein, pmTurquoise2, to verify expression. DRG neurons were biolistically transfected with Nav1.6r and one of the chimeric constructs. As a control, tag only was expressed instead of a chimeric subunit. Nav1.6r currents were isolated by pharmacological (500nM TTXR) and genetic (Nav1.8shRNA) inhibition of endogenous sodium currents as previously described. Using the recording protocols previously described we examined the biophysical properties of Nav1.6r with co-expression of β4(F2A) or F2A(β4) and investigated if the

chimeric constructs modulated resurgent currents. Representative traces of accumulation of long-term inactivation for each group are shown in Figure 26A. β4(F2A) slightly increased the accumulation of long-term inactivation relative to control (Figure 26B: minimum sodium channel availability $p<0.05$: β4(F2A) 84 ± 2%, n=12; Control 89 ± 2%, n=14), whereas, F2A(β4) did not alter accumulation of long-term inactivation (88 ± 2%, n=9). Expression of either chimera, β4(F2A) or F2A(β4) did not alter the current density relative to control (current density $p=0.8$ and $p=0.4$ respectively: β4(F2A) 1.6 ± 0.3nA/pF, n=12; F2A(β4) 1.1 ± 0.3nA/pF, n=9; control 4.2 ± 2.6nA/pF, n=14). In a similar pattern as seen with FHF2A, F2A(β4) expression shifted the voltage-dependence of activation (Figure 26C) and inactivation (Figure 26D) of Nav1.6r to positive potentials by 5mV relative to control, whereas β4(F2A) did not alter either (Table 6). Expression of F2A(β4) enhanced Nav1.6r recovery from steady-state inactivation relative to control (Figure 26E Inset). β4(F2A) did not slow or enhance Nav1.6r recovery from inactivation relative to control (Figure 26E and Table 6).

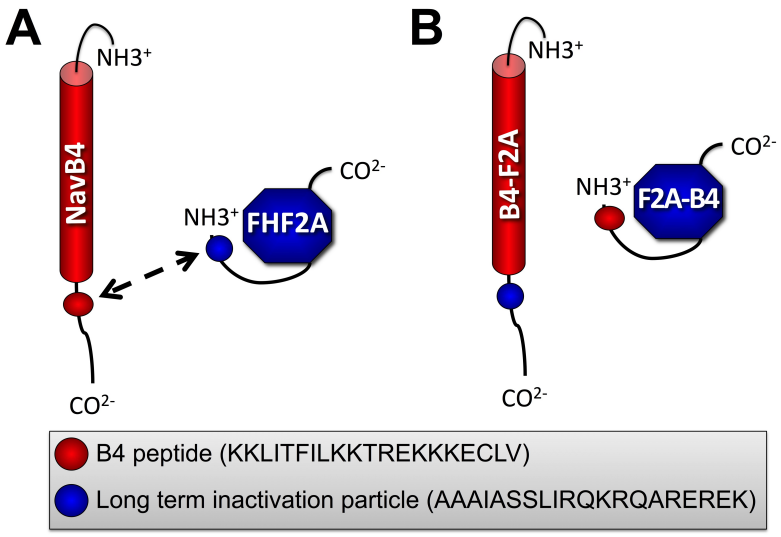

Figure 25: Chimeric constructs of FHF2A and Navβ4. ***A*****,** Illustration of FHF2A and Navβ4 subunits. The Navβ4 subunit consists of an extracellular N-terminal domain, single transmembrane and a cytosolic domain C-terminal domain. The cytosolic domain contains a sequence of amino acids proposed to mediate open channel block that generate resurgent currents (red sphere represents β4 peptide sequence, amino acids 183-203(197, 199)). The FHF2A subunit is a cytosolic protein, which contains a core region homologous to all FHF with a C-terminal epitope that enables interaction with the cytoplasmic C-terminal region of sodium channels (160). Distinct from its FHF2B counterpart, the FHF2A N-terminus sequence is much longer and contains a sequence identified as the long-term inactivation particle (yellow sphere, amino acids 1-20 (175). Arrow between the subunits highlights the region that was exchanged between these subunits to generate the chimeric constructs. ***B***, Illustration of the resulting chimeric constructs. The β4(F2A) contains all components of the Navβ4 subunit with the exception of β4-peptide sequence, which was replaced with long-term inactivation particle sequence. The F2A(β4) contains all domains of the FHF2A protein except the long-term inactivation particle, which was replaced with the β4 peptide sequence. ***Inset***, depicts the figure legend for the β4-peptide and long-term inactivation particle with the corresponding amino acid sequence.

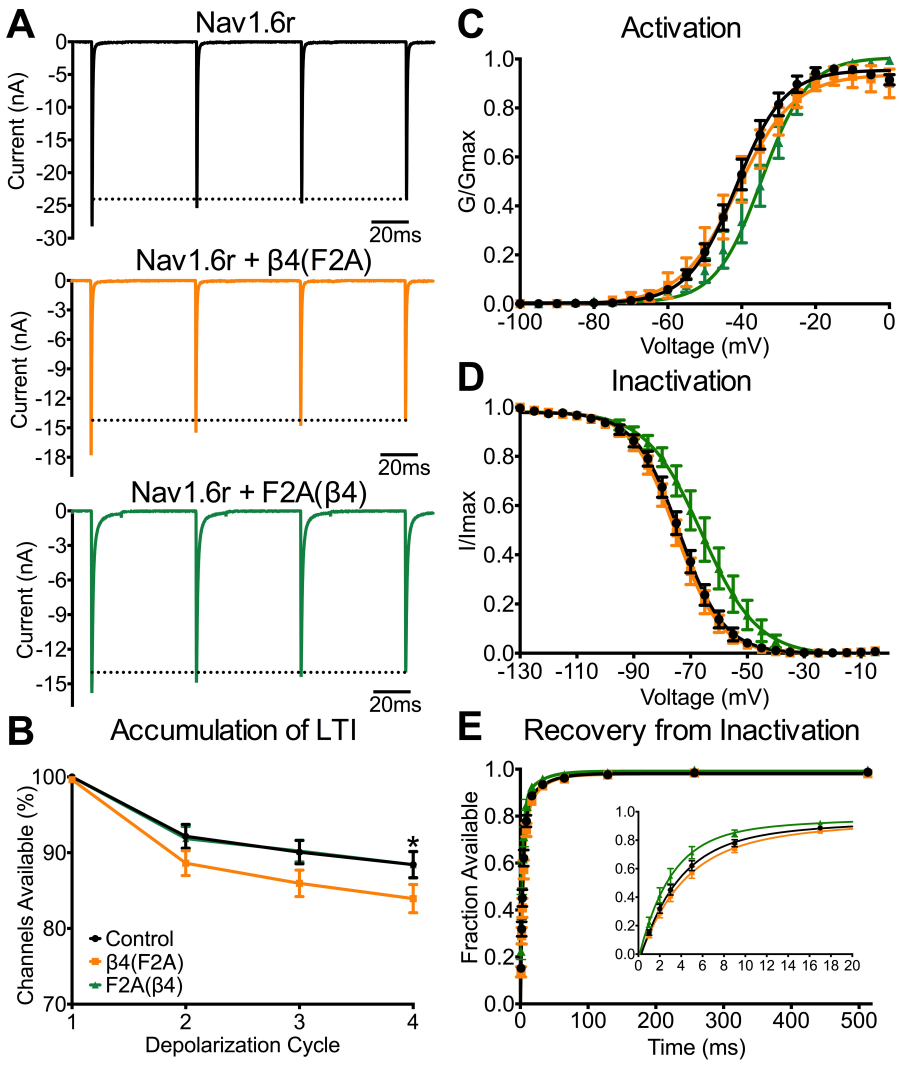

Figure 26: Biophysical properties of Nav1.6r modulated by β4(F2A) and F2A(β4) chimeras. ***A***, Representative traces of cycle-dependent reduction as a measure of long-term inactivation (LTI) for Nav1.6r isolated currents in DRG neurons with co-expression of fluorescent tag (control, black), F2A(β4) (green) and β4(F2A) (orange). ***B***, The percentage of channels available as a function of depolarization cycle shows increased accumulation of long-term inactivation for β4(F2A) group (orange squares, n=12) relative to control (black circles, n=16), whereas no difference is observed for F2A(β4) group (green triangles, n=8) relative to control. ***C***, Normalized conductance as a function of voltage shows that co-expression of F2A(β4) (n=8) shifted the voltage-dependence of activation to positive potentials relative to control (n=14), whereas, no change is observed for the β4(F2A) group (n=12). ***D***, Normalized current as a function of voltage shows that co-expression of F2A(β4) (n=9) shifted the voltage-dependence of steady-state inactivation to positive potentials relative to control (n=14), whereas, no change is observed for the β4(F2A) group (n=12). ***E***, Fraction of current available as a function of time shows that recovery is not significantly altered with co-expression of either chimera β4(F2A) (n=12) or F2A(β4) (n=9) relative to control (n=14). Asterisks (*) represent $p<0.05$ obtained from Student's t-test. Data are mean ± SEM.

	Activation		Inactivation		Recovery	
	$V_{1/2}$ (mV)	k	$V_{1/2}$ (mV)	k	τfast (ms)	τslow (ms)
Control	-40.3 ± 1.7	6.1 ± 0.8	- 73.8 ± 1.6	7.3 ± 0.3	4.8 ± 0.5	38.8 ± 5.6
n	14	14	14	14	14	14
β4(F2A)	-40.5 ± 3.2	5.2 ± 0.5	-75.17 ± 1.8	7.2 ± 0.4	4.8 ± 0.7	35.6 ± 7.1
n	12	12	12	12	12	12
F2A(β4)	-35.2 ± 2.5*	6.0 ± 0.5	-65.3 ± 3.3*	7.4 ± 0.4	2.7 ± 0.3*	43.0 ± 11
n	8	8	9	9	9	9

Table 6: Biophysical properties of Nav1.6r in control, F2A(β4) and β4(F2A) groups. Abbreviations are: τ, time constant; k, slope factor of activation or inactivation curve; $V_{1/2}$, midpoint of activation or inactivation curve. Groups were compared to control using Student's t-test (parametric) or Mann-Whitney U Test (non-parametric). *$p<0.05$ (vs. control). Data are mean ± SEM and n is the number of cells from which recordings were obtained.

Differential modulation of fast resurgent currents by F2A(β4) and β4(F2A) chimeras

We next examined Nav1.6r-mediated resurgent currents. Resurgent current amplitude was normalized to the peak sodium current obtained from the steady-state inactivation protocol and expressed as the percentage of peak current. Representative traces of resurgent currents for each condition are shown in Figure 27A. Figure 27B shows the distribution of resurgent current positive and resurgent current negative neurons for each condition. Overall the percentage of resurgent current positive neurons was not significantly different with expression of β4(F2A) or F2A(β4) relative to control ($p=0.30$ and $p=0.52$, respectively). The percentage of resurgent current positive neurons was 33% for β4(F2A), 67%for F2A(β4) and 53% for control. However, F2A(β4) expression increased the resurgent current amplitude by three-fold relative to control (Figure 27C peak resurgent current $p<0.05$: F2A(β4) 3.1 ± 0.8%, n=9; Control 1.2 ± 0.4%, n=15). In contrast, β4(F2A) reduced the amplitude of the resurgent current by two-fold (β4(F2A) $p<0.05$ 0.4 ± 0.2%, n=12).

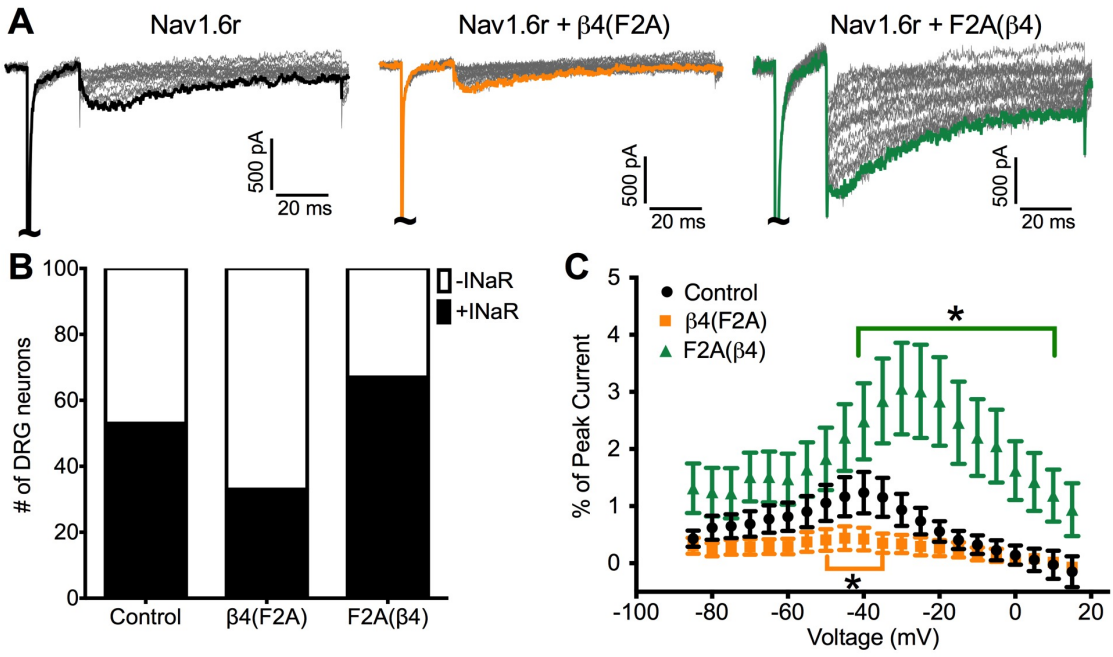

Figure 27: β4(F2A) and F2A(β4) differentially modulate fast resurgent currents. ***A***, Representative traces of Nav1.6r resurgent currents obtained from cultured DRG neurons with corresponding peak resurgent currents highlighted for control (black), β4(F2A) (orange) and F2A(β4) (green) groups. ***B***, Neither co-expression of β4(F2A) (n=12) nor co-expression of F2A(β4) (n=9) altered the distribution of resurgent current positive (+INaR)/resurgent current negative (-INaR) DRG neurons relative to control (n=16). ***C***, Resurgent current amplitude was decreased with co-expression of β4(F2A) (orange squares, n=12) in a range of voltages relative to control (black circles, n=15). In contrast, co-expression of F2A(β4) (green triangles, n=9) chimera increased resurgent current amplitude in a range of voltages relative to control. Note that resurgent currents were normalized to peak transient currents and plotted as a function of voltage. Asterisks (*) represent $p < 0.05$ obtained from Student's t-test. Summary data are mean ± SEM.

Inflammation causes differential effects on FHFAs and FHF2B isoforms

The results of overexpression of FHF2A and FHF2B, FHFA peptide and chimeric constructs suggest that the FHF2A and FHF2B isoforms regulate resurgent currents and may contribute to pain pathologies. Therefore, we chose to examine FHF2A and FHF2B expression in a radicular pain model in which we previously reported increased resurgent currents in a collaboration study with Dr. J-M. Zhang (242). In this model, localized inflammation of the DRG (LID) causes persistent mechanical hypersensitivity that starts as soon as post operative day 1 (14, 120, 121, 242). To examine FHF2A and FHF2B expression, Sprague Dawley Rats were injected with zymosan at a 2mg/mL concentration near L4 and L5 DRG in one side of the spine (see Methods). Sham operated rats that underwent the same procedure with the exception of the injections were used as a control. At post operative day 5, L4/L5 ipsilateral DRG were harvested from LID and Sham operated animals. FHFA and FHF2B levels were examined in primary DRG cultures with immunocytochemistry. One caveat with the FHFA antibody used is that it is not selective to the FHF2A isoform, because it targets the long-term inactivation particle which is highly conserved between all FHFAs. However, in adult DRG neurons, FHF4A is not expressed and FHF1A is downregulated in adulthood (164). FHF1A contains a nuclear localization signal that is functional in DRG neurons and targets the protein to the nucleus (164). In contrast, the nuclear localization signal for FHF2A is predicted to be inactive since staining is limited to the cell periphery and not detected in the nucleus in adult DRG neurons

(163). Therefore, given that our model uses adult DRG neurons we expect that cross-reaction is minimal and likely most of the antibody signal is reflecting FHF2A expression. Representative images of FHFA staining are shown in Figure 28A-B. Inflammation of the DRG reduced FHFAs levels relative to Sham control (Figure 28C, FHF2A Mean Intensity $p<0.0001$; LID 13.0 ± 0.3AU., n=1989, Sham 24.8 ± 0.8AU, n=1116). In contrast, FHF2B expression was modulated in the opposite direction as FHFAs. Representative images of FHF2B staining are shown in Figure 28D-E. FHF2B was upregulated in the LID group relative to Sham control (Figure 28F, FHF2B Mean Intensity $p<0.0001$; LID 29.5 ± 1.6AU, n=1121, Sham 21.04 ± 0.4AU, n=1164).

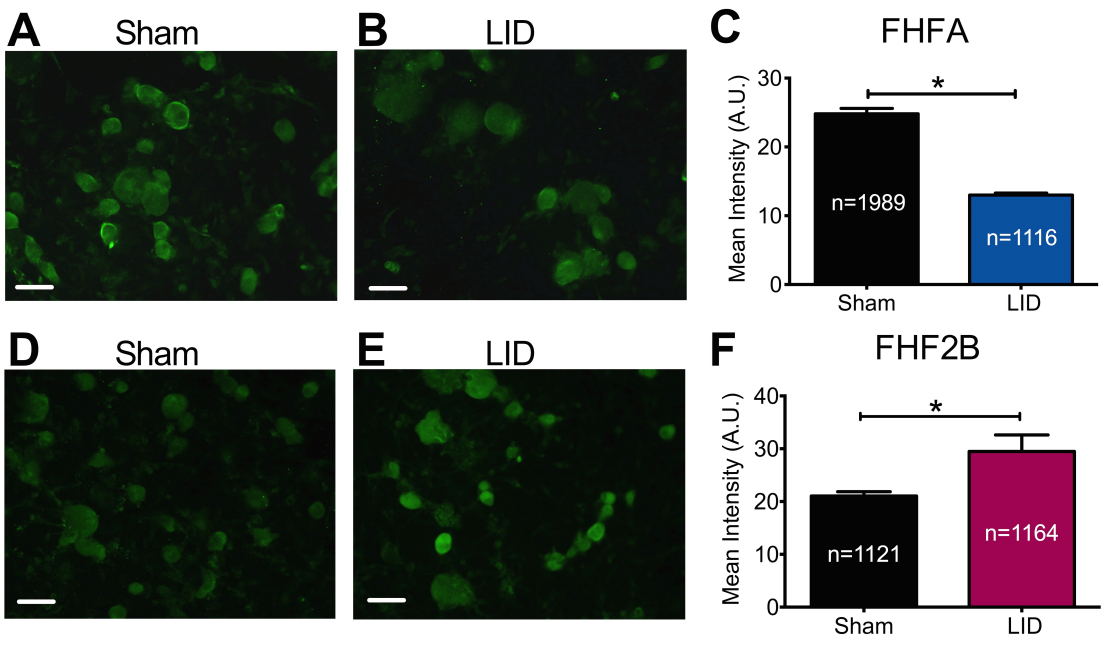

Figure 28: FHFA and FHF2B levels are differentially altered after local inflammation of the DRG. Examples of immunocytochemical staining against FHFAs in primary cultured DRG neurons from control (sham operated, ***A***) and induced local inflammation of the DRGs (LID, ***B***) animals at post operative day 5. ***C,*** DRG neurons from LID animals (n=1989) exhibited an increase in FHFA signal relative to sham control (n=1116). Examples of immunocytochemical staining against FHF2B in primary cultured DRG neurons from sham (***D***) and LID (***E***) animals at post operative day 5. ***F,*** DRG neurons from LID animals (n=1164) exhibited a decrease in FHF2B signal relative to sham control (n=1121). Five animals per group were examined. Asterisks (*) represent p <0.0001 obtained from Student's t-test. Summary data are mean ± SEM. Scale bar 50μm.

Discussion

In this study we show that FHF2A and FHF2B differentially regulate resurgent sodium currents in DRG sensory neurons. The first component of the third aim hypothesis was that FHF2A limits the capacity of sensory neurons to generate fast resurgent currents by mediating long-term inactivation. Three main findings support this hypothesis. First, overexpression of FHF2A reduced the resurgent current and increased the accumulation of channels in inactivated states resulting in delayed channel recovery. Secondly, a peptide derived from FHF2A`s long-term inactivation particle recapitulated the reduction in resurgent current generation and the enhancement of long-term inactivation. The peptide did not modulate the voltage-dependence of inactivation and activation as seen with full length FHF2A suggesting these changes do not account for negative regulation of resurgent current. Thirdly, the F2A(β4) chimera (in which the long-term inactivation particle was replaced with Navβ4's open channel blocker sequence) did not negatively regulate resurgent currents nor did it induce long-term inactivation. The chimera produced the opposite effect, an enhancement in resurgent current modulation suggesting this region is key for FHF2A`s resurgent current modulation.

The second component of our hypothesis was FHF2B increases resurgent currents by delaying inactivation. Our results support this hypothesis. FHF2B increased resurgent currents, shifted the voltage-dependence of inactivation to

positive potentials and enhanced recovery from inactivation. FHF2B's inability to mediate long-term inactivation while still shifting inactivation to positive potentials likely increased the accessibility of the putative open channel blocker. The faster recovery observed with overexpression of FHF2B supports this possibility, since recovery when the channel undergoes open channel block is reported to occur in a shorter time scale than channel recovery from fast inactivation (178). An alternative explanation is that FHF2B displaces the endogenous negative regulation exerted by FHF2A because all FHFs are predicted to bind to a conserved region within the C-terminus of VGSCs (160). FHF2A is expressed in neurons of all size classes and is particularly predominant in small diameter neurons (163). The transfected neurons examined in these studies were mostly in the small diameter range. Therefore, it is plausible that displacement of endogenous FHF2A by exogenous FHF2B contributes to some extent to FHF2B's positive regulation of fast resurgent currents.

Based on previous reports, the potential mechanism for FHF2A negative regulation is competition of the long-term inactivation particle with the Navβ4 open channel blocker activity (176, 203). The results from FHF2A and Navβ4 chimeras partially support this hypothesis, however the implications of results obtained with these chimeric proteins is limited by a few caveats. Our assumption was that by replacing the peptide sequence of long-term inactivation with the open channel blocker and vice-versa the activity of these peptide sequences would be retained in the resulting chimera. However, the β4(F2A) chimera failed

to delay channel recovery and produced only a very mild enhancement in accumulation of inactivated states; suggesting that the long-term inactivation particle is not fully functional in the chimeric construct. Therefore, the reduction in resurgent current observed with the expression of the β4(F2A) chimera is likely due to a dominant negative effect of an inactive Navβ4, likely competing with wildtype Navβ4 for α subunits. In a similar manner, there are two possible contributions underlying F2A(β4)'s resurgent current enhancement: 1) the Navβ4 open channel blocker sequence is active in the chimera and/or 2) loss of the long-term inactivation particle allowed other changes in the voltage-dependence to favor the endogenous open channel blocker interaction as seen with FHF2B. To further explore the first possibility, we tested the F2A(β4) chimera in a Nav1.5 HEK cell line that does not generate resurgent current unless the β4-peptide is introduced. We found that indeed the F2A(β4) chimera mediated resurgent currents (Figure 29) in a Nav1.5 cell-line. This result favors the possibility that the F2A(β4) chimera retains open channel blocker activity. However, it would be simplistic to assume that the resurgent current enhancement is only due to this activity. It is likely a combined effect of removing a limiting determinant (i.e. long-term inactivation particle), adding an active open channel blocker sequence and the shift in voltage-dependence of inactivation contributing to the overall enhancement of resurgent current. Overall, results from β4(F2A) and F2A(β4) chimeras confirmed that the N-terminus of FHF2A and the C-terminus of Navβ4 are important modulators of fast resurgent currents.

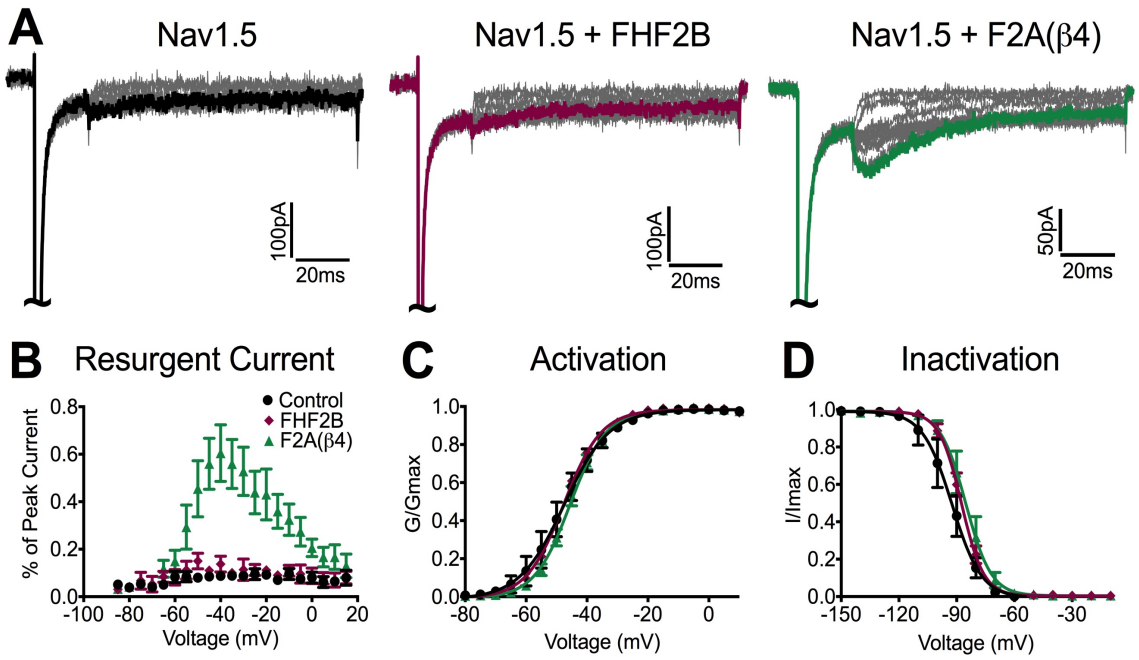

Figure 29: F2A(β4) but not FHF2B induced fast resurgent currents mediated by Nav1.5 in HEK cells. HEK293 cells stably expressing Nav1.5 were transfected with tagged-F2A(β4) or tagged-FHF2B. Non-transfected cells were used as a control. Resurgent currents were elicited with a standard resurgent current voltage protocol, in which cell membrane was initially depolarized to +30mV for 20ms, and then repolarized to voltages ranging from +15mV to -85 for 100ms in 5mV increments. ***A***, Representative traces of Nav1.5 resurgent currents are shown for control (black), FHF2B (purple) and F2A(β4) (green). Trace obtained at -40 mv is highlighted for each group. ***B***, Resurgent current amplitude was normalized to peak transient current. F2A(β4) (green triangles) generated a biphasic current voltage curve typically observed for resurgent currents, whereas, control (blue circles) or FHF2B (purple diamonds) did not. **C**, Effects of FHF2B and F2A(β4) on Nav1.5's voltage-dependence of activation. The $V_{1/2}$ values are -47.5 ± 0.9mV (control), -47.6 ± 0.3mV (FHF2B) and -45.5 ± 0.4mV (F2A(β4)), respectively. ***D***, Effects of FHF2B and F2A(β4) on voltage-dependence of inactivation. The $V_{1/2}$ values are -92.4 ± 1.2mV (control), -87.5 ± 0.5 mV (FHF2B) and -85.3 ± 1.0mV (F2A(β4)), respectively. The holding potential was -120 mV. Data are mean ± SEM and n=5 for each group.

FHFs binding to the C-terminus of VGSC can cause changes in the biophysical properties of the VGSC (134). Expression of FHF2A, FHF2B or F2A(β4) shifted the voltage-dependence of inactivation to positive potentials. Since the F2A(β4) chimera lacks the long-term inactivation particle sequence yet retained the ability to cause shifts in voltage-dependence of activation and inactivation, the results suggest that these modulations are mainly an effect of the FHF2 core region binding to the C-terminus of Nav1.6. The shift of inactivation to positive potentials is consistent with previous reports of FHF2 binding to the C-terminus of different sodium channels including Nav1.6 (157, 160, 162, 163). FHF2A and F2A(β4) also shifted activation to positive potentials. Since both F2A(β4) and FHF2A but not FHF2B exerted this effect, it is most likely that the N-terminus region that is conserved between F2A(β4) and FHF2A is responsible for this effect.

Interestingly, the chimeras generated for this study might serve as valuable tools for the study of resurgent currents in the future. The (β4)F2A chimera did not significantly alter the voltage-dependence of activation or inactivation, recovery from inactivation, or current density. The main effect we detected was a significant reduction in resurgent current. As such, overexpression of this protein in animal models or in vitro studies might serve as a tool to selectively target resurgent currents. On the other hand, the F2A(β4) chimera might serve as a tool to artificially induce fast resurgent currents. The applications for the F2A(β4) might be limited since it alters other channel

properties. However, we envision that the F2A(β4) chimera might be useful in high-throughput assays to identify compounds that might inhibit resurgent currents.

Overall our data suggest that FHF2A and FHF2B modulate resurgent currents in DRG neurons. The importance of this finding is more evident when we examine how these proteins are regulated in a radicular pain model induced by localized inflammation of the DRG. Our results show that after inflammation FHFA isoforms are downregulated, whereas FHF2B was upregulated. The change in expression of these isoforms likely contributes to the increased resurgent current generation and hyperexcitability reported in this model (116, 120, 242). The limitation of the antibody specificity precludes us from definitively attributing the effect solely to changes in the FHF2A isoform. However, the high conservation of the long-term inactivation particle between all FHFAs suggests that if other FHFAs were to interact with Nav1.6 they will likely have a similar negative regulation on resurgent currents. FHFs modulation might also contribute to other pain pathologies. For example, two studies using cDNA arrays reported FHF2 cDNA levels downregulated with no change in FHF1 and FHF4 after peripheral nerve injury (165, 166). Using the Expression Atlas (255) from European Bioinformatics Institute and European Molecular Biology Laboratory we found that FHF1 and FHF2 levels are downregulated in DRG neurons after spinal nerve ligation, a chronic pain model (256). Which of the FHF1 and FHF2 isoforms contribute most to these changes is unknown. Our study suggests that

FHFs might prove to be novel targets for regulating fast resurgent current in DRG neurons and further studies might provide new insight into possible therapeutic strategies for pain.

SUMMATION AND FUTURE DIRECTIONS

Increased fast resurgent currents in peripheral sensory neurons have been implicated in several pain pathologies. However, our knowledge of how these currents are modulated in sensory neurons is limited. The main goal of this dissertation was to identify fast resurgent current modulators in order to address the gap in our knowledge and potentially devise new therapeutic or experimental strategies. We focused on Nav1.6 mediated currents because this isoform is the main carrier of fast resurgent currents (27). Thus, our findings may be particularly relevant to pain pathologies associated with Nav1.6 channel activity that contributes to DRG's hyperexcitability.

Navβ4 and resurgent currents

The identity of the open channel blocker that mediates resurgent currents in DRG neurons was unclear. Results from the first aim of this dissertation suggest that Navβ4 is the major open channel blocker in DRG neurons. Overexpression of Navβ4 greatly increased resurgent currents, whereas, knockdown or overexpression of a mutant form of Navβ4 decreased resurgent current generation. The Navβ4 C-terminal mutant data suggests that in congruence with CNS studies, the C-terminal region of Navβ4 is important for resurgent current generation (180, 197, 199). In contrast, our results suggest that Navβ2 does not modulate fast resurgent currents.

Our interpretation of the results is limited because we did not directly examine if Navβ2 or Navβ4 associates with Nav1.6 in the DRG neuronal background. Future studies are needed to determine if Navβ4 resurgent current modulation is due to association with Nav1.6. One potential approach to determine whether there is an association between these subunits, would be to use identified mutations at the N-terminus of Navβ4 that disrupt association with α subunits (228, 230). If overexpression of an N-terminal Navβ4 mutant that does not associate with Nav1.6 modulates resurgent currents this might suggest that Navβ4's resurgent current modulation is independent of Nav1.6 association. An alternative approach would be to use pharmacological tools to determine the potential association of Navβ2 or Navβ4 with Nav1.6. For example, recent studies have found that Nav1.2 inhibition by ProTxII (a toxin isolated from the tarantula (257)) is disrupted by association of Navβ2 or Navβ4 (230, 231). It is unknown if the same effects are observed for Nav1.6 but would be an important avenue to explore. However, these studies might require a cell background that lacks robust expression of β-subunits. Biochemical assays such as co-immunoprecipitation of the β-subunit:α subunit complex in DRG tissue might be necessary to strengthen any findings.

Modulation of Nav1.6 by Navβ4 may also be due to direct or indirect interaction of Navβ4 protein fragments. β subunits are known substrates of proteases from the secretase family (Figure 30) (244). Sequential proteolysis can produce a variety of fragments. N-terminal cleavage generates a soluble IgG

extracellular fragment and a transmembrane C-terminal fragment (258). The C-terminal transmembrane fragment is further processed to yield a transmembrane fragment and a soluble C-terminal fragment (258, 259).

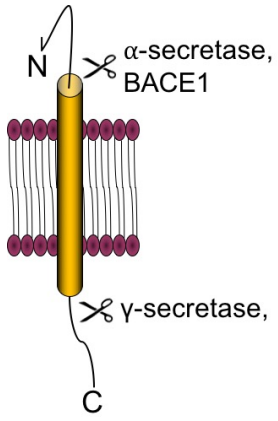

Figure 30: Schematic representation of secretase cleavage sites in β-subunits. The extracellular N-terminus region close to the transmembrane domain contains a cleavage site for β-site amyloid precursor protein-cleaving enzyme 1 (BACE1)(258, 260). Navβ2 contains an additional α-secretase cleavage site at the N-terminus (259). The C-terminus juxtamembrane region contains a γ-secretase cleaveage site(259).

A study by Huth el al, suggests that cleavage of Navβ4 by β-site amyloid precursor protein-cleaving enzyme 1 (BACE1) modulates the decay of resurgent sodium current in cerebellar neurons(261). Several studies concur that Navβ4 association with alpha subunits is dependent on the N-terminal domain of the beta subunit (198, 228, 230, 262). Thus, shedding of Navβ4's extracellular domain by BACE1 cleavage would potentially destabilize the association with an alpha subunit (261). It is unclear if the resulting C-terminal transmembrane domain can interact with Nav1.6 or if further processing of the C-terminal fragment yields a soluble peptide with open-channel blocker activity.

Proteolytic fragments may also indirectly modulate sodium channels (244, 263). For example, the soluble C-terminal fragment of Navβ2 translocates to the nucleus (263). It has been proposed that the nuclear fragment exerts transcriptional regulation of sodium channels by functioning as transcription factors (263). It is possible that Navβ4 regulates Nav1.6 expression in this manner or may modulate transcription of factors that modulate channel activity. Further studies are needed to examine the potential modulation of Nav1.6 or resurgent currents by Navβ4 proteolytic fragments in DRG neurons. Selective activators and inhibitors of different secretase enzymes may serve as tools to address this question (264).

Navβ4 and nociception

In the second part of this dissertation we examined the effects of Navβ4 knockdown in an inflammatory pain model. In the LID model, Nav1.6 has been proposed to contribute to mechanical hypersensitivity. However, it is unknown if fast resurgent currents are altered and if they contribute to the hyperexcitability of DRG neurons and mechanical hypersensitivity. Our results show that LID increases fast resurgent currents and transient currents in DRG neurons. Knockdown of Navβ4 prevented the increase in fast resurgent current, excitability and mechanical sensitivity. Navβ4 knockdown also reduced persistent currents. Our results suggests that in the LID model, Navβ4's modulation of resurgent and persistent currents contributes to hyperexcitability . Fast resurgent currents are

proposed to increase the firing frequency of DRG neurons (17, 19, 196, 249, 265, 266). Persistent currents depolarize the membrane, decreasing the stimulus needed to trigger an action potential (73, 265, 267, 268). Together these changes, could enable the spontaneous burst firing similar to the pattern observed in LID DRG neurons (238, 269). Future studies are needed to confirm the contribution of resurgent currents and persistent currents with DRG neuronal simulations since selective inhibition through pharmacological methods is not currently feasible.

One of the limitation of our study, is that the we performed patch clamp studies in cultured DRG neurons which lacked axonal projections and nerve endings. While we did detect Navβ4 upregulation in the soma and the axonal regions near the DRG, we did not examine if resurgent and persistent currents are also enhanced at the axon or nerve endings. Furthermore, we did not examine where spontaneous activity is initiated (i.e. at the soma or in other neuronal compartments). If spontaneous activity were to be generated at the neuronal soma, the action potentials generated may then be relayed to the periphery, spinal cord, or both. Transmission of action potentials toward the periphery may stimulate release of neurotransmitters and other chemical substances that in turn sensitize the nociceptive fibers to activation (270). On the other hand, constant release of neurotransmitters and other chemical mediators at the spinal cord may facilitate the activation of second order nociceptive neurons at the spinal cord (271, 272). In this manner, maladaptive changes at

the periphery or at the spinal cord may facilitate a nociceptive like-response to a normally innocuous stimulus. Future studies could examine the potential changes at the peripheral nerve endings or at the spinal cord in the LID model employing electrophysiological and immunohistochemical methods to elucidate these possibilities.

Although the location of spontaneous activity merits further examination, several studies have shown that spontaneous activity is key for the development of persistent pain (273-276). In particular, early blockade of afferent spontaneous activity (within 10 days of injury) in some models is sufficient to prevent the development of chronic mechanical and thermal hypersensitivity (119). Based on our results, agents that block both resurgent and persistent currents may be effective in reducing spontaneous activity. Our experimental LID paradigm in which β4-siRNA was injected at the time of inflammation, suggest that early blockade might be sufficient to prevent persistent mechanical hypersensitivity in this model. Future studies are needed to explore the therapeutic potential of agents that selectively target persistent and resurgent currents over the transient current that underlies the action potential upstroke. For example, a published collaboration study with R. Patel (277) suggests that cannabidiol, an active agent found in the cannabis plant, selectively targets persistent and resurgent currents. It would be important to determine if cannabidiol reduces spontaneous activity in the LID model and if it has a therapeutic effect. Alternatively, future studies might explore selective targeting of the Navβ4 C-terminal region. The available Navβ4

crystal structure might help identify compounds that target the Nav1.6 and Navβ4 interaction (230).

Aβ fibers and the LID model

In the LID pain model, hyperexcitability is mainly observed in Aβ fibers. To devise the best therapeutic strategy, it is important that we understand how Aβ fibers contribute to the pathology. The role of Aβ fibers in nociception has been controversial because these fibers were initially thought to be mainly activated by non-noxious mechanic stimulation (82). Thus, Aβ fibers have been classified as low-threshold mechanoreceptors. However, there is intriguing evidence that suggests a population of Aβ fibers is activated by noxious mechanic or heat stimuli (82, 278-285). Therefore, a fraction of Aβ fibers have been identified as putative nociceptors or high-threshold fibers.

There are two main ascending pathways by which Aβ fibers could modulate nociceptive impulses from reaching the CNS and alter pain perception. The pathways are known as the lemniscal pathway and the spinothalamic pathway (286, 287). One way to distinguish between these two pathways is by identifying the second order neurons to which the DRG's CNS branch mainly projects. The lemniscal pathway second order neurons are located in the medulla. In contrast, spinothalamic second order neurons are located in spinal cord. Second order neurons then project to third order neurons in the thalamus.

Under non-pathological conditions, nociceptive impulses are relayed through the spinothalamic pathway (226, 287). In contrast, non-nociceptive (low threshold) DRG neurons are proposed to mainly relay impulses through the lemniscal pathway (286). Aβ fibers form part of the lemniscal pathway. It is important to note that this is a simplified scheme of the circuitry. In reality there are many collateral projections at each relay point. For example, Aβ fibers that send projections to the medulla also send collateral projections to the spinal cord (226, 286). Importantly, the collateral projections of low-threshold and high-threshold Aβ fibers may modulate the activation of the spinothalamic pathway at the spinal cord.

In the spinal cord there is a variety of neurons that can be divided by the lamina (anatomical surface division) they occupy (288). Classic DRG nociceptors (i.e. C-fibers and Aδ-fibers) mainly project to lamina I-II nociceptive specific projection neurons (289, 290). Some DRG nociceptors may also project to wide-dynamic range (WDR) neurons, which are predominantly located in lamina V (226, 291, 292). WDR neurons can respond to a variety of stimuli intensities (low-threshold and high-threshold) (292). Nociceptive impulses from DRG neurons can be relayed by WDR or projection neurons through the spinothalamic pathway (226, 292). Lemniscal collaterals projections at the spinal cord can display different projection patterns. Putative Aβ nociceptors collaterals project to lamina I through V in a “flame-shaped” aspect (279-281). Thus, it has been proposed that these putative Aβ nociceptor projections may directly activate second order

nociceptive neurons at the spinal cord in lamina I-II or V, relaying impulses through the spinothalamic tract. However, it is not clear which neurons Aβ nociceptors communicate with at the spinal cord and if the net effect is inhibitory or excitatory. In contrast, low threshold Aβ mechanoreceptors collaterals mainly project to lamina III-V (and lamina II to a lesser extent) stimulating interneurons that activate and inhibit nociceptive neurons (291). The net effect of low threshold Aβ collaterals reduce the probability of nociceptive impulses from being relayed to the thalamus by activating inhibitory interneurons (293). It is proposed that activation of low threshold mechanoreceptors reduces the perception of pain by generating a segmental control or gate at the spinal cord level. Melznack and Wall introduced this concept in the gates control theory of pain (294, 295). They proposed that at each relay point, “gates” modulate the successful transmission of the nociceptive impulses to the next relay point. For example, descending pathways from the brain to the spinal cord can activate inhibitory interneurons at the spinal cord (293, 296-298).

Further studies are needed to explore which population of Aβ fibers might contribute to LID pain. If hyperexcitability of low threshold Aβ fibers are responsible for mechanical hypersensitivity then the normal circuitry may have been altered. One possibility is that inhibition control at the spinal cord is somehow compromised. Several studies have found a reduction in inhibitory signaling at the spinal cord in some pain conditions, although the mechanism is not clear (299-302). Other studies have suggested that a substantial portion of

non-nociceptive A-fibers sprout connections to laminas associated with nociceptive signaling, i.e. LaminaI/II (303-305). However, concerns regarding the selectivity of the neuronal tracers have questioned the interpretation of the results (306, 307). A more robust study, using neuronal tracers and selective markers, found a small portion of A-fibers sprout contacts into lamina II (308). It is possible that these abnormal contacts activate nociceptive specific neurons within lamina II overriding the inhibitory input. Interestingly, several studies have suggested that Navβ4 and Navβ4 proteolytic fragments promote neurite outgrowth (146, 147, 196). Future studies are needed to explore if upregulation of Navβ4 promotes sprouting of Aβ fibers. On the other hand, if hyperexcitability of nociceptive Aβ fibers contributes to mechanical hypersensitivity, this hyperexcitability may produce changes at the peripheral nerve endings or second order neurons at the spinal cord facilitating activation of the spinothalamic pathway as previously discussed. Further studies are required to elucidate how the Aβ fiber circuitry contributes to nociception under normal and LID conditions.

FHF2 and resurgent currents

Resurgent currents are observed in a subpopulation of DRG neurons (27), raising the possibility of endogenous negative regulators which restricts resurgent current generation (27). Our results suggest that FHF2A negatively regulates resurgent currents. We identified the long-term inactivation sequence (or particle) in the N-terminus of the FHF2A protein as being important for

FHF2A's negative regulation. The chimeric construct that lacked the long-term inactivation particle failed to negatively regulate resurgent currents. Furthermore, a peptide derived from FHF2A's long-term inactivation particle recapitulated negative regulation of resurgent currents. Based on our results it is possible that in neurons where FHF2A is abundant, resurgent currents may be repressed. In contrast, FHF2B, which lacks the long-term inactivation particle, greatly increased resurgent currents. This effect is likely mediated by FHF2B modulation of fast inactivation to positive potentials, which may increase the probability of the open channel blocker to bind to the sodium channel. The core regions of FHF2A and FHF2B bind at the same site in the C-terminus of the alpha subunit. Therefore, it is possible that the ratio of FHF2A and FHF2B levels may regulate the degree of fast resurgent current generation in a given DRG neuron.

However, the interpretation of our results is limited since we mainly used an overexpression approach of FHF2 isoforms and chimeric constructs. Overexpression of a given subunit may induce an interaction that may not endogenously occur otherwise. Therefore, different experimental approaches are required to provide a more complete picture. One potential approach would be to couple single cell analysis with electrophysiological recordings. Using this approach, we could determine if a given DRG neuron generates resurgent currents and what are the corresponding levels of FHF2A, FHF2B, Navβ4. If our model is correct, FHF2A levels would be negatively correlated with resurgent current amplitude. In contrast, we predict that FHF2B and Navβ4 levels would be

positively correlated with resurgent current amplitude. Alternatively, in-vivo knockdown of FHF2A or FHF2B would allow us to examine the effects on endogenous fast resurgent current.

In the LID pain model, we found that FHFA isoforms are upregulated, whereas, FHF2B is downregulated. Based on our overexpression results of the individual proteins, downregulation of FHF2A and upregulation of FHF2B may contribute to the enhanced resurgent currents we detected in the LID model (see part 2 results). Further studies are needed to examine which FHFA isoforms are downregulated. One approach would be to use Reverse transcription polymerase chain reaction (RT-PCR) or in-situ hybridization with specific primer probes to examine mRNA levels. While mRNA levels do not always correlate to protein expression, this approach would allow us to distinguish between FHFA isoforms and overcome the limitation of lack of specificity of current available antibodies.

Future studies might also explore the individual contribution of FHF2A and FHF2B subunits to nociception. For example, it will be interesting to determine if FHF2A knockdown or overexpression of FHF2B is sufficient to induce pain associated behaviors. While we have identified these two potential players, other FHFs might also modulate Nav1.6 or other α subunits. In addition to FHF2, FHF1 and FHF4 are expressed in adult DRGs. FHF3 mRNA is detected in embryonic DRG but expression has not been studied in adult DRG neurons (309).There is always a possibility that expression of these isoforms is modulated in specific

pathophysiologies. Additionally, there is some evidence that suggests FHFs interact with other partners such as kinases (150-152) and calcium channels (310) in CNS and cardiomyocytes. Therefore, it is possible that FHF modulation in DRG neurons alters other targets and may also contribute to pain pathologies. Further studies are necessary to determine such possibilities and provide more insights into FHFs potential role in peripheral sensory neurons.

FHF2A and FHF2B as potential therapeutic targets

Based on our findings FHF2A and FHF2B may be useful targets for therapeutic interventions in the LID model. One potential strategy for a therapeutic intervention would be to disrupt FHF2B interaction with Nav1.6. We hypothesize that FHF2B disruption with Nav1.6 attenuates the increase in resurgent currents and might decrease hyperexcitability observed in the LID model. However, selective disruption of FHF2B interaction with the C-terminus of Nav1.6 may prove to be difficult since the core binding region for Nav1.6 is conserved between FHF2A and FHF2B. Inadvertent disruption of the FHF2A interaction with Nav1.6 might end up exacerbating hyperexcitability by further reducing long-term inactivation.

An alternative strategy for a therapeutic intervention would be to increase FHF2A's long-term inactivation activity. We hypothesize that increasing long-term inactivation activity would reduce resurgent current generation and

hyperexcitability. Future studies might explore in-vivo overexpression of FHF2A in the LID model. An alternative approach would be to inject the long-term inactivation particle (175) in the form of a cell-penetrating peptide. Our preliminary in-vitro results with this approach are promising (Figure 31). The FHFA peptide sequence corresponding to FHF2A's long-term inactivation particle (175) was coupled with a transactivator of transcription (tat) motif to yield tatFHFA, a predicted cell membrane penetrating peptide (311). The tatFHFA peptide effectively reduced spontaneous activity in DRG neurons cultured from LID animals at POD5 (Figure 31A-B). In contrast, no spontaneous activity was observed in DRG neurons cultured from sham animals. Interestingly, the tatFHFA peptide also reduced spontaneous activity from DRG neurons transfected with Navβ4 (Figure 31C-D). Further studies are needed to confirm these results with additional controls such as a tat only peptide. Additional studies may also explore if tatFHFA is selective to Nav1.6. We speculate that it might not be. Therefore, one concern is that tatFHFA might have side effects that limit its therapeutic potential by targeting VGSCs in other parts of the body such as the CNS, heart or muscle tissues. For example, resurgent currents play a prominent role in the activity of cerebellar Purkinje neurons (17, 18, 167, 210). Reduction of cerebellar resurgent currents mediated by tatFHFA might impact motor coordination. Thus preliminary studies might explore the best dose and delivery method to minimize these side effects. Once optimized and proper controls are established, it will be interesting to see if the tatFHFA peptide can reduced hypersensitivity in the LID model or other pain models (16, 26).

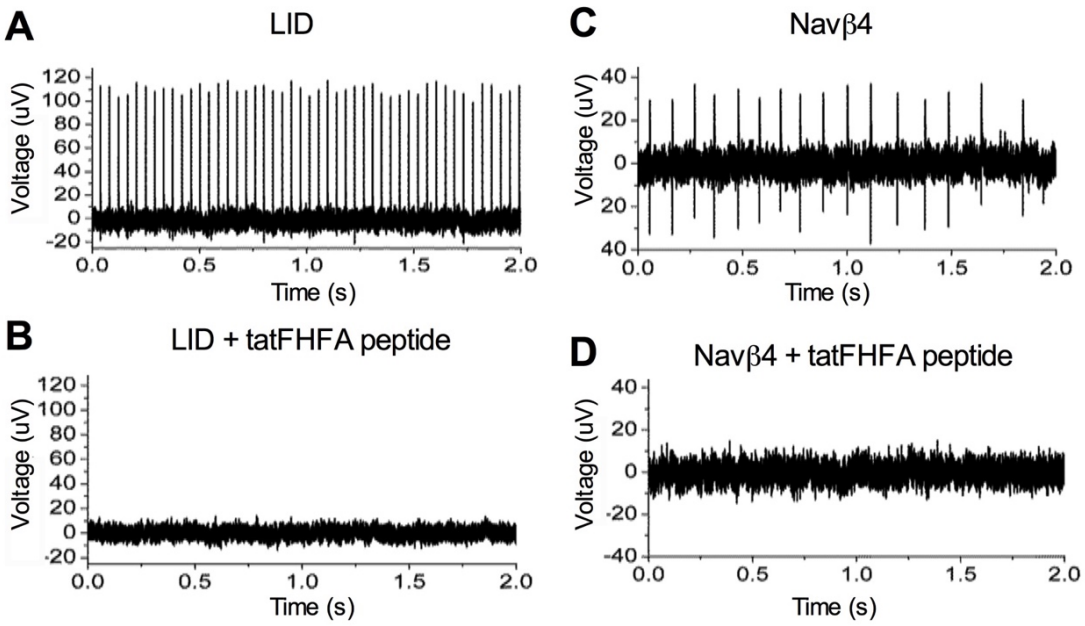

Figure 31: Preliminary results of tatFHFA peptide. ***A*****,** Representative trace of spontaneous activity recorded from cultured DRG neurons from a post operative day 5 animal that underwent LID surgery. No spontaneous activity was observed in sham control. ***B***, Spontaneous activity is abolished after a 20min incubation with tatFHFA peptide at a 1mM concentration. ***C***, Representative trace of spontaneous activity recorded from DRG neurons transfected with Navβ4. ***D***, After 20 min incubation with tatFHFA Navβ4 mediated spontaneous activity is abolished. Representative traces correspond to one electrode (n=1) from a multielectrode array unit which records extracellular activity from multiple neurons.

General Conclusions

Overall, this dissertation addressed key questions regarding the modulation of resurgent currents in DRG neurons. The results of this dissertation have provided key insights into how resurgent currents are modulated in normal and pathophysiological conditions such as inflammation. Our results can be integrated into a new working model for resurgent current modulation in DRG neurons (Figure 32), in which Navβ4 mediates resurgent currents, FHF2B enhances resurgent currents and FHF2A limits resurgent current generation. We propose these auxiliary subunits modulate resurgent currents and the biophysical

properties of Nav1.6 resulting in changes in neuronal excitability. In this manner, we propose that neuronal excitability can be modulated by enhancing or reducing resurgent currents. Regulatory auxiliary subunits may serve as alternative therapeutic targets to pore-forming Nav1.6. As such, our findings may prove to be useful for other conditions in which hyperexcitability contributes to the disorder. In, particularly, these results may be relevant to pathologies associated with enhanced resurgent currents such as epilepsy (312, 313).

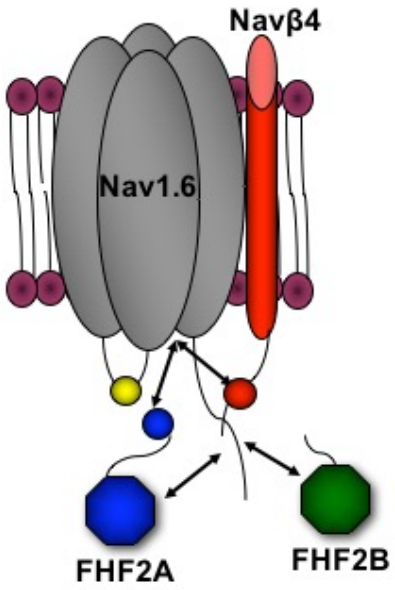

Figure 32: Proposed working model for Nav1.6 resurgent current modulation. Navβ4 (red cylinder) associates with Nav1.6 (grey tetramer). Part of C-terminal region of Navβ4, also known as the β4 peptide (red sphere), interacts with Nav1.6 to mediate resurgent currents. FHF2A (blue octagon) or FHF2B (green octagon) can bind to the C-terminal region of Nav1.6 and modulate biophysical properties of the channel. FHF2B binding delays fast inactivation (yellow sphere) increasing the probability of the β4 peptide interaction. FHF2A binding to the C-terminus of Nav1.6 also delays fast inactivation but introduces a new competitor which is the long-term inactivation particle (blue sphere) contained within FHF2A's N-terminal domain. If the long-term inactivation particle outcompetes the β4-peptide interaction it results in a decrease of resurgent current generation by Nav1.6.

REFERENCES

1. Relieving Pain in America: A Blueprint for Transforming Prevention, Care, Education, and Research. Washington (DC)2011.
2. Portenoy RK, Ugarte C, Fuller I, Haas G. Population-based survey of pain in the United States: differences among white, African American, and Hispanic subjects. J Pain. 2004;5(6):317-28. Epub 2004/09/01. doi: 10.1016/j.jpain.2004.05.005 S1526590004008247 [pii]. PubMed PMID: 15336636.
3. Dubin AE, Patapoutian A. Nociceptors: the sensors of the pain pathway. J Clin Invest. 2010;120(11):3760-72. doi: 10.1172/JCI42843. PubMed PMID: 21041958; PMCID: PMC2964977.
4. Baranauskas G, Nistri A. Sensitization of pain pathways in the spinal cord: cellular mechanisms. Progress in neurobiology. 1998;54(3):349-65. PubMed PMID: 9481803.
5. Millan MJ. The induction of pain: an integrative review. Progress in neurobiology. 1999;57(1):1-164. PubMed PMID: 9987804.
6. Cummins TR, Rush AM. Voltage-gated sodium channel blockers for the treatment of neuropathic pain. Expert Rev Neurother. 2007;7(11):1597-612. Epub 2007/11/14. doi: 10.1586/14737175.7.11.1597. PubMed PMID: 17997706.
7. Liu M, Wood JN. The roles of sodium channels in nociception: implications for mechanisms of neuropathic pain. Pain medicine. 2011;12 Suppl 3:S93-9. doi: 10.1111/j.1526-4637.2011.01158.x. PubMed PMID: 21752183.
8. Waxman SG, Dib-Hajj S, Cummins TR, Black JA. Sodium channels and pain. Proceedings of the National Academy of Sciences of the United States of America. 1999;96(14):7635-9. Epub 1999/07/08. PubMed PMID: 10393872; PMCID: 33593.
9. Dib-Hajj SD, Cummins TR, Black JA, Waxman SG. From genes to pain: Na v 1.7 and human pain disorders. Trends Neurosci. 2007;30(11):555-63. Epub 2007/10/24. doi: 10.1016/j.tins.2007.08.004. PubMed PMID: 17950472.
10. Cummins TR, Dib-Hajj SD, Black JA, Waxman SG. Sodium channels and the molecular pathophysiology of pain. Prog Brain Res. 2000;129:3-19. Epub 2000/12/01. doi: S0079-6123(00)29002-X [pii] 10.1016/S0079-6123(00)29002-X. PubMed PMID: 11098678.
11. Baker MD, Wood JN. Involvement of Na+ channels in pain pathways. Trends Pharmacol Sci. 2001;22(1):27-31. Epub 2001/02/13. doi: S0165-6147(00)01585-6 [pii]. PubMed PMID: 11165669.
12. Cummins TR, Sheets PL, Waxman SG. The roles of sodium channels in nociception: Implications for mechanisms of pain. Pain. 2007;131(3):243-57. Epub 2007/09/04. doi: S0304-3959(07)00430-7 [pii] 10.1016/j.pain.2007.07.026. PubMed PMID: 17766042; PMCID: 2055547.
13. Dib-Hajj SD, Cummins TR, Black JA, Waxman SG. Sodium channels in normal and pathological pain. Annu Rev Neurosci. 2010;33:325-47. Epub 2010/04/07. doi: 10.1146/annurev-neuro-060909-153234. PubMed PMID: 20367448.

14. Xie W, Strong JA, Ye L, Mao JX, Zhang J-M. Knockdown of sodium channel $Na_V1.6$ blocks mechanical pain and abnormal bursting activity of afferent neurons in inflamed sensory ganglia. Pain. 2013;154:1170-80.
15. Xie W, Strong JA, Zhang JM. Local knockdown of the Na1.6 sodium channel reduces pain behaviors, sensory neuron excitability, and sympathetic sprouting in rat models of neuropathic pain. Neuroscience. 2015. Epub 2015/02/18. doi: 10.1016/j.neuroscience.2015.02.010. PubMed PMID: 25686526.
16. Deuis JR, Zimmermann K, Romanovsky AA, Possani LD, Cabot PJ, Lewis RJ, Vetter I. An animal model of oxaliplatin-induced cold allodynia reveals a crucial role for Nav1.6 in peripheral pain pathways. Pain. 2013;154(9):1749-57. Epub 2013/05/29. doi: 10.1016/j.pain.2013.05.032. PubMed PMID: 23711479; PMCID: 3748219.
17. Khaliq ZM, Gouwens NW, Raman IM. The contribution of resurgent sodium current to high-frequency firing in Purkinje neurons: an experimental and modeling study. The Journal of neuroscience : the official journal of the Society for Neuroscience. 2003;23(12):4899-912. Epub 2003/07/02. doi: 23/12/4899 [pii]. PubMed PMID: 12832512.
18. Akemann W, Knopfel T. Interaction of Kv3 potassium channels and resurgent sodium current influences the rate of spontaneous firing of Purkinje neurons. The Journal of neuroscience : the official journal of the Society for Neuroscience. 2006;26(17):4602-12. Epub 2006/04/28. doi: 26/17/4602 [pii] 10.1523/JNEUROSCI.5204-05.2006. PubMed PMID: 16641240.
19. Jarecki BW, Piekarz AD, Jackson JO, 2nd, Cummins TR. Human voltage-gated sodium channel mutations that cause inherited neuronal and muscle channelopathies increase resurgent sodium currents. J Clin Invest. 2010;120(1):369-78. Epub 2009/12/30. doi: 10.1172/JCI40801 40801 [pii]. PubMed PMID: 20038812; PMCID: 2799199.
20. Sheets PL, Jackson JO, 2nd, Waxman SG, Dib-Hajj SD, Cummins TR. A Nav1.7 channel mutation associated with hereditary erythromelalgia contributes to neuronal hyperexcitability and displays reduced lidocaine sensitivity. The Journal of physiology. 2007;581(Pt 3):1019-31. Epub 2007/04/14. doi: jphysiol.2006.127027 [pii] 10.1113/jphysiol.2006.127027. PubMed PMID: 17430993; PMCID: 2170829.
21. Jarecki BW, Sheets PL, Jackson JO, 2nd, Cummins TR. Paroxysmal extreme pain disorder mutations within the D3/S4-S5 linker of Nav1.7 cause moderate destabilization of fast inactivation. The Journal of physiology. 2008;586(Pt 17):4137-53. Epub 2008/07/05. doi: 10.1113/jphysiol.2008.154906 jphysiol.2008.154906 [pii]. PubMed PMID: 18599537; PMCID: 2652197.
22. Dib-Hajj SD, Estacion M, Jarecki BW, Tyrrell L, Fischer TZ, Lawden M, Cummins TR, Waxman SG. Paroxysmal extreme pain disorder M1627K mutation in human Nav1.7 renders DRG neurons hyperexcitable. Mol Pain. 2008;4:37. Epub 2008/09/23. doi: 10.1186/1744-8069-4-37 1744-8069-4-37 [pii]. PubMed PMID: 18803825; PMCID: 2556659.
23. Klinger AB, Eberhardt M, Link AS, Namer B, Kutsche LK, Schuy ET, Sittl R, Hoffmann T, Alzheimer C, Huth T, Carr RW, Lampert A. Sea-anemone toxin ATX-II elicits A-fiber-dependent pain and enhances resurgent and persistent

sodium currents in large sensory neurons. Mol Pain. 2012;8:69. doi: 10.1186/1744-8069-8-69. PubMed PMID: 22978421; PMCID: 3495684.
24. Tan ZY, Priest BT, Krajewski JL, Knopp KL, Nisenbaum ES, Cummins TR. Protein kinase C enhances human sodium channel hNav1.7 resurgent currents via a serine residue in the domain III-IV linker. FEBS Lett. 2014;588(21):3964-9. doi: 10.1016/j.febslet.2014.09.011. PubMed PMID: 25240195.
25. Tan ZY, Piekarz AD, Priest BT, Knopp KL, Krajewski JL, McDermott JS, Nisenbaum ES, Cummins TR. Tetrodotoxin-resistant sodium channels in sensory neurons generate slow resurgent currents that are enhanced by inflammatory mediators. The Journal of neuroscience : the official journal of the Society for Neuroscience. 2014;34(21):7190-7. doi: 10.1523/JNEUROSCI.5011-13.2014. PubMed PMID: 24849353; PMCID: 4028496.
26. Sittl R, Lampert A, Huth T, Schuy ET, Link AS, Fleckenstein J, Alzheimer C, Grafe P, Carr RW. Anticancer drug oxaliplatin induces acute cooling-aggravated neuropathy via sodium channel subtype Na(V)1.6-resurgent and persistent current. Proceedings of the National Academy of Sciences of the United States of America. 2012;109(17):6704-9. Epub 2012/04/12. doi: 10.1073/pnas.1118058109
1118058109 [pii]. PubMed PMID: 22493249; PMCID: 3340057.
27. Cummins TR, Dib-Hajj SD, Herzog RI, Waxman SG. Nav1.6 channels generate resurgent sodium currents in spinal sensory neurons. FEBS Lett. 2005;579(10):2166-70. Epub 2005/04/07. doi: 10.1016/j.febslet.2005.03.009. PubMed PMID: 15811336.
28. Hodgkin AL, Huxley AF. The dual effect of membrane potential on sodium conductance in the giant axon of Loligo. The Journal of physiology. 1952;116(4):497-506. PubMed PMID: 14946715; PMCID: PMC1392212.
29. Hodgkin AL, Huxley AF. The components of membrane conductance in the giant axon of Loligo. The Journal of physiology. 1952;116(4):473-96. PubMed PMID: 14946714; PMCID: PMC1392209.
30. Hodgkin AL, Huxley AF. Currents carried by sodium and potassium ions through the membrane of the giant axon of Loligo. The Journal of physiology. 1952;116(4):449-72. PubMed PMID: 14946713; PMCID: PMC1392213.
31. Hodgkin AL, Huxley AF, Katz B. Measurement of current-voltage relations in the membrane of the giant axon of Loligo. The Journal of physiology. 1952;116(4):424-48. PubMed PMID: 14946712; PMCID: PMC1392219.
32. Cole KS. Dynamic electrical characteristics of squid axon membrane. Arch Sci Physiol. 1949;3:253-8.
33. Marmont G. Studies on the axon membrane; a new method. Journal of cellular physiology. 1949;34(3):351-82. PubMed PMID: 15406358.
34. Hodgkin AL, Huxley AF. A quantitative description of membrane current and its application to conduction and excitation in nerve. The Journal of physiology. 1952;117(4):500-44. Epub 1952/08/01. PubMed PMID: 12991237; PMCID: 1392413.
35. Hille B. The receptor for tetrodotoxin and saxitoxin. A structural hypothesis. Biophysical journal. 1975;15(6):615-9. doi: 10.1016/S0006-3495(75)85842-5. PubMed PMID: 1148362; PMCID: PMC1334742.

36. Hille B. Pharmacological modifications of the sodium channels of frog nerve. The Journal of general physiology. 1968;51(2):199-219. PubMed PMID: 5641635; PMCID: PMC2201123.
37. Narahashi T, Haas HG, Therrien EF. Saxitoxin and tetrodotoxin: comparison of nerve blocking mechanism. Science. 1967;157(3795):1441-2. PubMed PMID: 6037860.
38. Narahashi T, Moore JW, Scott WR. Tetrodotoxin Blockage of Sodium Conductance Increase in Lobster Giant Axons. The Journal of general physiology. 1964;47:965-74. PubMed PMID: 14155438; PMCID: PMC2195365.
39. Nakamura Y, Nakajima S, Grundfest H. The action of tetrodotoxin on electrogenic components of squid giant axons. The Journal of general physiology. 1965;48(6):975-96. PubMed PMID: 5855512; PMCID: PMC2195447.
40. Armstrong CM, Hille B. The inner quaternary ammonium ion receptor in potassium channels of the node of Ranvier. The Journal of general physiology. 1972;59(4):388-400. PubMed PMID: 4112955; PMCID: PMC2203187.
41. Tasaki I, Hagiwar AS. Demonstration of two stable potential states in the squid giant axon under tetraethylammonium chloride. The Journal of general physiology. 1957;40(6):859-85. PubMed PMID: 13439165; PMCID: PMC2147584.
42. Hille B. The permeability of the sodium channel to organic cations in myelinated nerve. The Journal of general physiology. 1971;58(6):599-619. PubMed PMID: 5315827; PMCID: PMC2226049.
43. Hille B. The permeability of the sodium channel to metal cations in myelinated nerve. The Journal of general physiology. 1972;59(6):637-58. PubMed PMID: 5025743; PMCID: PMC2203202.
44. Hille B. Ionic selectivity, saturation, and block in sodium channels. A four-barrier model. The Journal of general physiology. 1975;66(5):535-60. PubMed PMID: 1194886; PMCID: PMC2226224.
45. Armstrong CM, Bezanilla F. Currents related to movement of the gating particles of the sodium channels. Nature. 1973;242(5398):459-61. PubMed PMID: 4700900.
46. Hille B, Woodhull AM, Shapiro BI. Negative surface charge near sodium channels of nerve: divalent ions, monovalent ions, and pH. Philos Trans R Soc Lond B Biol Sci. 1975;270(908):301-18. PubMed PMID: 238230.
47. Hille B. An essential ionized acid group in sodium channels. Fed Proc. 1975;34(5):1318-21. PubMed PMID: 235474.
48. Armstrong CM, Bezanilla F, Rojas E. Destruction of sodium conductance inactivation in squid axons perfused with pronase. The Journal of general physiology. 1973;62(4):375-91. PubMed PMID: 4755846; PMCID: PMC2226121.
49. Beneski DA, Catterall WA. Covalent labeling of protein components of the sodium channel with a photoactivable derivative of scorpion toxin. Proceedings of the National Academy of Sciences of the United States of America. 1980;77(1):639-43. PubMed PMID: 6928649; PMCID: PMC348330.
50. Hartshorne RP, Catterall WA. Purification of the saxitoxin receptor of the sodium channel from rat brain. Proceedings of the National Academy of Sciences

of the United States of America. 1981;78(7):4620-4. PubMed PMID: 6270687; PMCID: PMC319845.
51. Hartshorne RP, Messner DJ, Coppersmith JC, Catterall WA. The saxitoxin receptor of the sodium channel from rat brain. Evidence for two nonidentical beta subunits. The Journal of biological chemistry. 1982;257(23):13888-91. PubMed PMID: 6292214.
52. Noda M, Ikeda T, Suzuki H, Takeshima H, Takahashi T, Kuno M, Numa S. Expression of functional sodium channels from cloned cDNA. Nature. 1986;322(6082):826-8. PubMed PMID: 2427955.
53. Noda M, Shimizu S, Tanabe T, Takai T, Kayano T, Ikeda T, Takahashi H, Nakayama H, Kanaoka Y, Minamino N, et al. Primary structure of Electrophorus electricus sodium channel deduced from cDNA sequence. Nature. 1984;312(5990):121-7. Epub 1984/11/08. PubMed PMID: 6209577.
54. Sakmann B, Neher E. Patch clamp techniques for studying ionic channels in excitable membranes. Annu Rev Physiol. 1984;46:455-72. doi: 10.1146/annurev.ph.46.030184.002323. PubMed PMID: 6143532.
55. Hamill OP, Marty A, Neher E, Sakmann B, Sigworth FJ. Improved patch-clamp techniques for high-resolution current recording from cells and cell-free membrane patches. Pflugers Arch. 1981;391(2):85-100. PubMed PMID: 6270629.
56. Hille B. Ion Channels of Excitable Membranes. Third ed. Sunderland, MA: Sinauer Associates, Inc; 2001.
57. Payandeh J, Scheuer T, Zheng N, Catterall WA. The crystal structure of a voltage-gated sodium channel. Nature. 2011;475(7356):353-8. Epub 2011/07/12. doi: 10.1038/nature10238. PubMed PMID: 21743477; PMCID: 3266868.
58. Catterall WA. From ionic currents to molecular mechanisms: the structure and function of voltage-gated sodium channels. Neuron. 2000;26(1):13-25. Epub 2000/05/08. doi: S0896-6273(00)81133-2 [pii]. PubMed PMID: 10798388.
59. West JW, Patton DE, Scheuer T, Wang Y, Goldin AL, Catterall WA. A cluster of hydrophobic amino acid residues required for fast Na(+)-channel inactivation. Proceedings of the National Academy of Sciences of the United States of America. 1992;89(22):10910-4. Epub 1992/11/15. PubMed PMID: 1332060; PMCID: 50452.
60. Moorman JR, Kirsch GE, Brown AM, Joho RH. Changes in sodium channel gating produced by point mutations in a cytoplasmic linker. Science. 1990;250(4981):688-91. PubMed PMID: 2173138.
61. Armstrong CM, Bezanilla F. Charge movement associated with the opening and closing of the activation gates of the Na channels. The Journal of general physiology. 1974;63(5):533-52. PubMed PMID: 4824995; PMCID: 2203568.
62. de Lera Ruiz M, Kraus RL. Voltage-Gated Sodium Channels: Structure, Function, Pharmacology, and Clinical Indications. Journal of medicinal chemistry. 2015;58(18):7093-118. doi: 10.1021/jm501981g. PubMed PMID: 25927480.
63. Trimmer JS, Cooperman SS, Tomiko SA, Zhou JY, Crean SM, Boyle MB, Kallen RG, Sheng ZH, Barchi RL, Sigworth FJ, et al. Primary structure and

functional expression of a mammalian skeletal muscle sodium channel. Neuron. 1989;3(1):33-49. Epub 1989/07/01. PubMed PMID: 2559760.
64. Rogart RB, Cribbs LL, Muglia LK, Kephart DD, Kaiser MW. Molecular cloning of a putative tetrodotoxin-resistant rat heart Na+ channel isoform. Proceedings of the National Academy of Sciences of the United States of America. 1989;86(20):8170-4. PubMed PMID: 2554302; PMCID: PMC298237.
65. Beckh S, Noda M, Lubbert H, Numa S. Differential regulation of three sodium channel messenger RNAs in the rat central nervous system during development. The EMBO journal. 1989;8(12):3611-6. Epub 1989/12/01. PubMed PMID: 2555170; PMCID: 402042.
66. Trimmer JS, Rhodes KJ. Localization of voltage-gated ion channels in mammalian brain. Annu Rev Physiol. 2004;66:477-519. doi: 10.1146/annurev.physiol.66.032102.113328. PubMed PMID: 14977411.
67. Kwong K, Carr MJ. Voltage-gated sodium channels. Curr Opin Pharmacol. 2015;22:131-9. doi: 10.1016/j.coph.2015.04.007. PubMed PMID: 26043074.
68. Devor M. Unexplained peculiarities of the dorsal root ganglion. Pain. 1999;Suppl 6:S27-35. Epub 1999/09/24. PubMed PMID: 10491970.
69. Rush AM, Cummins TR, Waxman SG. Multiple sodium channels and their roles in electrogenesis within dorsal root ganglion neurons. The Journal of physiology. 2007;579(Pt 1):1-14. Epub 2006/12/13. doi: jphysiol.2006.121483 [pii]
10.1113/jphysiol.2006.121483. PubMed PMID: 17158175; PMCID: 2075388.
70. Caffrey JM, Eng DL, Black JA, Waxman SG, Kocsis JD. Three types of sodium channels in adult rat dorsal root ganglion neurons. Brain Res. 1992;592(1-2):283-97. PubMed PMID: 1280518.
71. Waxman SG, Kocsis JD, Black JA. Type III sodium channel mRNA is expressed in embryonic but not adult spinal sensory neurons, and is reexpressed following axotomy. Journal of neurophysiology. 1994;72(1):466-70. PubMed PMID: 7965028.
72. Crill WE. Persistent sodium current in mammalian central neurons. Annu Rev Physiol. 1996;58:349-62. PubMed PMID: 8815799.
73. Taddese A, Bean BP. Subthreshold sodium current from rapidly inactivating sodium channels drives spontaneous firing of tuberomammillary neurons. Neuron. 2002;33(4):587-600. PubMed PMID: 11856532.
74. Elliott AA, Elliott JR. Characterization of TTX-sensitive and TTX-resistant sodium currents in small cells from adult rat dorsal root ganglia. The Journal of physiology. 1993;463:39-56. PubMed PMID: 8246189; PMCID: 1175332.
75. Cummins TR, Dib-Hajj SD, Black JA, Akopian AN, Wood JN, Waxman SG. A novel persistent tetrodotoxin-resistant sodium current in SNS-null and wild-type small primary sensory neurons. The Journal of neuroscience : the official journal of the Society for Neuroscience. 1999;19(24):RC43. PubMed PMID: 10594087.
76. Habib AM, Wood JN, Cox JJ. Sodium channels and pain. Handb Exp Pharmacol. 2015;227:39-56. Epub 2015/04/08. doi: 10.1007/978-3-662-46450-2_3. PubMed PMID: 25846613.

77. Blair NT, Bean BP. Roles of tetrodotoxin (TTX)-sensitive Na+ current, TTX-resistant Na+ current, and Ca2+ current in the action potentials of nociceptive sensory neurons. The Journal of neuroscience : the official journal of the Society for Neuroscience. 2002;22(23):10277-90. Epub 2002/11/27. doi: 22/23/10277 [pii]. PubMed PMID: 12451128.
78. Renganathan M, Cummins TR, Waxman SG. Contribution of Na(v)1.8 sodium channels to action potential electrogenesis in DRG neurons. Journal of neurophysiology. 2001;86(2):629-40. Epub 2001/08/10. PubMed PMID: 11495938.
79. Renganathan M, Dib-Hajj S, Waxman SG. Na(v)1.5 underlies the 'third TTX-R sodium current' in rat small DRG neurons. Brain research Molecular brain research. 2002;106(1-2):70-82. Epub 2002/10/24. PubMed PMID: 12393266.
80. Kerr NC, Gao Z, Holmes FE, Hobson SA, Hancox JC, Wynick D, James AF. The sodium channel Nav1.5a is the predominant isoform expressed in adult mouse dorsal root ganglia and exhibits distinct inactivation properties from the full-length Nav1.5 channel. Molecular and cellular neurosciences. 2007;35(2):283-91. Epub 2007/04/17. doi: 10.1016/j.mcn.2007.03.002. PubMed PMID: 17433712; PMCID: 2726334.
81. Beaulieu P, International Association for the Study of Pain. Pharmacology of pain. Seattle, WA: IASP Press; 2010. xiv, 622 p. p.
82. Djouhri L, Lawson SN. Abeta-fiber nociceptive primary afferent neurons: a review of incidence and properties in relation to other afferent A-fiber neurons in mammals. Brain research Brain research reviews. 2004;46(2):131-45. Epub 2004/10/07. doi: 10.1016/j.brainresrev.2004.07.015. PubMed PMID: 15464202.
83. Ho C, O'Leary ME. Single-cell analysis of sodium channel expression in dorsal root ganglion neurons. Molecular and cellular neurosciences. 2011;46(1):159-66. Epub 2010/09/08. doi: 10.1016/j.mcn.2010.08.017 S1044-7431(10)00208-3 [pii]. PubMed PMID: 20816971; PMCID: 3005531.
84. Djouhri L, Fang X, Okuse K, Wood JN, Berry CM, Lawson SN. The TTX-resistant sodium channel Nav1.8 (SNS/PN3): expression and correlation with membrane properties in rat nociceptive primary afferent neurons. The Journal of physiology. 2003;550(Pt 3):739-52. Epub 2003/06/10. doi: 10.1113/jphysiol.2003.042127. PubMed PMID: 12794175; PMCID: 2343087.
85. Shields SD, Ahn HS, Yang Y, Han C, Seal RP, Wood JN, Waxman SG, Dib-Hajj SD. Nav1.8 expression is not restricted to nociceptors in mouse peripheral nervous system. Pain. 2012;153(10):2017-30. Epub 2012/06/19. doi: 10.1016/j.pain.2012.04.022. PubMed PMID: 22703890.
86. Ramachandra R, McGrew SY, Baxter JC, Howard JR, Elmslie KS. NaV1.8 channels are expressed in large, as well as small, diameter sensory afferent neurons. Channels. 2013;7(1):34-7. Epub 2012/10/16. doi: 10.4161/chan.22445. PubMed PMID: 23064159; PMCID: 3589279.
87. Okuse K, Chaplan SR, McMahon SB, Luo ZD, Calcutt NA, Scott BP, Akopian AN, Wood JN. Regulation of expression of the sensory neuron-specific sodium channel SNS in inflammatory and neuropathic pain. Molecular and cellular neurosciences. 1997;10(3-4):196-207. PubMed PMID: 9532581.

88. Cummins TR, Waxman SG. Downregulation of tetrodotoxin-resistant sodium currents and upregulation of a rapidly repriming tetrodotoxin-sensitive sodium current in small spinal sensory neurons after nerve injury. The Journal of neuroscience : the official journal of the Society for Neuroscience. 1997;17(10):3503-14. Epub 1997/05/15. PubMed PMID: 9133375.
89. Tanaka M, Cummins TR, Ishikawa K, Dib-Hajj SD, Black JA, Waxman SG. SNS Na+ channel expression increases in dorsal root ganglion neurons in the carrageenan inflammatory pain model. Neuroreport. 1998;9(6):967-72. PubMed PMID: 9601651.
90. Dib-Hajj SD, Fjell J, Cummins TR, Zheng Z, Fried K, LaMotte R, Black JA, Waxman SG. Plasticity of sodium channel expression in DRG neurons in the chronic constriction injury model of neuropathic pain. Pain. 1999;83(3):591-600. Epub 1999/11/24. doi: S0304395999001694 [pii]. PubMed PMID: 10568868.
91. Gold MS, Reichling DB, Shuster MJ, Levine JD. Hyperalgesic agents increase a tetrodotoxin-resistant Na+ current in nociceptors. Proceedings of the National Academy of Sciences of the United States of America. 1996;93(3):1108-12. PubMed PMID: 8577723.
92. Faber CG, Lauria G, Merkies IS, Cheng X, Han C, Ahn HS, Persson AK, Hoeijmakers JG, Gerrits MM, Pierro T, Lombardi R, Kapetis D, Dib-Hajj SD, Waxman SG. Gain-of-function Nav1.8 mutations in painful neuropathy. Proceedings of the National Academy of Sciences of the United States of America. 2012;109(47):19444-9. Epub 2012/11/02. doi: 10.1073/pnas.1216080109
1216080109 [pii]. PubMed PMID: 23115331; PMCID: 3511073.
93. Han C, Vasylyev D, Macala LJ, Gerrits MM, Hoeijmakers JG, Bekelaar KJ, Dib-Hajj SD, Faber CG, Merkies IS, Waxman SG. The G1662S NaV1.8 mutation in small fibre neuropathy: impaired inactivation underlying DRG neuron hyperexcitability. J Neurol Neurosurg Psychiatry. 2014;85(5):499-505. Epub 2013/09/06. doi: 10.1136/jnnp-2013-306095
jnnp-2013-306095 [pii]. PubMed PMID: 24006052.
94. Zhang XY, Wen J, Yang W, Wang C, Gao L, Zheng LH, Wang T, Ran K, Li Y, Li X, Xu M, Luo J, Feng S, Ma X, Ma H, Chai Z, Zhou Z, Yao J, Zhang X, Liu JY. Gain-of-function mutations in SCN11A cause familial episodic pain. Am J Hum Genet. 2013;93(5):957-66. Epub 2013/11/12. doi: 10.1016/j.ajhg.2013.09.016
S0002-9297(13)00456-4 [pii]. PubMed PMID: 24207120; PMCID: 3824123.
95. Huang J, Han C, Estacion M, Vasylyev D, Hoeijmakers JG, Gerrits MM, Tyrrell L, Lauria G, Faber CG, Dib-Hajj SD, Merkies IS, Waxman SG. Gain-of-function mutations in sodium channel Na(v)1.9 in painful neuropathy. Brain. 2014;137(Pt 6):1627-42. Epub 2014/04/30. doi: 10.1093/brain/awu079
awu079 [pii]. PubMed PMID: 24776970.
96. Leipold E, Liebmann L, Korenke GC, Heinrich T, Giesselmann S, Baets J, Ebbinghaus M, Goral RO, Stodberg T, Hennings JC, Bergmann M, Altmuller J, Thiele H, Wetzel A, Nurnberg P, Timmerman V, De Jonghe P, Blum R, Schaible HG, Weis J, Heinemann SH, Hubner CA, Kurth I. A de novo gain-of-function

mutation in SCN11A causes loss of pain perception. Nat Genet. 2013;45(11):1399-404. Epub 2013/09/17. doi: 10.1038/ng.2767 ng.2767 [pii]. PubMed PMID: 24036948.
97. Fertleman CR, Baker MD, Parker KA, Moffatt S, Elmslie FV, Abrahamsen B, Ostman J, Klugbauer N, Wood JN, Gardiner RM, Rees M. SCN9A mutations in paroxysmal extreme pain disorder: allelic variants underlie distinct channel defects and phenotypes. Neuron. 2006;52(5):767-74. doi: 10.1016/j.neuron.2006.10.006. PubMed PMID: 17145499.
98. Jarecki BW, Sheets PL, Jackson Ii JO, Cummins TR. Paroxysmal Extreme Pain Disorder mutations within the D3/S4-S5 Linker of Nav1.7 cause moderate destabilization of fast-inactivation. The Journal of physiology. 2008. PubMed PMID: 18599537.
99. Cox JJ, Reimann F, Nicholas AK, Thornton G, Roberts E, Springell K, Karbani G, Jafri H, Mannan J, Raashid Y, Al-Gazali L, Hamamy H, Valente EM, Gorman S, Williams R, McHale DP, Wood JN, Gribble FM, Woods CG. An SCN9A channelopathy causes congenital inability to experience pain. Nature. 2006;444(7121):894-8. doi: 10.1038/nature05413. PubMed PMID: 17167479.
100. Goldberg YP, MacFarlane J, MacDonald ML, Thompson J, Dube MP, Mattice M, Fraser R, Young C, Hossain S, Pape T, Payne B, Radomski C, Donaldson G, Ives E, Cox J, Younghusband HB, Green R, Duff A, Boltshauser E, Grinspan GA, Dimon JH, Sibley BG, Andria G, Toscano E, Kerdraon J, Bowsher D, Pimstone SN, Samuels ME, Sherrington R, Hayden MR. Loss-of-function mutations in the Nav1.7 gene underlie congenital indifference to pain in multiple human populations. Clinical genetics. 2007;71(4):311-9. doi: 10.1111/j.1399-0004.2007.00790.x. PubMed PMID: 17470132.
101. Minett MS, Falk S, Santana-Varela S, Bogdanov YD, Nassar MA, Heegaard AM, Wood JN. Pain without nociceptors? Nav1.7-independent pain mechanisms. Cell Rep. 2014;6(2):301-12. doi: 10.1016/j.celrep.2013.12.033. PubMed PMID: 24440715; PMCID: PMC3969273.
102. Burgess DL, Kohrman DC, Galt J, Plummer NW, Jones JM, Spear B, Meisler MH. Mutation of a new sodium channel gene, Scn8a, in the mouse mutant 'motor endplate disease'. Nat Genet. 1995;10(4):461-5. doi: 10.1038/ng0895-461. PubMed PMID: 7670495.
103. Schaller KL, Caldwell JH. Developmental and regional expression of sodium channel isoform NaCh6 in the rat central nervous system. J Comp Neurol. 2000;420(1):84-97. PubMed PMID: 10745221.
104. Schaller KL, Krzemien DM, Yarowsky PJ, Krueger BK, Caldwell JH. A novel, abundant sodium channel expressed in neurons and glia. The Journal of neuroscience : the official journal of the Society for Neuroscience. 1995;15(5 Pt 1):3231-42. PubMed PMID: 7751906.
105. Tzoumaka E, Tischler AC, Sangameswaran L, Eglen RM, Hunter JC, Novakovic SD. Differential distribution of the tetrodotoxin-sensitive rPN4/NaCh6/Scn8a sodium channel in the nervous system. J Neurosci Res. 2000;60(1):37-44. PubMed PMID: 10723066.
106. Musarella M, Alcaraz G, Caillol G, Boudier JL, Couraud F, Autillo-Touati A. Expression of Nav1.6 sodium channels by Schwann cells at neuromuscular

junctions: role in the motor endplate disease phenotype. Glia. 2006;53(1):13-23. doi: 10.1002/glia.20252. PubMed PMID: 16078241.
107. Noujaim SF, Kaur K, Milstein M, Jones JM, Furspan P, Jiang D, Auerbach DS, Herron T, Meisler MH, Jalife J. A null mutation of the neuronal sodium channel NaV1.6 disrupts action potential propagation and excitation-contraction coupling in the mouse heart. FASEB J. 2012;26(1):63-72. doi: 10.1096/fj.10-179770. PubMed PMID: 21948246; PMCID: PMC3250234.
108. Craner MJ, Damarjian TG, Liu S, Hains BC, Lo AC, Black JA, Newcombe J, Cuzner ML, Waxman SG. Sodium channels contribute to microglia/macrophage activation and function in EAE and MS. Glia. 2005;49(2):220-9. doi: 10.1002/glia.20112. PubMed PMID: 15390090.
109. Black JA, Liu S, Waxman SG. Sodium channel activity modulates multiple functions in microglia. Glia. 2009;57(10):1072-81. doi: 10.1002/glia.20830. PubMed PMID: 19115387.
110. Blanchard MG, Willemsen MH, Walker JB, Dib-Hajj SD, Waxman SG, Jongmans MC, Kleefstra T, van de Warrenburg BP, Praamstra P, Nicolai J, Yntema HG, Bindels RJ, Meisler MH, Kamsteeg EJ. De novo gain-of-function and loss-of-function mutations of SCN8A in patients with intellectual disabilities and epilepsy. J Med Genet. 2015;52(5):330-7. doi: 10.1136/jmedgenet-2014-102813. PubMed PMID: 25725044; PMCID: PMC4413743.
111. Ohba C, Kato M, Takahashi S, Lerman-Sagie T, Lev D, Terashima H, Kubota M, Kawawaki H, Matsufuji M, Kojima Y, Tateno A, Goldberg-Stern H, Straussberg R, Marom D, Leshinsky-Silver E, Nakashima M, Nishiyama K, Tsurusaki Y, Miyake N, Tanaka F, Matsumoto N, Saitsu H. Early onset epileptic encephalopathy caused by de novo SCN8A mutations. Epilepsia. 2014;55(7):994-1000. doi: 10.1111/epi.12668. PubMed PMID: 24888894.
112. O'Brien JE, Meisler MH. Sodium channel SCN8A (Nav1.6): properties and de novo mutations in epileptic encephalopathy and intellectual disability. Front Genet. 2013;4:213. doi: 10.3389/fgene.2013.00213. PubMed PMID: 24194747; PMCID: PMC3809569.
113. Jones JM, Dionne L, Dell'Orco J, Parent R, Krueger JN, Cheng X, Dib-Hajj SD, Bunton-Stasyshyn RK, Sharkey LM, Dowling JJ, Murphy GG, Shakkottai VG, Shrager P, Meisler MH. Single amino acid deletion in transmembrane segment D4S6 of sodium channel Scn8a (Nav1.6) in a mouse mutant with a chronic movement disorder. Neurobiol Dis. 2016;89:36-45. doi: 10.1016/j.nbd.2016.01.018. PubMed PMID: 26807988.
114. Meisler MH, Plummer NW, Burgess DL, Buchner DA, Sprunger LK. Allelic mutations of the sodium channel SCN8A reveal multiple cellular and physiological functions. Genetica. 2004;122(1):37-45. PubMed PMID: 15619959.
115. Strong JA, Xie W, Bataille FJ, Zhang JM. Preclinical studies of low back pain. Mol Pain. 2013;9:17. Epub 2013/03/30. doi: 10.1186/1744-8069-9-17 1744-8069-9-17 [pii]. PubMed PMID: 23537369; PMCID: 3617092.
116. Xie WR, Deng H, Li H, Bowen TL, Strong JA, Zhang JM. Robust increase of cutaneous sensitivity, cytokine production and sympathetic sprouting in rats with localized inflammatory irritation of the spinal ganglia. Neuroscience.

2006;142(3):809-22. doi: 10.1016/j.neuroscience.2006.06.045. PubMed PMID: 16887276; PMCID: PMC1661830.
117. Zhang JM, Song XJ, LaMotte RH. Enhanced excitability of sensory neurons in rats with cutaneous hyperalgesia produced by chronic compression of the dorsal root ganglion. Journal of neurophysiology. 1999;82(6):3359-66. PubMed PMID: 10601467.
118. Song XJ, Hu SJ, Greenquist KW, Zhang JM, LaMotte RH. Mechanical and thermal hyperalgesia and ectopic neuronal discharge after chronic compression of dorsal root ganglia. Journal of neurophysiology. 1999;82(6):3347-58. PubMed PMID: 10601466.
119. Xie W, Strong JA, Meij JT, Zhang JM, Yu L. Neuropathic pain: early spontaneous afferent activity is the trigger. Pain. 2005;116(3):243-56. doi: 10.1016/j.pain.2005.04.017. PubMed PMID: 15964687; PMCID: PMC1343516.
120. Xie W, Strong JA, Zhang JM. Increased excitability and spontaneous activity of rat sensory neurons following in vitro stimulation of sympathetic fiber sprouts in the isolated dorsal root ganglion. Pain. 2010;151(2):447-59. doi: 10.1016/j.pain.2010.08.006. PubMed PMID: 20800969; PMCID: PMC2955761.
121. Xie W, Strong JA, Li H, Zhang J-M. Sympathetic sprouting near sensory neurons after nerve injury occurs preferentially on spontaneously active cells and is reduced by early nerve block. Journal of neurophysiology. 2007;97(1):492-502. PubMed PMID: 17065247.
122. Loh L, Nathan PW. Painful peripheral states and sympathetic blocks. J Neurol Neurosurg Psychiatry. 1978;41(7):664-71. PubMed PMID: 690645; PMCID: PMC493113.
123. Saif MW, Reardon J. Management of oxaliplatin-induced peripheral neuropathy. Ther Clin Risk Manag. 2005;1(4):249-58. PubMed PMID: 18360567; PMCID: PMC1661634.
124. Argyriou AA, Polychronopoulos P, Iconomou G, Chroni E, Kalofonos HP. A review on oxaliplatin-induced peripheral nerve damage. Cancer Treat Rev. 2008;34(4):368-77. doi: 10.1016/j.ctrv.2008.01.003. PubMed PMID: 18281158.
125. Webster RG, Brain KL, Wilson RH, Grem JL, Vincent A. Oxaliplatin induces hyperexcitability at motor and autonomic neuromuscular junctions through effects on voltage-gated sodium channels. Br J Pharmacol. 2005;146(7):1027-39. doi: 10.1038/sj.bjp.0706407. PubMed PMID: 16231011; PMCID: PMC1751225.
126. Adelsberger H, Quasthoff S, Grosskreutz J, Lepier A, Eckel F, Lersch C. The chemotherapeutic oxaliplatin alters voltage-gated Na(+) channel kinetics on rat sensory neurons. Eur J Pharmacol. 2000;406(1):25-32. PubMed PMID: 11011028.
127. Grolleau F, Gamelin L, Boisdron-Celle M, Lapied B, Pelhate M, Gamelin E. A possible explanation for a neurotoxic effect of the anticancer agent oxaliplatin on neuronal voltage-gated sodium channels. Journal of neurophysiology. 2001;85(5):2293-7. PubMed PMID: 11353042.
128. Henry MA, Freking AR, Johnson LR, Levinson SR. Sodium channel Nav1.6 accumulates at the site of infraorbital nerve injury. BMC neuroscience.

2007;8:56. Epub 2007/07/31. doi: 10.1186/1471-2202-8-56. PubMed PMID: 17662136; PMCID: 1941742.
129. Susuki K. Node of Ranvier disruption as a cause of neurological diseases. ASN Neuro. 2013;5(3):209-19. doi: 10.1042/AN20130025. PubMed PMID: 23834220; PMCID: PMC3736360.
130. Craner MJ, Klein JP, Renganathan M, Black JA, Waxman SG. Changes of sodium channel expression in experimental painful diabetic neuropathy. Annals of neurology. 2002;52(6):786-92. Epub 2002/11/26. doi: 10.1002/ana.10364. PubMed PMID: 12447933.
131. Hong S, Morrow TJ, Paulson PE, Isom LL, Wiley JW. Early painful diabetic neuropathy is associated with differential changes in tetrodotoxin-sensitive and -resistant sodium channels in dorsal root ganglion neurons in the rat. The Journal of biological chemistry. 2004;279(28):29341-50. Epub 2004/05/05. doi: 10.1074/jbc.M404167200. PubMed PMID: 15123645; PMCID: 1828032.
132. Ren YS, Qian NS, Tang Y, Liao YH, Yang YL, Dou KF, Toi M. Sodium channel Nav1.6 is up-regulated in the dorsal root ganglia in a mouse model of type 2 diabetes. Brain Res Bull. 2012;87(2-3):244-9. doi: 10.1016/j.brainresbull.2011.10.015. PubMed PMID: 22075254.
133. Chahine M, O'Leary ME. Regulatory Role of Voltage-Gated Na Channel beta Subunits in Sensory Neurons. Front Pharmacol. 2011;2:70. Epub 2011/11/30. doi: 10.3389/fphar.2011.00070. PubMed PMID: 22125538; PMCID: 3221288.
134. Zhang X, Bao L, Yang L, Wu Q, Li S. Roles of intracellular fibroblast growth factors in neural development and functions. Sci China Life Sci. 2012;55(12):1038-44. doi: 10.1007/s11427-012-4412-x. PubMed PMID: 23233218.
135. Isom LL. Sodium channel beta subunits: anything but auxiliary. Neuroscientist. 2001;7(1):42-54. PubMed PMID: 11486343.
136. Patino GA, Isom LL. Electrophysiology and beyond: multiple roles of Na+ channel beta subunits in development and disease. Neurosci Lett. 2010;486(2):53-9. Epub 2010/07/06. doi: 10.1016/j.neulet.2010.06.050 S0304-3940(10)00810-4 [pii]. PubMed PMID: 20600605; PMCID: 2964441.
137. Catterall WA, Goldin AL, Waxman SG. International Union of Pharmacology. XLVII. Nomenclature and structure-function relationships of voltage-gated sodium channels. Pharmacol Rev. 2005;57(4):397-409. Epub 2005/12/31. doi: 57/4/397 [pii]
10.1124/pr.57.4.4. PubMed PMID: 16382098.
138. Ho C, Zhao J, Malinowski S, Chahine M, O'Leary ME. Differential expression of sodium channel beta subunits in dorsal root ganglion sensory neurons. The Journal of biological chemistry. 2012;287(18):15044-53. doi: 10.1074/jbc.M111.333740. PubMed PMID: 22408255; PMCID: 3340221.
139. Takahashi N, Kikuchi S, Dai Y, Kobayashi K, Fukuoka T, Noguchi K. Expression of auxiliary beta subunits of sodium channels in primary afferent neurons and the effect of nerve injury. Neuroscience. 2003;121(2):441-50. Epub 2003/10/03. PubMed PMID: 14522002.

140. O'Malley HA, Isom LL. Sodium channel beta subunits: emerging targets in channelopathies. Annu Rev Physiol. 2015;77:481-504. doi: 10.1146/annurev-physiol-021014-071846. PubMed PMID: 25668026.
141. Lopez-Santiago LF, Pertin M, Morisod X, Chen C, Hong S, Wiley J, Decosterd I, Isom LL. Sodium channel beta2 subunits regulate tetrodotoxin-sensitive sodium channels in small dorsal root ganglion neurons and modulate the response to pain. The Journal of neuroscience : the official journal of the Society for Neuroscience. 2006;26(30):7984-94. doi: 10.1523/JNEUROSCI.2211-06.2006. PubMed PMID: 16870743.
142. Lopez-Santiago LF, Brackenbury WJ, Chen C, Isom LL. Na+ channel Scn1b gene regulates dorsal root ganglion nociceptor excitability in vivo. The Journal of biological chemistry. 2011;286(26):22913-23. doi: 10.1074/jbc.M111.242370. PubMed PMID: 21555511; PMCID: PMC3123059.
143. Shah BS, Stevens EB, Gonzalez MI, Bramwell S, Pinnock RD, Lee K, Dixon AK. beta3, a novel auxiliary subunit for the voltage-gated sodium channel, is expressed preferentially in sensory neurons and is upregulated in the chronic constriction injury model of neuropathic pain. Eur J Neurosci. 2000;12(11):3985-90. PubMed PMID: 11069594.
144. Shah BS, Gonzalez MI, Bramwell S, Pinnock RD, Lee K, Dixon AK. Beta3, a novel auxiliary subunit for the voltage gated sodium channel is upregulated in sensory neurones following streptozocin induced diabetic neuropathy in rat. Neurosci Lett. 2001;309(1):1-4. PubMed PMID: 11489532.
145. Isom LL, Catterall WA. Na+ channel subunits and Ig domains. Nature. 1996;383(6598):307-8. doi: 10.1038/383307b0. PubMed PMID: 8848042.
146. Oyama F, Miyazaki H, Sakamoto N, Becquet C, Machida Y, Kaneko K, Uchikawa C, Suzuki T, Kurosawa M, Ikeda T, Tamaoka A, Sakurai T, Nukina N. Sodium channel beta4 subunit: down-regulation and possible involvement in neuritic degeneration in Huntington's disease transgenic mice. J Neurochem. 2006;98(2):518-29. doi: 10.1111/j.1471-4159.2006.03893.x. PubMed PMID: 16805843.
147. Zhou TT, Zhang ZW, Liu J, Zhang JP, Jiao BH. Glycosylation of the sodium channel beta4 subunit is developmentally regulated and involves in neuritic degeneration. Int J Biol Sci. 2012;8(5):630-9. doi: 10.7150/ijbs.3684. PubMed PMID: 22553463; PMCID: PMC3341604.
148. Goldfarb M. Fibroblast growth factor homologous factors: evolution, structure, and function. Cytokine Growth Factor Rev. 2005;16(2):215-20. Epub 2005/05/03. doi: S1359-6101(05)00012-2 [pii]
10.1016/j.cytogfr.2005.02.002. PubMed PMID: 15863036; PMCID: 3212846.
149. Wu QF, Yang L, Li S, Wang Q, Yuan XB, Gao X, Bao L, Zhang X. Fibroblast growth factor 13 is a microtubule-stabilizing protein regulating neuronal polarization and migration. Cell. 2012;149(7):1549-64. Epub 2012/06/26. doi: 10.1016/j.cell.2012.04.046. PubMed PMID: 22726441.
150. Wildburger NC, Ali SR, Hsu WC, Shavkunov AS, Nenov MN, Lichti CF, LeDuc RD, Mostovenko E, Panova-Elektronova NI, Emmett MR, Nilsson CL, Laezza F. Quantitative proteomics reveals protein-protein interactions with fibroblast growth factor 12 as a component of the voltage-gated sodium channel

1.2 (nav1.2) macromolecular complex in Mammalian brain. Mol Cell Proteomics. 2015;14(5):1288-300. doi: 10.1074/mcp.M114.040055. PubMed PMID: 25724910; PMCID: PMC4424400.
151. Schoorlemmer J, Goldfarb M. Fibroblast growth factor homologous factors and the islet brain-2 scaffold protein regulate activation of a stress-activated protein kinase. The Journal of biological chemistry. 2002;277(51):49111-9. doi: 10.1074/jbc.M205520200. PubMed PMID: 12244047; PMCID: PMC4266389.
152. Schoorlemmer J, Goldfarb M. Fibroblast growth factor homologous factors are intracellular signaling proteins. Curr Biol. 2001;11(10):793-7. Epub 2001/05/30. doi: S0960-9822(01)00232-9 [pii]. PubMed PMID: 11378392; PMCID: 3216481.
153. Konig HG, Fenner BJ, Byrne JC, Schwamborn RF, Bernas T, Jefferies CA, Prehn JH. Fibroblast growth factor homologous factor 1 interacts with NEMO to regulate NF-kappaB signaling in neurons. J Cell Sci. 2012;125(Pt 24):6058-70. doi: 10.1242/jcs.111880. PubMed PMID: 23097049.
154. Yan H, Pablo JL, Pitt GS. FGF14 regulates presynaptic Ca2+ channels and synaptic transmission. Cell Rep. 2013;4(1):66-75. doi: 10.1016/j.celrep.2013.06.012. PubMed PMID: 23831029; PMCID: PMC3736584.
155. Munoz-Sanjuan I, Smallwood PM, Nathans J. Isoform diversity among fibroblast growth factor homologous factors is generated by alternative promoter usage and differential splicing. The Journal of biological chemistry. 2000;275(4):2589-97. Epub 2000/01/25. PubMed PMID: 10644718.
156. Smallwood PM, Munoz-Sanjuan I, Tong P, Macke JP, Hendry SH, Gilbert DJ, Copeland NG, Jenkins NA, Nathans J. Fibroblast growth factor (FGF) homologous factors: new members of the FGF family implicated in nervous system development. Proceedings of the National Academy of Sciences of the United States of America. 1996;93(18):9850-7. Epub 1996/09/03. PubMed PMID: 8790420; PMCID: 38518.
157. Wang C, Wang C, Hoch EG, Pitt GS. Identification of novel interaction sites that determine specificity between fibroblast growth factor homologous factors and voltage-gated sodium channels. The Journal of biological chemistry. 2011;286(27):24253-63. doi: 10.1074/jbc.M111.245803. PubMed PMID: 21566136; PMCID: PMC3129206.
158. Wang C, Chung BC, Yan H, Lee SY, Pitt GS. Crystal structure of the ternary complex of a NaV C-terminal domain, a fibroblast growth factor homologous factor, and calmodulin. Structure. 2012;20(7):1167-76. doi: 10.1016/j.str.2012.05.001. PubMed PMID: 22705208; PMCID: PMC3610540.
159. Liu C, Dib-Hajj SD, Waxman SG. Fibroblast growth factor homologous factor 1B binds to the C terminus of the tetrodotoxin-resistant sodium channel rNav1.9a (NaN). The Journal of biological chemistry. 2001;276(22):18925-33. Epub 2001/05/29. doi: 10.1074/jbc.M101606200 M101606200 [pii]. PubMed PMID: 11376006.
160. Goetz R, Dover K, Laezza F, Shtraizent N, Huang X, Tchetchik D, Eliseenkova AV, Xu CF, Neubert TA, Ornitz DM, Goldfarb M, Mohammadi M. Crystal structure of a fibroblast growth factor homologous factor (FHF) defines a conserved surface on FHFs for binding and modulation of voltage-gated sodium

channels. The Journal of biological chemistry. 2009;284(26):17883-96. Epub 2009/05/02. doi: 10.1074/jbc.M109.001842
M109.001842 [pii]. PubMed PMID: 19406745; PMCID: 2719427.
161. Pablo JL, Pitt GS. Fibroblast Growth Factor Homologous Factors: New Roles in Neuronal Health and Disease. Neuroscientist. 2016;22(1):19-25. doi: 10.1177/1073858414562217. PubMed PMID: 25492945; PMCID: PMC4555190.
162. Wittmack EK, Rush AM, Craner MJ, Goldfarb M, Waxman SG, Dib-Hajj SD. Fibroblast growth factor homologous factor 2B: association with Nav1.6 and selective colocalization at nodes of Ranvier of dorsal root axons. The Journal of neuroscience : the official journal of the Society for Neuroscience. 2004;24(30):6765-75. Epub 2004/07/30. doi: 10.1523/JNEUROSCI.1628-04.2004
24/30/6765 [pii]. PubMed PMID: 15282281.
163. Rush AM, Wittmack EK, Tyrrell L, Black JA, Dib-Hajj SD, Waxman SG. Differential modulation of sodium channel Na(v)1.6 by two members of the fibroblast growth factor homologous factor 2 subfamily. Eur J Neurosci. 2006;23(10):2551-62. Epub 2006/07/05. doi: EJN4789 [pii]
10.1111/j.1460-9568.2006.04789.x. PubMed PMID: 16817858.
164. Hubert T, Bourane S, Venteo S, Mechaly I, Puech S, Valmier J, Carroll P, Fichard-Carroll A. Fibroblast growth factor homologous factor 1 (FHF1) is expressed in a subpopulation of calcitonin gene-related peptide-positive nociceptive neurons in the murine dorsal root ganglia. J Comp Neurol. 2008;507(4):1588-601. Epub 2008/01/29. doi: 10.1002/cne.21631. PubMed PMID: 18220257.
165. Li GD, Wo Y, Zhong MF, Zhang FX, Bao L, Lu YJ, Huang YD, Xiao HS, Zhang X. Expression of fibroblast growth factors in rat dorsal root ganglion neurons and regulation after peripheral nerve injury. Neuroreport. 2002;13(15):1903-7. PubMed PMID: 12395088.
166. Xiao HS, Huang QH, Zhang FX, Bao L, Lu YJ, Guo C, Yang L, Huang WJ, Fu G, Xu SH, Cheng XP, Yan Q, Zhu ZD, Zhang X, Chen Z, Han ZG, Zhang X. Identification of gene expression profile of dorsal root ganglion in the rat peripheral axotomy model of neuropathic pain. Proceedings of the National Academy of Sciences of the United States of America. 2002;99(12):8360-5. doi: 10.1073/pnas.122231899. PubMed PMID: 12060780; PMCID: PMC123072.
167. Yan H, Pablo JL, Wang C, Pitt GS. FGF14 modulates resurgent sodium current in mouse cerebellar Purkinje neurons. Elife. 2014;3:e04193. doi: 10.7554/eLife.04193. PubMed PMID: 25269146; PMCID: PMC4356139.
168. Savio-Galimberti E, Gollob MH, Darbar D. Voltage-gated sodium channels: biophysics, pharmacology, and related channelopathies. Front Pharmacol. 2012;3:124. doi: 10.3389/fphar.2012.00124. PubMed PMID: 22798951; PMCID: PMC3394224.
169. Goldin AL. Mechanisms of sodium channel inactivation. Curr Opin Neurobiol. 2003;13(3):284-90. Epub 2003/07/10. doi: S0959438803000655 [pii]. PubMed PMID: 12850212.

170. Ulbricht W. Sodium channel inactivation: molecular determinants and modulation. Physiol Rev. 2005;85(4):1271-301. Epub 2005/09/27. doi: 85/4/1271 [pii]
10.1152/physrev.00024.2004. PubMed PMID: 16183913.
171. Dib-Hajj S, Black JA, Cummins TR, Waxman SG. NaN/Nav1.9: a sodium channel with unique properties. Trends Neurosci. 2002;25(5):253-9. PubMed PMID: 11972962.
172. Sheets PL, Jarecki BW, Cummins TR. Lidocaine reduces the transition to slow inactivation in Na(v)1.7 voltage-gated sodium channels. Br J Pharmacol. 2011;164(2b):719-30. doi: 10.1111/j.1476-5381.2011.01209.x. PubMed PMID: 21232038; PMCID: 3188891.
173. Blair NT, Bean BP. Role of tetrodotoxin-resistant Na+ current slow inactivation in adaptation of action potential firing in small-diameter dorsal root ganglion neurons. The Journal of neuroscience : the official journal of the Society for Neuroscience. 2003;23(32):10338-50. Epub 2003/11/14. doi: 23/32/10338 [pii]. PubMed PMID: 14614093.
174. Zimmermann K, Leffler A, Babes A, Cendan CM, Carr RW, Kobayashi J, Nau C, Wood JN, Reeh PW. Sensory neuron sodium channel Nav1.8 is essential for pain at low temperatures. Nature. 2007;447(7146):855-8. PubMed PMID: 17568746.
175. Dover K, Solinas S, D'Angelo E, Goldfarb M. Long-term inactivation particle for voltage-gated sodium channels. The Journal of physiology. 2010;588(Pt 19):3695-711. Epub 2010/08/04. doi: 10.1113/jphysiol.2010.192559 jphysiol.2010.192559 [pii]. PubMed PMID: 20679355; PMCID: 2998221.
176. Venkatesan K, Liu Y, Goldfarb M. Fast-onset long-term open-state block of sodium channels by A-type FHFs mediates classical spike accommodation in hippocampal pyramidal neurons. The Journal of neuroscience : the official journal of the Society for Neuroscience. 2014;34(48):16126-39. Epub 2014/11/28. doi: 10.1523/JNEUROSCI.1271-14.2014. PubMed PMID: 25429153; PMCID: 4244476.
177. Lewis AH, Raman IM. Interactions among DIV voltage-sensor movement, fast inactivation, and resurgent Na current induced by the NaVbeta4 open-channel blocking peptide. The Journal of general physiology. 2013;142(3):191-206. Epub 2013/08/14. doi: 10.1085/jgp.201310984. PubMed PMID: 23940261; PMCID: PMC3753608.
178. Raman IM, Bean BP. Inactivation and recovery of sodium currents in cerebellar Purkinje neurons: evidence for two mechanisms. Biophysical journal. 2001;80(2):729-37. doi: 10.1016/S0006-3495(01)76052-3. PubMed PMID: 11159440; PMCID: 1301271.
179. Cannon SC, Bean BP. Sodium channels gone wild: resurgent current from neuronal and muscle channelopathies. J Clin Invest. 2010;120(1):80-3. Epub 2009/12/30. doi: 10.1172/JCI41340
41340 [pii]. PubMed PMID: 20038809; PMCID: 2798702.
180. Grieco TM, Malhotra JD, Chen C, Isom LL, Raman IM. Open-channel block by the cytoplasmic tail of sodium channel beta4 as a mechanism for

resurgent sodium current. Neuron. 2005;45(2):233-44. Epub 2005/01/25. doi: S0896627304008360 [pii]
10.1016/j.neuron.2004.12.035. PubMed PMID: 15664175.
181. Patel RR, Barbosa C, Xiao Y, Cummins TR. Human Nav1.6 Channels Generate Larger Resurgent Currents than Human Nav1.1 Channels, but the Navbeta4 Peptide Does Not Protect Either Isoform from Use-Dependent Reduction. PloS one. 2015;10(7):e0133485. Epub 2015/07/17. doi: 10.1371/journal.pone.0133485. PubMed PMID: 26182346; PMCID: 4504674.
182. Cruz JS, Silva DF, Ribeiro LA, Araujo IG, Magalhaes N, Medeiros A, Freitas C, Araujo IC, Oliveira FA. Resurgent Na+ current: a new avenue to neuronal excitability control. Life Sci. 2011;89(15-16):564-9. Epub 2011/06/21. doi: 10.1016/j.lfs.2011.05.016
S0024-3205(11)00262-1 [pii]. PubMed PMID: 21683085.
183. Theile JW, Jarecki BW, Piekarz AD, Cummins TR. Nav1.7 mutations associated with paroxysmal extreme pain disorder, but not erythromelalgia, enhance Navbeta4 peptide-mediated resurgent sodium currents. The Journal of physiology. 2011;589(Pt 3):597-608. Epub 2010/12/01. doi: 10.1113/jphysiol.2010.200915
jphysiol.2010.200915 [pii]. PubMed PMID: 21115638; PMCID: 3055545.
184. Choi JS, Boralevi F, Brissaud O, Sanchez-Martin J, Te Morsche RH, Dib-Hajj SD, Drenth JP, Waxman SG. Paroxysmal extreme pain disorder: a molecular lesion of peripheral neurons. Nature reviews Neurology. 2011;7(1):51-5. Epub 2010/11/17. doi: 10.1038/nrneurol.2010.162. PubMed PMID: 21079636.
185. Jarecki BW, Sheets PL, Xiao Y, Jackson JO, 2nd, Cummins TR. Alternative splicing of Na(V)1.7 exon 5 increases the impact of the painful PEPD mutant channel I1461T. Channels. 2009;3(4):259-67. PubMed PMID: 19633428; PMCID: 2856339.
186. Alsen C. Biological significance of peptides from Anemonia sulcata. Fed Proc. 1983;42(1):101-8. PubMed PMID: 6129161.
187. Moran Y, Gordon D, Gurevitz M. Sea anemone toxins affecting voltage-gated sodium channels--molecular and evolutionary features. Toxicon. 2009;54(8):1089-101. doi: 10.1016/j.toxicon.2009.02.028. PubMed PMID: 19268682; PMCID: PMC2807626.
188. Chahine M, George AL, Jr., Zhou M, Ji S, Sun W, Barchi RL, Horn R. Sodium channel mutations in paramyotonia congenita uncouple inactivation from activation. Neuron. 1994;12(2):281-94. PubMed PMID: 8110459.
189. Ji S, George AL, Jr., Horn R, Barchi RL. Paramyotonia congenita mutations reveal different roles for segments S3 and S4 of domain D4 in hSkM1 sodium channel gating. The Journal of general physiology. 1996;107(2):183-94. PubMed PMID: 8833340; PMCID: PMC2219264.
190. Kuhn FJ, Greeff NG. Movement of voltage sensor S4 in domain 4 is tightly coupled to sodium channel fast inactivation and gating charge immobilization. The Journal of general physiology. 1999;114(2):167-83. PubMed PMID: 10435996; PMCID: PMC2230646.

191. Stevens M, Peigneur S, Tytgat J. Neurotoxins and their binding areas on voltage-gated sodium channels. Front Pharmacol. 2011;2:71. doi: 10.3389/fphar.2011.00071. PubMed PMID: 22084632; PMCID: PMC3210964.
192. Richardson JD, Vasko MR. Cellular mechanisms of neurogenic inflammation. J Pharmacol Exp Ther. 2002;302(3):839-45. doi: 10.1124/jpet.102.032797. PubMed PMID: 12183638.
193. Hucho T, Levine JD. Signaling pathways in sensitization: toward a nociceptor cell biology. Neuron. 2007;55(3):365-76. doi: 10.1016/j.neuron.2007.07.008. PubMed PMID: 17678851.
194. Chattopadhyay M, Mata M, Fink DJ. Continuous delta-opioid receptor activation reduces neuronal voltage-gated sodium channel (NaV1.7) levels through activation of protein kinase C in painful diabetic neuropathy. The Journal of neuroscience : the official journal of the Society for Neuroscience. 2008;28(26):6652-8. doi: 10.1523/JNEUROSCI.5530-07.2008. PubMed PMID: 18579738; PMCID: PMC3321315.
195. Vijayaragavan K, Boutjdir M, Chahine M. Modulation of Nav1.7 and Nav1.8 peripheral nerve sodium channels by protein kinase A and protein kinase C. Journal of neurophysiology. 2004;91(4):1556-69. doi: 10.1152/jn.00676.2003. PubMed PMID: 14657190.
196. Miyazaki H, Oyama F, Inoue R, Aosaki T, Abe T, Kiyonari H, Kino Y, Kurosawa M, Shimizu J, Ogiwara I, Yamakawa K, Koshimizu Y, Fujiyama F, Kaneko T, Shimizu H, Nagatomo K, Yamada K, Shimogori T, Hattori N, Miura M, Nukina N. Singular localization of sodium channel beta4 subunit in unmyelinated fibres and its role in the striatum. Nature communications. 2014;5:5525. doi: 10.1038/ncomms6525. PubMed PMID: 25413837.
197. Bant JS, Raman IM. Control of transient, resurgent, and persistent current by open-channel block by Na channel beta4 in cultured cerebellar granule neurons. Proceedings of the National Academy of Sciences of the United States of America. 2010;107(27):12357-62. Epub 2010/06/23. doi: 10.1073/pnas.1005633107
1005633107 [pii]. PubMed PMID: 20566860; PMCID: 2901465.
198. Yu FH, Westenbroek RE, Silos-Santiago I, McCormick KA, Lawson D, Ge P, Ferriera H, Lilly J, DiStefano PS, Catterall WA, Scheuer T, Curtis R. Sodium channel beta4, a new disulfide-linked auxiliary subunit with similarity to beta2. The Journal of neuroscience : the official journal of the Society for Neuroscience. 2003;23(20):7577-85. PubMed PMID: 12930796.
199. Lewis AH, Raman IM. Cross-species conservation of open-channel block by Na channel beta4 peptides reveals structural features required for resurgent Na current. The Journal of neuroscience : the official journal of the Society for Neuroscience. 2011;31(32):11527-36. doi: 10.1523/JNEUROSCI.1428-11.2011. PubMed PMID: 21832183; PMCID: 3178407.
200. Aman TK, Grieco-Calub TM, Chen C, Rusconi R, Slat EA, Isom LL, Raman IM. Regulation of persistent Na current by interactions between beta subunits of voltage-gated Na channels. The Journal of neuroscience : the official journal of the Society for Neuroscience. 2009;29(7):2027-42. Epub 2009/02/21. doi: 10.1523/JNEUROSCI.4531-08.2009

29/7/2027 [pii]. PubMed PMID: 19228957; PMCID: 2667244.
201. Wang GK, Edrich T, Wang SY. Time-dependent block and resurgent tail currents induced by mouse beta4(154-167) peptide in cardiac Na+ channels. The Journal of general physiology. 2006;127(3):277-89. Epub 2006/03/01. doi: 10.1085/jgp.200509399. PubMed PMID: 16505148; PMCID: 2151501.
202. Chen Y, Yu FH, Sharp EM, Beacham D, Scheuer T, Catterall WA. Functional properties and differential neuromodulation of Na(v)1.6 channels. Molecular and cellular neurosciences. 2008;38(4):607-15. Epub 2008/07/05. doi: 10.1016/j.mcn.2008.05.009. PubMed PMID: 18599309; PMCID: 3433175.
203. Barbosa C, Tan ZY, Wang R, Xie W, Strong JA, Patel RR, Vasko MR, Zhang JM, Cummins TR. Navbeta4 regulates fast resurgent sodium currents and excitability in sensory neurons. Mol Pain. 2015;11:60. doi: 10.1186/s12990-015-0063-9. PubMed PMID: 26408173; PMCID: PMC4582632.
204. Devor M. Ectopic discharge in Abeta afferents as a source of neuropathic pain. Exp Brain Res. 2009;196(1):115-28. doi: 10.1007/s00221-009-1724-6. PubMed PMID: 19242687.
205. Bedi SS, Yang Q, Crook RJ, Du J, Wu Z, Fishman HM, Grill RJ, Carlton SM, Walters ET. Chronic spontaneous activity generated in the somata of primary nociceptors is associated with pain-related behavior after spinal cord injury. The Journal of neuroscience : the official journal of the Society for Neuroscience. 2010;30(44):14870-82. doi: 10.1523/JNEUROSCI.2428-10.2010. PubMed PMID: 21048146; PMCID: PMC3073589.
206. Nieto FR, Cobos EJ, Tejada MA, Sanchez-Fernandez C, Gonzalez-Cano R, Cendan CM. Tetrodotoxin (TTX) as a therapeutic agent for pain. Mar Drugs. 2012;10(2):281-305. doi: 10.3390/md10020281. PubMed PMID: 22412801; PMCID: PMC3296997.
207. Berger JV, Knaepen L, Janssen SP, Jaken RJ, Marcus MA, Joosten EA, Deumens R. Cellular and molecular insights into neuropathy-induced pain hypersensitivity for mechanism-based treatment approaches. Brain Res Rev. 2011;67(1-2):282-310. doi: 10.1016/j.brainresrev.2011.03.003. PubMed PMID: 21440003.
208. Xie W, Strong JA, Mao J, Zhang JM. Highly localized interactions between sensory neurons and sprouting sympathetic fibers observed in a transgenic tyrosine hydroxylase reporter mouse. Mol Pain. 2011;7:53. doi: 10.1186/1744-8069-7-53. PubMed PMID: 21794129; PMCID: PMC3152901.
209. Xie W, Strong JA, Zhang JM. Early blockade of injured primary sensory afferents reduces glial cell activation in two rat neuropathic pain models. Neuroscience. 2009;160(4):847-57. doi: 10.1016/j.neuroscience.2009.03.016. PubMed PMID: 19303429; PMCID: PMC2777638.
210. Raman IM, Bean BP. Resurgent sodium current and action potential formation in dissociated cerebellar Purkinje neurons. The Journal of neuroscience : the official journal of the Society for Neuroscience. 1997;17(12):4517-26. Epub 1997/06/15. PubMed PMID: 9169512.
211. Goldfarb M. Voltage-gated sodium channel-associated proteins and alternative mechanisms of inactivation and block. Cell Mol Life Sci.

2012;69(7):1067-76. Epub 2011/09/29. doi: 10.1007/s00018-011-0832-1. PubMed PMID: 21947499; PMCID: 3272111.
212. Herzog RI, Cummins TR, Ghassemi F, Dib-Hajj SD, Waxman SG. Distinct repriming and closed-state inactivation kinetics of Nav1.6 and Nav1.7 sodium channels in mouse spinal sensory neurons. The Journal of physiology. 2003;551(Pt 3):741-50. doi: 10.1113/jphysiol.2003.047357. PubMed PMID: 12843211; PMCID: 2343279.
213. Leffler A, Herzog RI, Dib-Hajj SD, Waxman SG, Cummins TR. Pharmacological properties of neuronal TTX-resistant sodium channels and the role of a critical serine pore residue. Pflugers Arch. 2005;451(3):454-63. Epub 2005/06/28. doi: 10.1007/s00424-005-1463-x. PubMed PMID: 15981012.
214. Mikami M, Yang J. Short hairpin RNA-mediated selective knockdown of NaV1.8 tetrodotoxin-resistant voltage-gated sodium channel in dorsal root ganglion neurons. Anesthesiology. 2005;103(4):828-36. PubMed PMID: 16192776.
215. Gavet O, Pines J. Progressive activation of CyclinB1-Cdk1 coordinates entry to mitosis. Developmental cell. 2010;18(4):533-43. Epub 2010/04/24. doi: 10.1016/j.devcel.2010.02.013. PubMed PMID: 20412769; PMCID: 3325599.
216. Fjell J, Cummins TR, Dib-Hajj SD, Fried K, Black JA, Waxman SG. Differential role of GDNF and NGF in the maintenance of two TTX-resistant sodium channels in adult DRG neurons. Brain research Molecular brain research. 1999;67(2):267-82. PubMed PMID: 10216225.
217. Cummins TR, Renganathan M, Stys PK, Herzog RI, Scarfo K, Horn R, Dib-Hajj SD, Waxman SG. The pentapeptide QYNAD does not block voltage-gated sodium channels. Neurology. 2003;60(2):224-9. PubMed PMID: 12552035.
218. Dib-Hajj SD, Choi JS, Macala LJ, Tyrrell L, Black JA, Cummins TR, Waxman SG. Transfection of rat or mouse neurons by biolistics or electroporation. Nat Protoc. 2009;4(8):1118-26. Epub 2009/07/21. doi: 10.1038/nprot.2009.90
nprot.2009.90 [pii]. PubMed PMID: 19617884.
219. Cummins TR, Aglieco F, Renganathan M, Herzog RI, Dib-Hajj SD, Waxman SG. Nav1.3 sodium channels: rapid repriming and slow closed-state inactivation display quantitative differences after expression in a mammalian cell line and in spinal sensory neurons. The Journal of neuroscience : the official journal of the Society for Neuroscience. 2001;21(16):5952-61. Epub 2001/08/07. doi: 21/16/5952 [pii]. PubMed PMID: 11487618.
220. Herzog RI, Liu C, Waxman SG, Cummins TR. Calmodulin binds to the C terminus of sodium channels Nav1.4 and Nav1.6 and differentially modulates their functional properties. The Journal of neuroscience : the official journal of the Society for Neuroscience. 2003;23(23):8261-70. PubMed PMID: 12967988.
221. Bowman CL, Baglioni A. Application of the Goldman-Hodgkin-Katz current equation to membrane current-voltage data. J Theor Biol. 1984;108(1):1-29. PubMed PMID: 6748675.
222. Black JA, Renganathan M, Waxman SG. Sodium channel Na(v)1.6 is expressed along nonmyelinated axons and it contributes to conduction. Brain

research Molecular brain research. 2002;105(1-2):19-28. PubMed PMID: 12399104.
223. Xie W, Strong JA, Kays J, Nicol GD, Zhang JM. Knockdown of the sphingosine-1-phosphate receptor S1PR1 reduces pain behaviors induced by local inflammation of the rat sensory ganglion. Neurosci Lett. 2012;515(1):61-5. doi: 10.1016/j.neulet.2012.03.019. PubMed PMID: 22445889; PMCID: 3322267.
224. Streit J, Lux HD. Voltage dependent calcium currents in PC12 growth cones and cells during NGF-induced cell growth. Pflugers Arch. 1987;408(6):634-41. PubMed PMID: 3601647.
225. Fatt P, Katz B. Spontaneous subthreshold activity at motor nerve endings. The Journal of physiology. 1952;117(1):109-28. PubMed PMID: 14946732; PMCID: PMC1392564.
226. Fein A. Nociceptors and the perception of pain. Farmington, CT2012.
227. Zhao J, O'Leary ME, Chahine M. Regulation of Nav1.6 and Nav1.8 peripheral nerve Na+ channels by auxiliary beta-subunits. Journal of neurophysiology. 2011;106(2):608-19. doi: 10.1152/jn.00107.2011. PubMed PMID: 21562192; PMCID: 3296273.
228. Buffington SA, Rasband MN. Na+ channel-dependent recruitment of Navbeta4 to axon initial segments and nodes of Ranvier. The Journal of neuroscience : the official journal of the Society for Neuroscience. 2013;33(14):6191-202. doi: 10.1523/JNEUROSCI.4051-12.2013. PubMed PMID: 23554500; PMCID: 3643000.
229. Chen C, Calhoun JD, Zhang Y, Lopez-Santiago L, Zhou N, Davis TH, Salzer JL, Isom LL. Identification of the cysteine residue responsible for disulfide linkage of Na+ channel alpha and beta2 subunits. The Journal of biological chemistry. 2012;287(46):39061-9. doi: 10.1074/jbc.M112.397646. PubMed PMID: 22992729; PMCID: 3493947.
230. Gilchrist J, Das S, Van Petegem F, Bosmans F. Crystallographic insights into sodium-channel modulation by the beta4 subunit. Proceedings of the National Academy of Sciences of the United States of America. 2013;110(51):E5016-24. Epub 2013/12/04. doi: 10.1073/pnas.1314557110. PubMed PMID: 24297919; PMCID: PMC3870679.
231. Das S, Gilchrist J, Bosmans F, Van Petegem F. Binary architecture of the Nav1.2-beta2 signaling complex. Elife. 2016;5. doi: 10.7554/eLife.10960. PubMed PMID: 26894959; PMCID: PMC4769172.
232. Grieco TM, Raman IM. Production of resurgent current in NaV1.6-null Purkinje neurons by slowing sodium channel inactivation with beta-pompilidotoxin. The Journal of neuroscience : the official journal of the Society for Neuroscience. 2004;24(1):35-42. Epub 2004/01/13. doi: 10.1523/JNEUROSCI.3807-03.2004
24/1/35 [pii]. PubMed PMID: 14715935.
233. Do MT, Bean BP. Sodium currents in subthalamic nucleus neurons from Nav1.6-null mice. Journal of neurophysiology. 2004;92(2):726-33. Epub 2004/04/02. doi: 10.1152/jn.00186.2004. PubMed PMID: 15056687.

234. Kearney J. Voltage-gated ion channel accessory subunits: sodium, potassium, or both? Epilepsy Curr. 2013;13(1):30-1. doi: 10.5698/1535-7511-13.1.30. PubMed PMID: 23447736; PMCID: PMC3577083.
235. Marionneau C, Carrasquillo Y, Norris AJ, Townsend RR, Isom LL, Link AJ, Nerbonne JM. The sodium channel accessory subunit Navbeta1 regulates neuronal excitability through modulation of repolarizing voltage-gated K(+) channels. The Journal of neuroscience : the official journal of the Society for Neuroscience. 2012;32(17):5716-27. doi: 10.1523/JNEUROSCI.6450-11.2012. PubMed PMID: 22539834; PMCID: PMC3347704.
236. Pongs O. Regulation of excitability by potassium channels. Results Probl Cell Differ. 2008;44:145-61. doi: 10.1007/400_2007_032. PubMed PMID: 17579818.
237. Grieco TM, Afshari FS, Raman IM. A role for phosphorylation in the maintenance of resurgent sodium current in cerebellar purkinje neurons. The Journal of neuroscience : the official journal of the Society for Neuroscience. 2002;22(8):3100-7. Epub 2002/04/12. doi: 20026319
22/8/3100 [pii]. PubMed PMID: 11943813.
238. Xie W, Strong JA, Kim D, Shahrestani S, Zhang JM. Bursting activity in myelinated sensory neurons plays a key role in pain behavior induced by localized inflammation of the rat sensory ganglion. Neuroscience. 2012;206:212-23. doi: 10.1016/j.neuroscience.2012.01.007. PubMed PMID: 22265726; PMCID: PMC3294034.
239. Chaplan SR, Bach FW, Pogrel JW, Chung JM, Yaksh TL. Quantitative assessment of tactile allodynia in the rat paw. J Neurosci Methods. 1994;53(1):55-63. PubMed PMID: 7990513.
240. Stebbing MJ, Eschenfelder S, Habler HJ, Acosta MC, Janig W, McLachlan EM. Changes in the action potential in sensory neurones after peripheral axotomy in vivo. Neuroreport. 1999;10(2):201-6. PubMed PMID: 10203309.
241. Ye L, Xie W, Strong JA, Zhang JM. Blocking the mineralocorticoid receptor improves effectiveness of steroid treatment for low back pain in rats. Anesthesiology. 2014;121(3):632-43. doi: 10.1097/ALN.0000000000000277. PubMed PMID: 24781496; PMCID: PMC4165848.
242. Xie W, Tan ZY, Barbosa C, Strong JA, Cummins TR, Zhang JM. Upregulation of the sodium channel NaVbeta4 subunit and its contributions to mechanical hypersensitivity and neuronal hyperexcitability in a rat model of radicular pain induced by local DRG inflammation. Pain. 2015. doi: 10.1097/j.pain.0000000000000453. PubMed PMID: 26785322.
243. Everill B, Cummins TR, Waxman SG, Kocsis JD. Sodium currents of large (Abeta-type) adult cutaneous afferent dorsal root ganglion neurons display rapid recovery from inactivation before and after axotomy. Neuroscience. 2001;106(1):161-9. Epub 2001/09/21. doi: S0306-4522(01)00258-5 [pii]. PubMed PMID: 11564426; PMCID: 2605362.
244. Brackenbury WJ, Isom LL. Na Channel beta Subunits: Overachievers of the Ion Channel Family. Front Pharmacol. 2011;2:53. doi: 10.3389/fphar.2011.00053. PubMed PMID: 22007171; PMCID: PMC3181431.

245. Krzemien DM, Schaller KL, Levinson SR, Caldwell JH. Immunolocalization of sodium channel isoform NaCh6 in the nervous system. J Comp Neurol. 2000;420(1):70-83. PubMed PMID: 10745220.
246. Isom LL, Ragsdale DS, De Jongh KS, Westenbroek RE, Reber BF, Scheuer T, Catterall WA. Structure and function of the beta 2 subunit of brain sodium channels, a transmembrane glycoprotein with a CAM motif. Cell. 1995;83(3):433-42. PubMed PMID: 8521473.
247. Jenkins SM, Bennett V. Ankyrin-G coordinates assembly of the spectrin-based membrane skeleton, voltage-gated sodium channels, and L1 CAMs at Purkinje neuron initial segments. J Cell Biol. 2001;155(5):739-46. doi: 10.1083/jcb.200109026. PubMed PMID: 11724816; PMCID: PMC2150881.
248. Malhotra JD, Kazen-Gillespie K, Hortsch M, Isom LL. Sodium channel beta subunits mediate homophilic cell adhesion and recruit ankyrin to points of cell-cell contact. The Journal of biological chemistry. 2000;275(15):11383-8. PubMed PMID: 10753953.
249. Lewis AH, Raman IM. Resurgent current of voltage-gated Na(+) channels. The Journal of physiology. 2014;592(Pt 22):4825-38. doi: 10.1113/jphysiol.2014.277582. PubMed PMID: 25172941; PMCID: PMC4259529.
250. Belkouch M, Dansereau MA, Tetreault P, Biet M, Beaudet N, Dumaine R, Chraibi A, Melik-Parsadaniantz S, Sarret P. Functional up-regulation of Nav1.8 sodium channel in Abeta afferent fibers subjected to chronic peripheral inflammation. J Neuroinflammation. 2014;11:45. doi: 10.1186/1742-2094-11-45. PubMed PMID: 24606981; PMCID: PMC4007624.
251. Strong JA, Xie W, Coyle DE, Zhang JM. Microarray analysis of rat sensory ganglia after local inflammation implicates novel cytokines in pain. PloS one. 2012;7(7):e40779. doi: 10.1371/journal.pone.0040779. PubMed PMID: 22815815; PMCID: PMC3397953.
252. Geer LY, Marchler-Bauer A, Geer RC, Han L, He J, He S, Liu C, Shi W, Bryant SH. The NCBI BioSystems database. Nucleic Acids Res. 2010;38(Database issue):D492-6. doi: 10.1093/nar/gkp858. PubMed PMID: 19854944; PMCID: PMC2808896.
253. Zhang J-M. Localized Inflammatory Irritation of the Lumbar Ganglia: An Animal Model of Chemogenic Low Back Pain and Radiculopathy. In: Ma C, Zhang J-M, editors. Animal Models of Pain. Springer Protocols: Humana Press; 2011. p. 89-102.
254. Wang C, Hennessey JA, Kirkton RD, Wang C, Graham V, Puranam RS, Rosenberg PB, Bursac N, Pitt GS. Fibroblast growth factor homologous factor 13 regulates Na+ channels and conduction velocity in murine hearts. Circ Res. 2011;109(7):775-82. doi: 10.1161/CIRCRESAHA.111.247957. PubMed PMID: 21817159; PMCID: PMC3383600.
255. Petryszak R, Burdett T, Fiorelli B, Fonseca NA, Gonzalez-Porta M, Hastings E, Huber W, Jupp S, Keays M, Kryvych N, McMurry J, Marioni JC, Malone J, Megy K, Rustici G, Tang AY, Taubert J, Williams E, Mannion O, Parkinson HE, Brazma A. Expression Atlas update--a database of gene and transcript expression from microarray- and sequencing-based functional

genomics experiments. Nucleic Acids Res. 2014;42(Database issue):D926-32. doi: 10.1093/nar/gkt1270. PubMed PMID: 24304889; PMCID: PMC3964963.
256. Hammer P, Banck MS, Amberg R, Wang C, Petznick G, Luo S, Khrebtukova I, Schroth GP, Beyerlein P, Beutler AS. mRNA-seq with agnostic splice site discovery for nervous system transcriptomics tested in chronic pain. Genome Res. 2010;20(6):847-60. doi: 10.1101/gr.101204.109. PubMed PMID: 20452967; PMCID: PMC2877581.
257. Middleton RE, Warren VA, Kraus RL, Hwang JC, Liu CJ, Dai G, Brochu RM, Kohler MG, Gao YD, Garsky VM, Bogusky MJ, Mehl JT, Cohen CJ, Smith MM. Two tarantula peptides inhibit activation of multiple sodium channels. Biochemistry. 2002;41(50):14734-47. PubMed PMID: 12475222.
258. Wong HK, Sakurai T, Oyama F, Kaneko K, Wada K, Miyazaki H, Kurosawa M, De Strooper B, Saftig P, Nukina N. beta Subunits of voltage-gated sodium channels are novel substrates of beta-site amyloid precursor protein-cleaving enzyme (BACE1) and gamma-secretase. The Journal of biological chemistry. 2005;280(24):23009-17. doi: 10.1074/jbc.M414648200. PubMed PMID: 15824102.
259. Kim DY, Ingano LA, Carey BW, Pettingell WH, Kovacs DM. Presenilin/gamma-secretase-mediated cleavage of the voltage-gated sodium channel beta2-subunit regulates cell adhesion and migration. The Journal of biological chemistry. 2005;280(24):23251-61. doi: 10.1074/jbc.M412938200. PubMed PMID: 15833746.
260. Gersbacher MT, Kim DY, Bhattacharyya R, Kovacs DM. Identification of BACE1 cleavage sites in human voltage-gated sodium channel beta 2 subunit. Mol Neurodegener. 2010;5:61. doi: 10.1186/1750-1326-5-61. PubMed PMID: 21182789; PMCID: PMC3022600.
261. Huth T, Rittger A, Saftig P, Alzheimer C. beta-Site APP-cleaving enzyme 1 (BACE1) cleaves cerebellar Na+ channel beta4-subunit and promotes Purkinje cell firing by slowing the decay of resurgent Na+ current. Pflugers Arch. 2011;461(3):355-71. doi: 10.1007/s00424-010-0913-2. PubMed PMID: 21246381.
262. Namadurai S, Yereddi NR, Cusdin FS, Huang CL, Chirgadze DY, Jackson AP. A new look at sodium channel beta subunits. Open biology. 2015;5(1):140192. doi: 10.1098/rsob.140192. PubMed PMID: 25567098; PMCID: PMC4313373.
263. Kim DY, Carey BW, Wang H, Ingano LA, Binshtok AM, Wertz MH, Pettingell WH, He P, Lee VM, Woolf CJ, Kovacs DM. BACE1 regulates voltage-gated sodium channels and neuronal activity. Nat Cell Biol. 2007;9(7):755-64. doi: 10.1038/ncb1602. PubMed PMID: 17576410; PMCID: PMC2747787.
264. De Strooper B, Vassar R, Golde T. The secretases: enzymes with therapeutic potential in Alzheimer disease. Nature reviews Neurology. 2010;6(2):99-107. doi: 10.1038/nrneurol.2009.218. PubMed PMID: 20139999; PMCID: PMC2879045.
265. Kim JH, Kushmerick C, von Gersdorff H. Presynaptic resurgent Na+ currents sculpt the action potential waveform and increase firing reliability at a CNS nerve terminal. The Journal of neuroscience : the official journal of the

Society for Neuroscience. 2010;30(46):15479-90. doi: 10.1523/JNEUROSCI.3982-10.2010. PubMed PMID: 21084604; PMCID: PMC3073539.
266. Afshari FS, Ptak K, Khaliq ZM, Grieco TM, Slater NT, McCrimmon DR, Raman IM. Resurgent Na currents in four classes of neurons of the cerebellum. Journal of neurophysiology. 2004;92(5):2831-43. Epub 2004/06/24. doi: 10.1152/jn.00261.2004
00261.2004 [pii]. PubMed PMID: 15212420.
267. Stafstrom CE, Schwindt PC, Chubb MC, Crill WE. Properties of persistent sodium conductance and calcium conductance of layer V neurons from cat sensorimotor cortex in vitro. Journal of neurophysiology. 1985;53(1):153-70. PubMed PMID: 2579215.
268. Stafstrom CE, Schwindt PC, Crill WE. Negative slope conductance due to a persistent subthreshold sodium current in cat neocortical neurons in vitro. Brain Res. 1982;236(1):221-6. PubMed PMID: 6279236.
269. Xie W, Strong JA, Zhang JM. Local knockdown of the NaV1.6 sodium channel reduces pain behaviors, sensory neuron excitability, and sympathetic sprouting in rat models of neuropathic pain. Neuroscience. 2015;291:317-30. Epub 2015/02/18. doi: 10.1016/j.neuroscience.2015.02.010. PubMed PMID: 25686526; PMCID: 4369447.
270. Gold MS, Gebhart GF. Nociceptor sensitization in pain pathogenesis. Nat Med. 2010;16(11):1248-57. doi: 10.1038/nm.2235. PubMed PMID: 20948530.
271. Latremoliere A, Woolf CJ. Central sensitization: a generator of pain hypersensitivity by central neural plasticity. J Pain. 2009;10(9):895-926. doi: 10.1016/j.jpain.2009.06.012. PubMed PMID: 19712899; PMCID: PMC2750819.
272. Costigan M, Scholz J, Woolf CJ. Neuropathic pain: a maladaptive response of the nervous system to damage. Annu Rev Neurosci. 2009;32:1-32. doi: 10.1146/annurev.neuro.051508.135531. PubMed PMID: 19400724; PMCID: PMC2768555.
273. Chaplan SR, Guo HQ, Lee DH, Luo L, Liu C, Kuei C, Velumian AA, Butler MP, Brown SM, Dubin AE. Neuronal hyperpolarization-activated pacemaker channels drive neuropathic pain. The Journal of neuroscience : the official journal of the Society for Neuroscience. 2003;23(4):1169-78. PubMed PMID: 12598605.
274. Lai J, Gold MS, Kim CS, Bian D, Ossipov MH, Hunter JC, Porreca F. Inhibition of neuropathic pain by decreased expression of the tetrodotoxin-resistant sodium channel, NaV1.8. Pain. 2002;95(1-2):143-52. PubMed PMID: 11790477.
275. Xiao WH, Bennett GJ. Synthetic omega-conopeptides applied to the site of nerve injury suppress neuropathic pains in rats. J Pharmacol Exp Ther. 1995;274(2):666-72. PubMed PMID: 7636726.
276. Yoon YW, Na HS, Chung JM. Contributions of injured and intact afferents to neuropathic pain in an experimental rat model. Pain. 1996;64(1):27-36. PubMed PMID: 8867245.
277. Patel R, Barbosa C, Brustovetsky T, Brustovetsky N, Cummins T. Aberrant Epilepsy-Associated Mutant Voltage-Gated Sodium Channel Activity can be targeted with Cannabidiol. Brain. 2016.

278. Lawson SN. Phenotype and function of somatic primary afferent nociceptive neurones with C-, Adelta- or Aalpha/beta-fibres. Exp Physiol. 2002;87(2):239-44. PubMed PMID: 11856969.
279. Woodbury CJ, Koerber HR. Widespread projections from myelinated nociceptors throughout the substantia gelatinosa provide novel insights into neonatal hypersensitivity. The Journal of neuroscience : the official journal of the Society for Neuroscience. 2003;23(2):601-10. PubMed PMID: 12533620.
280. Woodbury CJ, Kullmann FA, McIlwrath SL, Koerber HR. Identity of myelinated cutaneous sensory neurons projecting to nocireceptive laminae following nerve injury in adult mice. J Comp Neurol. 2008;508(3):500-9. doi: 10.1002/cne.21693. PubMed PMID: 18335545; PMCID: PMC2664515.
281. Boada MD, Woodbury CJ. Myelinated skin sensory neurons project extensively throughout adult mouse substantia gelatinosa. The Journal of neuroscience : the official journal of the Society for Neuroscience. 2008;28(9):2006-14. doi: 10.1523/JNEUROSCI.5609-07.2008. PubMed PMID: 18305235.
282. Burgess PR, Petit D, Warren RM. Receptor types in cat hairy skin supplied by myelinated fibers. Journal of neurophysiology. 1968;31(6):833-48. PubMed PMID: 5710537.
283. Treede RD, Meyer RA, Campbell JN. Myelinated mechanically insensitive afferents from monkey hairy skin: heat-response properties. Journal of neurophysiology. 1998;80(3):1082-93. PubMed PMID: 9744923.
284. Burgess PR, Perl ER. Myelinated afferent fibres responding specifically to noxious stimulation of the skin. The Journal of physiology. 1967;190(3):541-62. PubMed PMID: 6051786; PMCID: PMC1365427.
285. Lynn B, Carpenter SE. Primary afferent units from the hairy skin of the rat hind limb. Brain Res. 1982;238(1):29-43. PubMed PMID: 6282398.
286. Purves D, Augustine G, Fitzpatrick D. Mechanosensory Information: The Dorsal Column-Medial Lemniscus System. . 2001. In: Neuroscience, 2nd edition [Internet]. Sunderland, MA: Sinauer Associates. Available from: http://www.ncbi.nlm.nih.gov/books/NBK11142/.
287. Purves D, Augustine G, Fitzpatrick D. Central Pain Pathways: The Spinothalamic Tract. 2001. In: Neuroscience, 2nd edition [Internet]. Sunderland, MA: Sinauer Associates. Available from: http://www.ncbi.nlm.nih.gov/books/NBK10967/.
288. Defrin R, Devor M, Brill S. Tactile allodynia in patients with lumbar radicular pain (sciatica). Pain. 2014;155(12):2551-9. doi: 10.1016/j.pain.2014.09.015. PubMed PMID: 25242568.
289. Maxwell DJ, Réthelyi M. Ultrastructure and synaptic connections of cutaneous afferent fibres in the spinal cord. Trends in neurosciences. 1987;10(3):117-23. doi: http://dx.doi.org/10.1016/0166-2236(87)90056-7.
290. Sengul G. Chapter 5 - Primary Afferent Projections to the Spinal Cord A2 - Paxinos, George. The Rat Nervous System (Fourth Edition). San Diego: Academic Press; 2015. p. 77-85.

291. Todd AJ. Neuronal circuitry for pain processing in the dorsal horn. Nat Rev Neurosci. 2010;11(12):823-36. doi: 10.1038/nrn2947. PubMed PMID: 21068766; PMCID: PMC3277941.
292. D'Mello R, Dickenson AH. Spinal cord mechanisms of pain. British Journal of Anaesthesia. 2008;101(1):8-16. doi: 10.1093/bja/aen088.
293. Greer KR, Hoyt JW. Pain: theory, anatomy, and physiology. Crit Care Clin. 1990;6(2):227-34. PubMed PMID: 2160851.
294. Melzack R, Wall PD. Pain mechanisms: a new theory. Science. 1965;150(3699):971-9. PubMed PMID: 5320816.
295. Moayedi M, Davis KD. Theories of pain: from specificity to gate control. Journal of neurophysiology. 2013;109(1):5-12. doi: 10.1152/jn.00457.2012. PubMed PMID: 23034364.
296. Basbaum AI, Fields HL. Endogenous pain control systems: brainstem spinal pathways and endorphin circuitry. Annu Rev Neurosci. 1984;7:309-38. doi: 10.1146/annurev.ne.07.030184.001521. PubMed PMID: 6143527.
297. Millan MJ. Descending control of pain. Progress in neurobiology. 2002;66(6):355-474. PubMed PMID: 12034378.
298. Heinricher MM, Tavares I, Leith JL, Lumb BM. Descending control of nociception: Specificity, recruitment and plasticity. Brain Res Rev. 2009;60(1):214-25. doi: 10.1016/j.brainresrev.2008.12.009. PubMed PMID: 19146877; PMCID: PMC2894733.
299. Zimmermann M. Pathobiology of neuropathic pain. Eur J Pharmacol. 2001;429(1-3):23-37. PubMed PMID: 11698024.
300. Baron R. [Neuropathic pain. The long path from mechanisms to mechanism-based treatment]. Anaesthesist. 2000;49(5):373-86. PubMed PMID: 10883351.
301. Duan B, Cheng L, Bourane S, Britz O, Padilla C, Garcia-Campmany L, Krashes M, Knowlton W, Velasquez T, Ren X, Ross SE, Lowell BB, Wang Y, Goulding M, Ma Q. Identification of spinal circuits transmitting and gating mechanical pain. Cell. 2014;159(6):1417-32. doi: 10.1016/j.cell.2014.11.003. PubMed PMID: 25467445; PMCID: PMC4258511.
302. Berrocal YA, Almeida VW, Puentes R, Knott EP, Hechtman JF, Garland M, Pearse DD. Loss of central inhibition: implications for behavioral hypersensitivity after contusive spinal cord injury in rats. Pain Res Treat. 2014;2014:178278. doi: 10.1155/2014/178278. PubMed PMID: 25180088; PMCID: PMC4142659.
303. Woolf CJ, Shortland P, Reynolds M, Ridings J, Doubell T, Coggeshall RE. Reorganization of central terminals of myelinated primary afferents in the rat dorsal horn following peripheral axotomy. J Comp Neurol. 1995;360(1):121-34. doi: 10.1002/cne.903600109. PubMed PMID: 7499558.
304. Doubell TP, Mannion RJ, Woolf CJ. Intact sciatic myelinated primary afferent terminals collaterally sprout in the adult rat dorsal horn following section of a neighbouring peripheral nerve. J Comp Neurol. 1997;380(1):95-104. PubMed PMID: 9073085.

305. Coggeshall RE, Lekan HA, Doubell TP, Allchorne A, Woolf CJ. Central changes in primary afferent fibers following peripheral nerve lesions. Neuroscience. 1997;77(4):1115-22. PubMed PMID: 9130791.
306. Tong YG, Wang HF, Ju G, Grant G, Hokfelt T, Zhang X. Increased uptake and transport of cholera toxin B-subunit in dorsal root ganglion neurons after peripheral axotomy: possible implications for sensory sprouting. J Comp Neurol. 1999;404(2):143-58. PubMed PMID: 9934990.
307. Blomqvist A, Craig AD. Is neuropathic pain caused by the activation of nociceptive-specific neurons due to anatomic sprouting in the dorsal horn? J Comp Neurol. 2000;428(1):1-4. PubMed PMID: 11058220.
308. Bao L, Wang HF, Cai HJ, Tong YG, Jin SX, Lu YJ, Grant G, Hokfelt T, Zhang X. Peripheral axotomy induces only very limited sprouting of coarse myelinated afferents into inner lamina II of rat spinal cord. Eur J Neurosci. 2002;16(2):175-85. PubMed PMID: 12169100.
309. Hadjab S, Franck MC, Wang Y, Sterzenbach U, Sharma A, Ernfors P, Lallemend F. A local source of FGF initiates development of the unmyelinated lineage of sensory neurons. The Journal of neuroscience : the official journal of the Society for Neuroscience. 2013;33(45):17656-66. doi: 10.1523/JNEUROSCI.1090-13.2013. PubMed PMID: 24198358.
310. Hennessey JA, Wei EQ, Pitt GS. Fibroblast growth factor homologous factors modulate cardiac calcium channels. Circ Res. 2013;113(4):381-8. doi: 10.1161/CIRCRESAHA.113.301215. PubMed PMID: 23804213; PMCID: PMC3813963.
311. Fawell S, Seery J, Daikh Y, Moore C, Chen LL, Pepinsky B, Barsoum J. Tat-mediated delivery of heterologous proteins into cells. Proceedings of the National Academy of Sciences of the United States of America. 1994;91(2):664-8. PubMed PMID: 8290579; PMCID: PMC43009.
312. Hargus NJ, Merrick EC, Nigam A, Kalmar CL, Baheti AR, Bertram EH, 3rd, Patel MK. Temporal lobe epilepsy induces intrinsic alterations in Na channel gating in layer II medial entorhinal cortex neurons. Neurobiol Dis. 2011;41(2):361-76. doi: 10.1016/j.nbd.2010.10.004. PubMed PMID: 20946956; PMCID: PMC3014455.
313. Hargus NJ, Nigam A, Bertram EH, 3rd, Patel MK. Evidence for a role of Nav1.6 in facilitating increases in neuronal hyperexcitability during epileptogenesis. Journal of neurophysiology. 2013;110(5):1144-57. doi: 10.1152/jn.00383.2013. PubMed PMID: 23741036; PMCID: PMC3763090.

CURRICULUM VITAE

Cindy M. Barbosa Nuñez

EDUCATION

Ph.D. Indiana University
Department of Pharmacology and Toxicology
Indianapolis, IN
Advisor, Theodore R. Cummins, Ph.D.

B.S. University of Puerto Rico
Department of Chemistry
San Juan, PR
Advisor, Jorge L. Colón, Ph.D.

HONORS AND AWARDS

- K.K. Chen Fellowship Award, Indiana University, 2015
- F31 (NS090837-01) Predoctoral Ruth L. Kirschstein National Research Service Award (NRSA), National Institute of Neurological Disorders and Stroke, NIH, 2014.
- Society for Neuroscience (SfN)-Neuroscience Scholars Program Associate, 2014-16
- Society for Advancement of Hispanic/Chicanos and Native Americans in Science Chapter at Indiana University Purdue University Indianapolis, President, 2014-15
- American Pain Society Young Investigator Travel Award, 2014
- Paradise Travel Award, Indiana University, 2013
- Indiana University School of Medicine Graduate Student Travel Award, 2013
- Summer Program in Neuroscience, Ethics and Survival (SPINES) Fellowship, Marine Biological Laboratory, 2013
- National Institute of Neurological Disorders and Stroke Diversity Supplement Award, NIH (NS053422), 2012-2015
- American Association for the Advancement of Science (AAAS)/Science Program for Excellence in Science, 2012-14
- Research Initiative for Scientific Enhancement Internship, University of Puerto Rico, 2009-2010
- Outstanding Poster Presentation Award (Physiology Category), Annual Biomedical Research Conference for Minority Students, 2009
- T-35 Summer Fellowship, Indiana University, 2009
- Academic Excellence in Science and Mathematic Award, University of Puerto Rico, 2009
- Academic Excellence in Science and Mathematic Award, University of Puerto Rico, 2008

- Academic Excellence in Science and Mathematic Award, University of Puerto Rico, 2007
- Puerto Rico-Louis Stokes Alliances for Minority Participation Summer Internship, University of Puerto Rico, 2007

PEER-REVIEWED PUBLICATIONS

- Patel RR, **Barbosa C** and Cummins TR. Epilepsy associated mutant voltage-gated sodium channels alter resurgent current generation that could be preferentially targeted with cannabidiol. Brain. In press.
- Xie W, Tan ZY, **Barbosa C**, Strong JA, Cummins TR, Zhang JM. Upregulation of the sodium channel NaVbeta4 subunit and its contributions to mechanical hypersensitivity and neuronal hyperexcitability in a rat model of radicular pain induced by local DRG inflammation. Pain. 2015. doi: 10.1097/j.pain.0000000000000453. PubMed PMID: 26785322..
- **Barbosa C** and Cummins TR. Current Topics in Membranes Book Series: Sodium Channels across phyla. Chapter: Unusual voltage-gated sodium currents as targets for pain. El Sevier. Accepted.
- **Barbosa C**, Tan ZY, Wang R, Xie W, Strong JA, Patel RR, Vasko MR, Zhang JM, Cummins TR. Navbeta4 regulates fast resurgent sodium currents and excitability in sensory neurons. Mol Pain. 2015;11:60. doi: 10.1186/s12990-015-0063-9. PubMed PMID: 26408173; PMCID: PMC4582632.
- Patel RR, **Barbosa C**, Xiao, Y and Cummins. Human Nav1.6 channels generate larger resurgent currents than human Nav1.1 channels, but the Navβ4 peptide does not protect either isoform from use-dependent reduction. PLoS ONE 10(7): e0133485. doi: 10.1371/journal.pone.0133485
- Casañas-Montes B, Díaz A, **Barbosa C**, Ramos C, Collazo C, Meléndez E, Queffelec C, Fayon F, Clearfield A, Bujoli B, Colón JL. Molybdocene dichloride intercalation into zirconium phosphate nanoparticles. Journal of Organometallic Chemistry. May 2015;05;031.
- Lee H, Park KD, Torregrosa R, Yang XF, Dustrude E, Wang Y, Wilson S, **Barbosa C**, Xiao Y, Cummins TR, Khanna R and Kohn H. Substituted N-(Biphenyl-4'-yl)methyl (R)-2-Acetamido-3-methoxypropionamides: Potent Anticonvulsants That Affect Frequency (Use)-Dependence and Slow Inactivation of Sodium Channels. Journal of Medicinal Chemistry. 2014; 57(14): 6165–82. doi: 10.1021/jm500707r. PubMed PMID: 25004277
- King AM, Yang XF, Wang Y, Dustrude ET, **Barbosa C**, Due MR, et al. Identification of the benzyloxyphenyl pharmacophore: a structural unit that promotes sodium channel slow inactivation. ACS Chemical Neuroscience. 2012;3(12):1037-49. E['gpub 2012/12/22.

doi: 10.1021/cn300129d. PubMed PMID: 23259039; PubMed Central PMCID: PMCPMC3526970.

- Kumar S, Chakraborty S, **Barbosa C**, Brustovetsky T, Brustovetsky N, Obukhov AG. Mechanisms controlling neurite outgrowth in a pheochromocytoma cell line: the role of TRPC channels. Journal of Cellular Physiology. 2012;227(4):1408-19. doi: 10.1002/jcp.22855. PubMed PMID: 21618530.
- Rivera EJ, **Barbosa C**, Torres R, Rivera H, Fachini ER, Green TW, et al. Luminescence rigidochromism and redox chemistry of pyrazolate-bridged binuclear platinum(II) diimine complex intercalated into zirconium phosphate layers. Inorganic Chemistry. 2012;51(5):2777-84. Epub 2012/02/22. doi: 10.1021/ic201423q. PubMed PMID: 22339702.
- Rivera EJ, **Barbosa C**, Torres R, Grove L, Taylor S, Connick WB, et al. Vapochromic and vapoluminescent response of materials based on platinum(ii) complexes intercalated into layered zirconium phosphate. Journal of Materials Chemistry. 2011;21(40):15899-902. doi: 10.1039/C1JM12053K.

PUBLICATIONS UNDER REVIEW

- **Barbosa C,** Johnson A and Cummins TR. FHF2 isoform differentially regulate Nav1.6 mediated resurgent sodium currents in dorsal root ganglion neurons. Submitted.

PUBLICATIONS IN PREPARATION

- Xiao Y**, Barbosa C,** Cummins TR. Increased resurgent sodium currents in Nav1.8 contribute to nociceptive sensory neurons hyperexcitability in small fiber neuropathy. In preparation

ABSTRACTS

- Xiao Y, **Barbosa Nunez C** and Cummins TR. Increased resurgent sodium currents in Nav1.8 contribute to nociceptive sensory neuron hyperexcitability in small fiber neuropathy. Soc Neurosci Abstracts. October 17-21, 2015.
- **Barbosa Nunez C** and Cummins TR. FHF2A negatively regulates resurgent currents in sensory neurons. Soc Neurosci Abstracts. October 17-21, 2015.
- Patel RR, **Barbosa Nunez C** and Cummins TR. Epilepsy associated mutant voltage-gated sodium channels alter resurgent current generation that could be preferentially targeted with cannabidiol. American Epilepsy Society Conference. December, 2014.
- Patel RR, **Barbosa Nunez C** and Cummins TR. Epilepsy associated mutant voltage-gated sodium channels alter resurgent current generation that could be preferentially targeted by cannabidiol. Soc Neurosci Abstracts. November 15-19, 2014.

- **Barbosa Nunez C,** Wang R, Xie W, Tan Z, Strong JA, Vasko MR, Zhang JM and Cummins TR. Navβ4 in sensory neurons regulates resurgent currents and excitability. Soc Neurosci Abstracts. November 15-19, 2014.
- Xie, W, Tan, Z, **Barbosa Nunez, C**., Strong, JA, Cummins, TR and Zhang, JM. (2014). Role of Navβ4 regulatory subunit and resurgent current in development of pathological pain. Soc Neurosci Abstracts. November 15-19, 2014.
- Patel RR, **Barbosa Nunez C** and Cummins TR. Epilepsy associated mutant voltage-gated sodium channels alter resurgent current generation that could be preferentially targeted with cannabidiol. 2014 Gill Symposium. October 15, 2014.
- Patel RR, **Barbosa Nunez C** and Cummins TR. Epilepsy associated mutant voltage-gated sodium channels alter resurgent current generation that could be preferentially targeted with cannabidiol. Ion Channels Gordon Research Seminar: Channel Structure, Function, Disease and Drugs. July 6, 2014.
- **Barbosa Nunez C**, Cummins TR. (279) Navβ4 in sensory neurons regulates resurgent currents and excitability. The journal of pain: official journal of the American Pain Society. 2014;15(4):S45. May 1, 2014.
- **Barbosa Nunez C** and Cummins TR. Navβ4 in sensory neurons regulates resurgent currents and excitability. Soc Neurosci Diversity Poster Session. November 11, 2013.
- **Barbosa Nunez C** and Cummins TR. Navβ4 in sensory neurons: potential regulator of resurgent currents. Midwest Regional Pain Interest Group Meeting. August 23, 2013.
- **Barbosa Nunez C**, Kumar S, Chakrabory S, Obukhov AG. The role of TRPC channels in regulating the length of neurites. Annual Biomedical Research Conference for Minorities. November 5, 2009.
- **Barbosa Nunez C**, Kumar S, Chakrabory S, Obukhov AG. The role of TRPC channels in regulating the length of neurites. CIC SROP Research Conference. July 25,2009.
- **Barbosa Nunez C**, Kumar S, Chakrabory S, Obukhov AG. The role of TRPC channels in regulating the length of neurites. IUPUI Summer Research Poster Symposium. July 22, 2009.

ORAL PRESENTATIONS

- **Barbosa Nunez C,** Wang R, Xie W, Tan Z, Strong JA, Vasko MR, Zhang JM and Cummins TR. Differential regulation of resurgent sodium currents by auxiliary proteins: potential therapeutic strategies for pain. Departmental Seminar. December 11, 2014.

- **Barbosa Nunez C,** Wang R, Xie W, Tan Z, Strong JA, Vasko MR, Zhang JM and Cummins TR. Navβ4 in sensory neurons regulates resurgent currents and excitability. Departmental Seminar. March2014.
- **Barbosa Nunez C** and Cummins TR. Navβ4 in sensory neurons: potential regulator of resurgent currents. SPINES Symposium. Marine Biology Lab, July 9, 2013.
- **Barbosa Nunez C** and Cummins TR. Navβ4 and FHF2A in sensory neurons: potential regulators of resurgent currents. Departmental Seminar. April 5, 2013
- **Barbosa Nunez C**, Casañas B, Colón JL. Intercalation of titanocene dichloride into zirconium phosphate layered nanomaterial envisioned as a drug delivery system. 30th Puerto Rico Interdisciplinary Scientific Meeting (45th Junior Technological Meeting). March 13, 2010.
- **Barbosa Nunez C**, Rivera E, Colón JL. Chemosensing applications of Binuclear Platinum(II) complex intercalated into Zirconium Phosphate Layers: Intercalation of Pt(4,4'dmbpy)(pz)-dimer into 10.3 Å ZrP phase. 28th Puerto Rico Interdisciplinary Scientific Meeting (43th Junior Technological Meeting). March 8, 2008.

PROFFESSIONAL MEMBERSHIPS

- Society for Advancement of Hispanic/Chicanos and Native Americans in Science, 2014-2016
- Society for Neuroscience, 2014-2016
- American Pain Society, 2013-2015
- American Association for the Advancement of Science, 2012-2015
- American Chemical Society, 2008-13